READING UNIVERSITY

Effective Robotic Control Through Anticipating Synchronisation

PhD Cybernetics

Brain Embodiment Lab, Department of Biomedical Engineering, School of Biological Sciences, University of Reading, Reading, RG6 6AH, United Kingdom

Henry Eberle

May 17, 2019

Abstract

This thesis describes the development of a robotic control scheme with a novel 'parallel' design that combines direct feedback control with the simultaneous output of a dynamical forward model. Unlike existing predictive control schemes with a serial 'sense-calculate-move' structure where the model fully determines the robot's behaviour, the parallel controller can adapt to overcome any feedback delay the system experiences without updating its parameters. This is thanks to replicating the key properties of anticipating synchronisation (AS), where a slave system (the robot) anticipates a similar master (a moving target) via delayed self-feedback. Since the robot and target possess very different dynamics, the output of the forward model is used to impose a suitable dynamical behaviour on the robot, while the direct feedback term simultaneously drives the robot itself to anticipate the target. This means that the forward model does not have to be

related to the robot's true dynamics so long as it represents a suitable AS slave system, and that any feedback delay will inevitably be opposed by a proportional degree of anticipation. The result is a highly robust and adaptable predictive controller that can be applied to a robot without requiring precise knowledge of its dynamics.

Contents

1 Individual Contributions

Chapters 2 to 4 of this thesis have been previously published as research articles under the same titles, while Chapter 5 is formatted as such for future publication. The author of this thesis, Henry Eberle (HE) is the first author of Chapters 2 ("Integration of Visual and Joint Information to Enable Linear Reaching Motions", published in Scientific Reports) and 4 ("Anticipation from Sensation: Using Anticipating Synchronisation to Stabilise a System with Inherent Sensory Delay", published in Royal Society Open Science) and the third author of Chapter 3 ("Renormalized time scale for anticipating and lagging synchronization", published in Physics Review E), after Yoshikatsu Hayashi (YN) and Slawomir J Nasuto (SJN). In all cases the co-authors are YN and SJN, HE's supervisors. HE set the research question, performed the literature review and carried out all experiments for Chapters 2 and 4, with YH and SJN providing guidance, discussing results and contributing to the format and editing of the manuscripts. For chapter 3, HE developed and performed all numerical simulations and experiments necessary to validate a hypothesis originated by YH, including producing all corresponding figures. HE is the sole author of all other chapters of the thesis, and developed all the code, simulations and models used to perform the experiments described therein.

Introduction

1 Introduction

Living things, but particularly animals, must respond correctly to a vast range of external phenomena and do so quickly, or risk their survival. The fundamental limitation to this comes from the many delays that exist within biological systems: muscles do not contract instantly, nor do nervous signals travel at the speed of light. Nonetheless, animals respond with minimal delay, to the point that a lagging response to stimuli is often indicative of a disease or disorder. The solution then, is that animals must be employing a form of anticipation; not reacting to current events, but responding to predicted future events. Traditional robotic manipulators do not experience these difficulties because a combination of high-gain motors and rigid linkages allows them to respond extremely rapidly to any given command. However, these robots are not suitable for mixed human environments because their rigidity, high speed and ability to exert injurious force make them dangerous to interact with. Softer, bio-inspired robots are safer, but bring with them the weaknesses and delays of biological systems. This thesis explores how a control scheme based on strong anticipation, specifically anticipating synchronisation, can be used to overcome uncertain or changing delay in a robotic system, displaying properties distinct from existing predictive control schemes.

This chapter is divided into three sections that summarise the research themes driving this thesis: the distinction between strong and so-called 'weak' or model-based anticipation, anticipating synchronisation, and the evidence for its existence within the human motor control system, and the intersection of the two with the control of robotic manipulators.

2 Strong and Weak Anticipation

Strong anticipation was first defined in contrast to 'weak anticipation' where an entity (biological or artificial) uses a model of its environment to predict external events and respond accordingly - what we would otherwise refer to as predictive control. The existance of a full and accurate dynamical model of the body allows instantaneous and flawless prediction of how it will respond to any given control input, and this ability has been placed as vitally important for human motor control, and even cognition, by many researchers. In terms of motor control, researchers such as Kawato [1] and Wolpert [2] have claimed that internal representations of the body are what allow humans to make quick, 'high gain' movements despite the appreciable neural transmission delay between muscle and brain and vice-versa. In this framework closed-loop control can be performed because a predictive model cancels out the delay that would otherwise cause instability. On a more cognitive level, Blakemore, Frith and Wolpert suggested in 2001 [3] that such a simulation of the body is responsible for the sensation of body ownership or agency - selectively cancelling the sensory feedback that arises from volitional movement such that we can separate outside influences from the consequences of our own actions. What all of these theories have in common is that they treat the body as a 'dumb' object that has no role in motor cognition - much like a robot. According to Dubois [4], strong anticipation differs in that is an "endo-anticipation" - the system, brain and body, predicts the environment with reference to its own behaviour, rather than relying on a model of itself.

Functionally this means that no computational predictions of some n seconds into the future occur; the appropriate 'predictive' behaviour can arise directly out of an organism's coupling with its environment (in this context 'coupling' refers to a feedback response to sensory input). The classic analogy, as laid out by Stepp and Turvey [5], is that of a baseball outfielder catching a thrown ball. Intercepting the ball can be achieved with an analytic solution, modeling the ball's ballistic trajectory and moving to where it will land, or a non-analytic solution where the outfielder moves continuously such that the ball's movement appears straight. This strategy will place the catcher in the right place at the right time simply using a negative feedback loop with a well-chosen error term. Strong (as opposed to 'weak', or model-based) anticipation is to prediction as the outfielder is to feedback control: anticipating events through a continuous sensory-motor coupling with the

environment, rather than a predictive model. One can easily see how strong anticipation, when applied to living organisms, overlaps with many of the concepts of embodied cognition. In Wilson's break down of the six major claims [6] of embodied cognition, it is only the last (that non-motor human cognition is performed with reference to the motor system) that is not familiar. Otherwise, both theories stress that cognition and behaviour must be viewed as a continuous interaction between the organism and the environment that is deeply embedded within their local timescale (as opposed to cognition and action being decoupled). A distinction can be made that embodied cognition is concerned with discovering how actions and cognitive events are produced by the interplay of body, brain and environment, while strong anticipation is focused on how these actions can become anticipatory, rather than merely reactive.

Strong anticipation is attractive in its parsimony, but potential examples remain highly specific (like the outfielder), and 'weak' model-based anticipation has many more years of primary research invested in it. One of the most well-researched potential forms of model-based anticipation is based around the concept of one or more 'forward models' within the human central nervous system (CNS). Such a forward model takes the current sensory input and a motor control signal and predicts the sensory data that will result. In principle this can counteract any physiological delay by predicting the delayed feedback signal before it arrives and later using the prediction error to refine the model. This may be paired with an inverse model, which calculates the correct motor commands for the body to produce a desired sensory response.

A forward model (and the associated inverse model that controls the body) that can encompass all the different ways in which the human body's kinematics and dynamics can change when using tools and interacting with the environments would be massively complex, which has led some to question whether such a unified model could exist within the brain. The modular selection and identification for control (MOSAIC) model, as defined by Wolpert and Kawato [7] and expanded upon by Haruno et al. [8] is intended to be an answer to this problem: it consists of a limited number of forward/inverse model pairs (modules), each corresponding to a specific sensorimotor context. Which models are actively engaged in controlling the body is determined by a 'responsibility estimator' which calculates the prediction error for each for-

ward model and weights the corresponding pair's contribution in proportion. This allows previously learned control strategies to be combined to perform 'intermediate' tasks, increasing the ability to generalise. The physiological evidence provided for this hypothesis is the fact that while adaptation to a novel control task is initially slow, 'de-adaptation' once the task is over is always quick. The authors took this as evidence that a new module is being learned for the new task, then quickly switched to an existing module once in a familar context.

All these methods lack what could be described as the key benefit of strong anticipation; in each case, the delay in reality must be learned and matched by some internal parameter in order to produce lag-free control. In truly strong anticipation, this information is encoded into the continuous sensorimotor interaction with the environment rather than an internal model and does not need to be learned. This may seem like a vague condition, but the most rigorous implementation of strong anticipation, anticipating synchronisation (AS), has a number of characteristics that can be tested for behaviourally.

2.1 Anticipating Synchronisation

AS is a now well-recognised extension of the phenomenon of synchronised dynamical systems; returning to Stepp and Turvey's 2010 paper [5], it is telling that it occupies the greater part of the discussion. Since at least the 15th century, it has been known that interacting dynamical systems can synchronise and thus behave identically. More surprisingly, it has recently been proven that one dynamical system can synchronise with the future state of another, acting as a predictor. In Voss's initial study [9] this phenomenon was demonstrated specifically in the context of chaotic dynamical systems, which thanks to their hypersensitivity to initial conditions, are extremely difficult to predict accurately using a model. The first form identified by Voss was only applicable to systems with an explicit delay dependence. He showed that such a system (the 'master') could be predicted by an otherwise identical system (the 'slave') in which the delayed term is replaced with the current state of the master as in Eq. 1 and 2:

$$\dot{x}(t) = -ax(t) + f(x(t-\tau) \tag{1}$$

$$\dot{y}(t) = -ay(t) + f(x(t)) \tag{2}$$

where $x(t)$ is the master at time t, $y(t)$ is the slave and $x(t-\tau)$ is the master's state delayed by τ. This creates an anticipating manifold that is globally attractive, such that the slave will always converge on to the master's future state until $y = x(t+\tau)$. The anticipation period can be increased to an arbitrary multiple of τ by creating a chain of slaves, each of which anticipates the last.

Stepp also defined a second, more generally applicable form that can predict dynamical systems that do not contain an explicit delay term. This relies on a dissipative coupling as shown in Eq. 3 and 4:

$$\dot{x}(t) = f(x(t)) \tag{3}$$

$$\dot{y}(t) = f(y(t)) + K[x(t) - y(t-\tau)] \tag{4}$$

where τ is a time delay that only exists in the coupling imposed on the slave and K is a constant governing the coupling strength. This creates an anticipation manifold that is only locally attracting, and the slave will not anticipate the master if their initial conditions differ too much and the anticipation period that can be achieved is smaller. Nevertheless, this second method can be applied to a vast family of dynamical systems, and because of this it is the one that has captured the interest of the most subsequent researchers. The slave can anticipate the master because of the similar vector fields of the two systems; the coupling constitutes a local gradient that accelerates the time evolution of the slave until $y(t) = x(t+\tau)$. As an example, consider a pair of the simple oscillating system governed by Eqs. 5 (master) and 6 (slave)

$$\dot{\boldsymbol{x}}(t) = a\left(\begin{bmatrix} d \\ 0 \end{bmatrix} + \begin{bmatrix} 0 & -1 \\ 1 & 0 \end{bmatrix} \boldsymbol{x}(t)\right) \tag{5}$$

$$\dot{\boldsymbol{y}}(t) = a\left(\begin{bmatrix} d \\ 0 \end{bmatrix} + \begin{bmatrix} 0 & -1 \\ 1 & 0 \end{bmatrix} \boldsymbol{y}(t)\right) + K[\boldsymbol{x}(t) - \boldsymbol{y}(t-\tau)] \tag{6}$$

where x and y are two-dimensional state vectors, d is a driving term, a is a time constant, K is the coupling constant and τ is the coupling constant. The two systems are identical save for the dissipative delay coupling term added to the slave which, as shown in Fig. 1 causes the slave to converge on the future state of the master after an initial transient behaviour, such

that $\boldsymbol{x}_s(t) = \boldsymbol{x}_m(t+\tau)$ from then on. If the master and slave are identical the coupling will disappear completely at this point, leaving two autonomous systems, one of which is τ seconds ahead of the other. If they are not identical, the coupling will never fully disappear and the slave's anticipation of the master's future state will not be fully accurate.

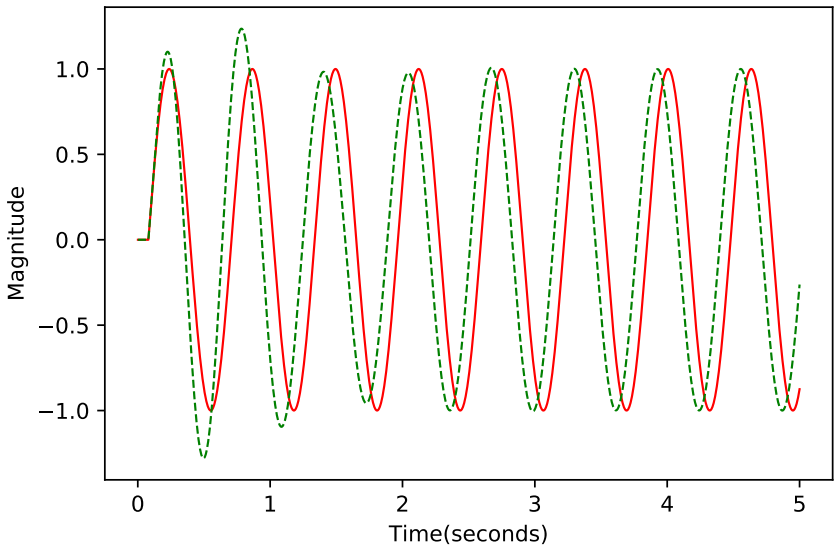

Figure 1: Example of anticipating synchronisation using a dissipative delay coupling Both master (red) and slave (green, dashed) are the X-axis evolution of simple oscillators governed by Eqs. 5 and 6, respectively. The coupling delay $\tau = 80$ms and the time constant $a = 1$.

Although a linear difference term is sufficient as a coupling to give a non-zero period of anticipation, typically a relatively small fraction of the characteristic timescale, it has been shown that this period can be greatly increased by taking into account the specific properties of the master and slave dynamics. In the 2008 study by Pyragas and Pyragienė [10] it was established that by applying a relatively simple rotational transformation to the coupling term, a Rössler chaotic attractor could be predicted by many times the initial anticipation period. This relied on the knowledge that the system is governed by two fixed points; an unstable spiral nearly coinciding with the xy plane and a stable manifold aligned with the z axis through

which the system detours back to the origin. Projecting the coupling difference term onto the unstable spiral and rotating it such that it was in phase with the slave allowed a 4x increase in the anticipation period. They went on to prove analytically that a similar improved coupling could be constructed for other Rössler-type systems and more complex double-scroll chaotic attractors. The 'chain' method of extending anticipation also works for the dissipative coupling, as established by Voss in 2000 [11]. In this way, an anticipation period of $n\tau$ can be achieved, where τ is the 'inter-slave' delay and n is the number of slaves. To prevent the initial transient of the first slave propagating through the entire chain and rendering the subsequent slaves unstable it was found necessary to implement an algorithm that limits the strength of the coupling where the difference between two adjacent systems is very large. This is because each identical slave can only synchronise with the 'normal' behaviour of the master, the transient behaviour being too different.

Although in principle it is difficult to distinguish AS from the forward model-based hypotheses mentioned in the previous section using behavioural studies, there is evience of a similar effect in some human motor behaviour. In a 2009 study by Stepp [12] participants were tasked with following an unpredictable target (governed by a chaotic Rössler attractor) using a cursor while their actual hand was hidden from them. The task was repeated multiple times, with an increasing delay between the movement of the subject's hand and the visual movement of the cursor. When the phase relationship between the target and the subjects' hand movements was analysed, it was apparent that as the delay increased the subjects transitioned from trailing the target (at a small delay of 20ms) to leading it (at 200 and 400ms), indicating anticipation. Crucially, they did not exercise their 'full' anticipation capability from the beginning, nor anticipate at the correct level to cancel out the delay, despite later demonstrating greater anticipation. Stepp concluded that this behaviour was not consistent with a forward model, which one would expect to initially under-anticipate before adapting to the delay. Instead it was posited that the human subjects were acting as the slave in Eq.3, with the imposed feedback delay corresponding to the term τ. This is maladaptive where additional feedback delay is imposed in the experiment, but it should be noted that under normal circumstances this effect would counteract natural physiological delay and lead to more responsive movement. An alternative explanation for these results was provided in a 2016 paper by Voss and Stepp [13] (following from Voss's paper in 2015) which

examined how the AS slave could be replaced with simple relaxation dynamics, retaining an anticipation-like effect in the form of frequency-dependent negative group delay. In such a system, different frequency components of the master signal are anticipated by different periods, while some may lag. However, this would be sufficient to explain the phenomenon observed in Stepp's study and would not require that Rössler dynamics exist within the human brain (which would seem unlikely).

It has not escaped notice that AS has applications for predictive control in artificial systems as, unlike many methods, it is not restricted by the linearity of the anticipated system (the local difference must be near-linear, but this is guaranteed if master and slave are sufficiently similar). The first studies on this subject have focused on how to insert AS into existing predictive control methodology in order to exploit this. In a study by Oguchi and Nijmeijer [14], a system with delayed control input is effectively controlled by placing it in series with a model with identical dynamics to the plant. The plant acts as the master system, while the model is the slave, subject to a coupling based on delayed self-feedback as in Eq.3. Provided the internal self-feedback delay matches the delay in the real system, it can be used to produce an anticipated control signal that 'cancels out' the delay and allows the system to behave as if it does not exist. Additionally, this required that the slave be driven by a non-delayed copy of the control signal. In a later study by Alvarez et al. (including Oguchi and Nijmeijer) [15], the same principle was used to control a mobile robot over a delayed internet connection between two hubs, one in the Netherlands and one in Japan. Due to the more complex nature of network delays, the self-feedback delay was not a static period, but either provided by a model of the internet connection or by sending the slave self feedback over the connection itself along with the control signal ('signal bouncing').

The artificial implementations treat the output of the plant and the slave dynamics as separate elements, and thus the *tau* term must be tuned or optimised to match the true system delay. Signal bouncing allows the true delay to be used in the slave self-feedback, but is only applicable in a network context. Thus existing implementations cannot match the interpretation from [12], which can only be resolved if the output of the plant and the slave are represented by the same term, strongly implying that the plant must be treated as the slave element (or part of it).

2.2 Applications in Robotic Manipulator Control

The difficulty in applying anticipating synchronisation as discussed above to robotics is that most robots, and most robotic control laws, are designed along entirely dissimilar principles. The classical robot, recognisable from hundreds if not thousands of theoretical papers (including some present in this thesis), is an assemblage of rigid rods or bars connected by either prismatic or revolute joints [16]. This machine which, to a greater or lesser extent, resembles nearly every robot used in research or industry makes a virtue of its simplified dynamics. The lack of flexibility and elasticity means that its kinematics are unchanging down to very high level of precision, which ensures that even when moving at very high velocities the position of the robot's endpoint can be described by the same set of coordinate transformations. The inverse of these kinematics can be iteratively solved in order to yield a controller that minimises total velocity, torque, energy use or any number of other objective functions and thanks to the robot's rigidity these calculations can be performed without an excess of time, processing power or memory.

Where dynamics are taken into account, it is to ensure that they do not interfere with the desired behaviour of the robot. In computed torque control schemes, a comprehensive dynamical model of a robotic manipulator is used to calculate a torque input that will linearise the robot's dynamics. This allows a controller to impose the linear behaviour that is assumed when designing kinematic control rules.

Once compliance or flexibility is introduced into a robot however, the computational costs of kinematic control become prohibitive (a good overview can be found here, by Rus and Tolley: [17]), which is why researchers have attempted to look for evidence of how animals (and particularly humans) control their soft bodies. Obviously, robots do not have an ecological niche, but their emulation of living organisms mean that some of principles of embodied cognition can be brought into play. An illustrative example of how can be seen in research by Mitsuda et al. with a humanoid robot arm [18], where they showed that expressing the robot's pose in binocular coordinates (vertical and horizontal rotation and vergence, or focal length) allowed effective control using a linear transformation that is much simpler than the kinematic calculations required when using Cartesian coordinates. This could be con-

sidered unsurprising, since the human motor and visual systems co-evolved. The other benefit of a control law based around a linear, static transformation is that it removes the dependence on precise knowledge of the robot's kinematics. As shown in the 2012 paper by Nishida et al. [19], convergence on a target in the robot's workspace can be ensured so long as the transformation matrix does not become orthogonal to the true kinematics during the movement. This is a relatively weak condition that can be easily fulfilled by selectively limiting the range of motion of the robot's revolute joints. Noticeably, this constraint is already present in the robot from the Mitsuda study, and the human arm it is based on. With convergence assured, the properties of the robot's motion becomes a feedback control, rather than a coordinate transformation problem.

Designing a robotic manipulator with autonomous dynamics ideal for displaying strong anticipation is beyond the scope of this thesis; instead it will examine how a suitable controller can modify a robot's dynamics such that the sensorimotor loop containing the robot and the controller behaves as a usable AS slave. The third chapter, previously published as "Integration of Visual and Joint Information to Enable Linear Reaching Motions" in Nature Scientific Reports is concerned with how a linear, static transformation (as discussed above) can cause a robot arm to converge on a specific trajectory shape - a straight line. The fourth chapter "Renormalized time scale for anticipating and lagging synchronization", published in Physical Review E, was a collaboration with Yoshikatsu Hayashi and Slawomir Nasuto, both of the Reading University Brain Embodiment Lab, in which this author performed the numerical simulations. The manuscript explored the mathematical basis of AS, showing that the effect of delay in the slave's self-feedback was well approximated by a renormalisation of the slave's time constant such that it evolves at a faster rate than the master. In combination, these two studies led to the hypothesis that a robot under proportional-derivative (PD) control could be considered as an AS slave if the master-slave coupling could be made more robust at higher delay values. Chapter four, published as "Anticipation from Sensation: Using Anticipating Synchronisation to Stabilise a System with Inherent Sensory Delay" in Royal Society Open Science, tested this hypothesis by defining two functional arrangements in which a robot could be coupled with a dynamical model such that it anticipated an external chaotic signal and display the properties identified in Stepp's 2009 study - the serial and parallel systems. Chapter five, "Synchronisation-Based

Control for a Collaborative Robot", applies the more robust parallel system to controlling a collaborative Baxter robotic platform and examines how this control system places in the wider context of strong anticipation.

3 Statement of Author Contributions

The third and fifth chapters of this thesis ("Integration of Visual and Joint Information to Enable Linear Reaching Motions" and "Anticipation from Sensation: Using Anticipating Synchronisation to Stabilise a System with Inherent Sensory Delay") were written by me (Henry Eberle) based on work undertaken by the same, with Dr. Yoshikatsu Hayashi and Prof. Slawomir Nasuto acting in their role as PhD supervisors to revise and moderate the manuscript before publication.

I performed the numerical analysis and simulations for the paper "Renormalized time scale for anticipating and lagging synchronization" which forms chapter four, as well as generating and formatting the figures.

I am the sole author of all other chapters in this thesis.

References

[1] Mitsuo Kawato, Tomoe Kuroda, Hiroshi Imamizu, Eri Nakano, Satoru Miyauchi, and Toshinori Yoshioka. Internal forward models in the cerebellum: fmri study on grip force and load force coupling. In *Progress in brain research*, volume 142, pages 171–188. Elsevier, 2003.

[2] Daniel M Wolpert, R Chris Miall, and Mitsuo Kawato. Internal models in the cerebellum. *Trends in cognitive sciences*, 2(9):338–347, 1998.

[3] Sarah-J Blakemore, Chris D Frith, and Daniel M Wolpert. The cerebellum is involved in predicting the sensory consequences of action. *Neuroreport*, 12(9):1879–1884, 2001.

[4] Daniel M Dubois. Mathematical foundations of discrete and functional systems with strong and weak anticipations. In *Anticipatory behavior in adaptive learning systems*, pages 110–132. Springer, 2003.

[5] Nigel Stepp and Michael T Turvey. On strong anticipation. *Cognitive Systems Research*, 11(2):148–164, 2010.

[6] Margaret Wilson. Six views of embodied cognition. *Psychonomic bulletin & review*, 9(4):625–636, 2002.

[7] Daniel M Wolpert and Mitsuo Kawato. Multiple paired forward and inverse models for motor control. *Neural networks*, 11(7):1317–1329, 1998.

[8] Masahiko Haruno, Daniel M Wolpert, and Mitsuo Kawato. Mosaic model for sensorimotor learning and control. *Neural computation*, 13(10):2201–2220, 2001.

[9] Henning U Voss. Anticipating chaotic synchronization. *Physical review E*, 61(5):5115, 2000.

[10] Kestutis Pyragas and Tatjana Pyragienė. Coupling design for a long-term anticipating synchronization of chaos. *Physical Review E*, 78(4):046217, 2008.

[11] Henning U Voss. Dynamic long-term anticipation of chaotic states. *Physical Review Letters*, 87(1):014102, 2001.

[12] Nigel Stepp. Anticipation in feedback-delayed manual tracking of a chaotic oscillator. *Experimental brain research*, 198(4):521–525, 2009.

[13] Henning U Voss and Nigel Stepp. A negative group delay model for feedback-delayed manual tracking performance. *Journal of computational neuroscience*, 41(3):295–304, 2016.

[14] Toshiki Oguchi and Henk Nijmeijer. Control of nonlinear systems with time-delay using state predictor based on synchronization. *Proc. of ENOC 2005*, pages 1150–1156, 2005.

[15] Alejandro Alvarez-Aguirre, Nathan van de Wouw, Toshiki Oguchi, and Henk Nijmeijer. Predictor-based remote tracking control of a mobile robot. *IEEE Transactions on Control Systems Technology*, 22(6):2087–2102, 2014.

[16] Lorenzo Sciavicco and Bruno Siciliano. *Modelling and control of robot manipulators*. Springer Science & Business Media, 2012.

[17] Daniela Rus and Michael T Tolley. Design, fabrication and control of soft robots. *Nature*, 521(7553):467, 2015.

[18] Binocular visual servoing based on linear time-invariant mapping.

[19] Ryosuke Nishida and Sadao Kawamura. A new feedback robot control method based on position/image sensor integration. In *Intelligent Robots and Systems (IROS), 2012 IEEE/RSJ International Conference on*, pages 5012–5017. IEEE, 2012.

Integration of Visual and Joint Information to Enable Linear Reaching Motions

Abstract

A new dynamics-driven control law was developed for a robot arm, based on the feedback control law which uses the linear transformation directly from work space to joint space. This was validated using a simulation of a two-joint planar robot arm and an optimisation algorithm was used to find the optimum matrix to generate straight trajectories of the end-effector in the work space. We found that this linear matrix can be decomposed into the rotation matrix representing the orientation of the goal direction and the joint relation matrix ($\boldsymbol{M}_{JRM}$) representing the joint response to errors in the Cartesian work space. The decomposition of the linear matrix indicates the separation of path planning in terms of the direction of the reaching motion and the synergies of joint coordination. Once the $\boldsymbol{M}_{JRM}$ is numerically obtained, the feedfoward planning of reaching direction allows us to provide asymptotically stable, linear trajectories in the entire work space through rotational transformation, completely avoiding the use of inverse kinematics. Our dynamics-driven control law suggests an interesting framework for interpreting human reaching motion control alternative to the dominant inverse method based explanations, avoiding expensive computation of the inverse kinematics and the point-to-point control along the desired trajectories.

Introduction

Path planning for reaching tasks is a fundamental problem both in robotics [1] and behavioural science [2] . While many control schemes can guarantee convergence of an end effector upon a target, controlling the path it takes is

much more complex. This is because traditionally, once a target has been defined in the robot's work space using its sensors, the necessary final pose to intercept the object must be calculated using some form of inverse kinematics: the explicit transformation of work space coordinates into joint angles. However, inverse kinematics are both computationally intensive and, more importantly, very sensitive to error. Small errors in the kinematic model used can translate into large deviations from the desired pose and unstable motion. Furthermore, if a robot is commanded to simply minimise the difference between its current joint state and a calculated final pose, it will execute a movement that is linear in terms of its joint space, but strongly curved in the work space in which it actually operates. While the end effector still converges upon the target, the trajectory is ultimately not determined in visual coordinates, making it difficult to navigate the external environment. Ideally, the end effector should execute a direct, straight path in the work space in which the target is defined. In order to produce a straight trajectory, most robot control systems must create an explicit path to the target. This requires a complete specification of the desired motion [3] and the leading methods all require a detailed specification of the robot's kinematics and/or dynamics [4] .

Human reaching motions have characteristic properties that distinguish them from those of robots, the most visible being that they are near-straight in the work space [5] . Human hand movements also have a distinctive 'bell-shaped' velocity profile that can be effectively described by the minimum jerk model. There are many theories of how this control is achieved, several of which rely on the existence of paired forward and inverse models used to calculate appropriate torques for any movement [6] . One model that does not rely on this assumption is the equilibrium point (EP) hypothesis, which holds that human motions are governed by the human central nervous system (CNS) modulating the resting length of muscles without reference to kinematics [7] . The EP hypothesis frames movements as the convergence of a dynamical system upon a stable point, rather than the product of a kinematic or geometric calculation. Although there is disagreement on what reference frame or frames the (CNS) operates in when executing reaching movements, the motions themselves are strongly influenced by visual feedback. It has been demonstrated in experiments by Wolpert et al. [8] and Flanagan and Rao [9] that by distorting subject's visual feedback on the position of their hand, the curvature of their reaching movements can be increased, implying that the

CNS is attempting to achieve a straight path in terms of the available visual feedback.

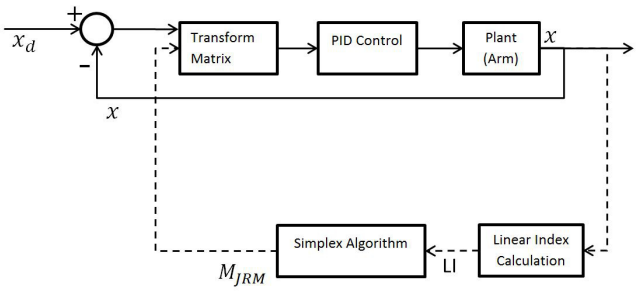

Figure 1: Block diagram of the robot control loop. The transform matrix is updated on a slow timescale in response to the performance of the control (the LI of its movements).

Some have stated that inverse dynamic models are a necessity for the control of the human body, arguing that it is the only way to execute specific motions with such a complex system [10] [11] . This paper comes from the viewpoint that computational complexity can be saved on the part of the controller by exploiting the dynamic properties of the system (a robot in this case).

Many researchers have utilised vision as a basis for controlling robots, either transforming visual data into feedback for a conventional robot controller (position-based visual servoing) [12] or attempting to align the robot's view with a specific scene corresponding to a work space target (image-based visual servoing) [13]. This often involves continuously recomputing the system Jacobian to obtain the correct joint velocities to reach the target, requiring detailed information on the robot's kinematics. Where this is not available, such as when a robot is physically modified, the central assumptions of kinematics-based control break down, and robust control can no longer be ensured.

Our study considered whether it is possible to cause an arm to generate a straight path with its end effector by correcting visual path deviations as

they arise during movement. This does not require a precise kinematic model and is thus much less sensitive to erroneous or incomplete data on the robot's link lengths and joint states. This method relies on the robot's nature as a dynamic system moving in the work space, as opposed to being derived from the system's statics, like the Jacobian transpose method. We thus also aim to demonstrate that this method is energy efficient compared to the Jacobian transpose method, based on this distinction.

It has been established that a control law based on a linear transformation of visual information can enable a robot end effector to converge on a target within a specific area of the work space [14] . It has also been shown that in a humanoid robot, the relationship between the binocular coordinates (viewing directions and vergence angle) of its end effector and the joint space coordinates of its arm is well-approximated by a linear transformation where the arm is positioned to occupy the front visual field of the robot [15] . However in these cases the linear transformation has been treated as an approximation of the kinematics, rather than being examined in terms of the dynamics.

In this paper, a control law based on a static linear transformation matrix $\boldsymbol{M}$ is used to complete the sensory-motor loop of a simulated robot arm, with the aim of creating straight movements in the end effector. The matrix $\boldsymbol{M}$ is reminiscent of the concept of a 'body schema', a dynamic representation of the body's behaviour. In humans this is the element of body representation that allows an understanding of how the body's elements will coordinate [16] [17] . In the simulated robot, $\boldsymbol{M}$ encodes a dynamic relationship between the arm's components that results in a stereotyped movement. Because $\boldsymbol{M}$ defines how the dynamics of the arm's joints interact, rather than acting as a computational model of the dynamics themselves, it is much simpler than the kinematic and dynamic models typically employed in the field of robotics.

Results

Proposed Control Law

The control law used in this study aims to coordinate the dynamics of the robot's individual joints such that its end effector moves in a straight line. To this end, a linear transformation matrix is applied to visual feedback to

constrain the joint's motion with respect to the work space, as can be seen in the system block diagram in Fig.1. The proposed control law can be seen below:

$$\boldsymbol{\tau} = \boldsymbol{M}(\boldsymbol{K_p}(\boldsymbol{x_d} - \boldsymbol{x}) - \boldsymbol{K_v}\dot{\boldsymbol{x}}), \tag{1}$$

where $\boldsymbol{M}$ is a static transformation matrix applied to the visual information to alter the arm's trajectory behaviour. $\boldsymbol{\tau}$ is the vector of joint torques and $\boldsymbol{x}$ is the work space position of the end effector. $\boldsymbol{x_d}$ is the target in the work space. $\boldsymbol{K_p}$ is a proportional gain matrix for the work space error, while $\boldsymbol{K_v}$ is a velocity gain matrix.

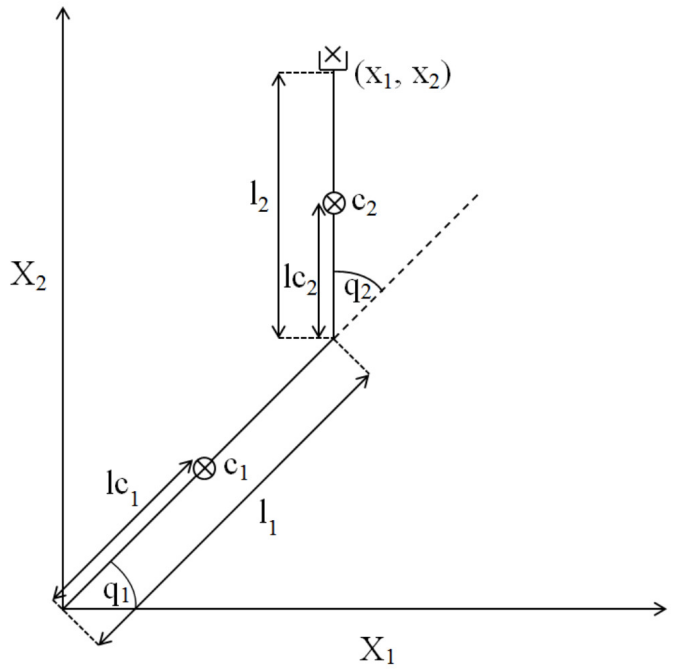

Figure 2: Image of the arm model: The location of the arm's 'hand', $\boldsymbol{x} = [x_1, x_2]$, is calculated from the arm's origin at its first joint. The vector $\boldsymbol{q} = [q_1, q_2]$ represents the rotation of the arm's two joints, while l_1 and l_2 are the link lengths. The lengths of the sections connecting the links' centres of mass (c_1, c_2) to the joints are represented by l_{c1} and l_{c2}.

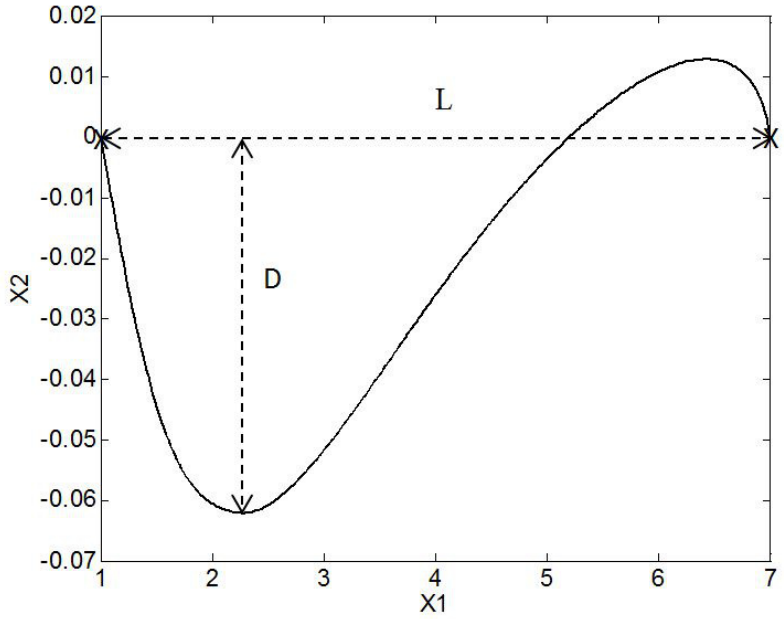

Figure 3: This figure shows the elements of the Linear Index (LI), which is a measure of the straightness of a path in Cartesian space. For this study $LI = D/L$ Where L is the absolute distance between the starting and end positions of the robot's end effector. D is the largest perpendicular deviation from the straight line vector that connects the start and end positions. In the line illustrated here, $L = 6$ and $D \approx 0.06$, so the LI is $\frac{0.06}{6} \approx 0.01$.

Due to the two-dimensional nature of the model's work space and joint space (illustrated in Fig.2), $\boldsymbol{M}$ becomes a 2x2 matrix composed of four parameters that must be optimised to produce direct, straight line trajectories. We used a simplex optimisation algorithm to optimise $\boldsymbol{M}$ automatically to produce desirable motions, defined as those with a low Linear Index (LI). The LI (see Fig. 3), as utilised by Desmurget et. al [18] is calculated by finding the greatest distance between the path taken by the end effector and the straight path connecting its starting and end points, as measured perpendicularly from the straight path:

$$LI = D/L \tag{2}$$

Where L is the absolute distance between the starting and end positions of the robot's end effector. D is the largest perpendicular deviation from the

straight line vector that connects the start and end positions. The mass of the links was set at 1 arbitrary unit each, and their lengths at 4 within the simulation to obtain the results presented here, although the behaviour at larger masses and longer lengths is not qualitatively different.

Properties of Simplex-Optimised Transformation Matrix

In order to eliminate the confounding effects of very large or small effective gains, each matrix produced by the optimisation algorithm was normalised by dividing it by its largest element. The optimised matrix was dependent on the orientation of the straight path from start point to target (θ), and appears to be the product of a 2D rotation matrix $\boldsymbol{T}(-\theta)$ and a constant matrix. At the angular origin of 0 radians on the X axis of the workspace the optimal matrix is $\left(\begin{smallmatrix} 1 & 1 \\ -1 & 1 \end{smallmatrix}\right)$, implying that this is the constant component, given this specific robot structure.

In order to validate that this was an invariant, 'base' component of $\boldsymbol{M}$, the procedure shown in Fig.4 was used, where targets are sampled at evenly spaced polar coordinates and reaching motions to the targets are then simulated. By mapping the LIs of the resulting trajectories to their intended targets in the work space as a heat map, it is possible to see how $\boldsymbol{M}$'s effectiveness varies with the angle of motion. LI was thresholded at 0.5 (largest perpendicular deviation is half the length of the ideal straight path) because the 0 to 0.5 range encompasses the vast majority of variation in 'successful' motions that converged on the target. Visual verification of simulations that produced LIs above 0.5 found that the end effector oscillated at high speeds without reaching the chosen target, so the visual representation can be safely divided into convergent (blue-green) and non-convergent (red) zones.

In Fig.5 it can be seen that while each of the simplex-optimised matrices is associated with linear motions at 0 radians (example trajectories for these M_{JRM} values can be seen in Fig.6), $\boldsymbol{M} = \left(\begin{smallmatrix} 1 & 1 \\ -1 & 1 \end{smallmatrix}\right)$. The closest to the value of $\boldsymbol{M}$ to $\left(\begin{smallmatrix} 1 & 1 \\ -1 & 1 \end{smallmatrix}\right)$ had the widest region of lowest LI centred around 0 radians, representing an optimal condition for straight motions in this direction (the matrices have been normalised with respect to their largest element to discount the effect of a higher control gain).

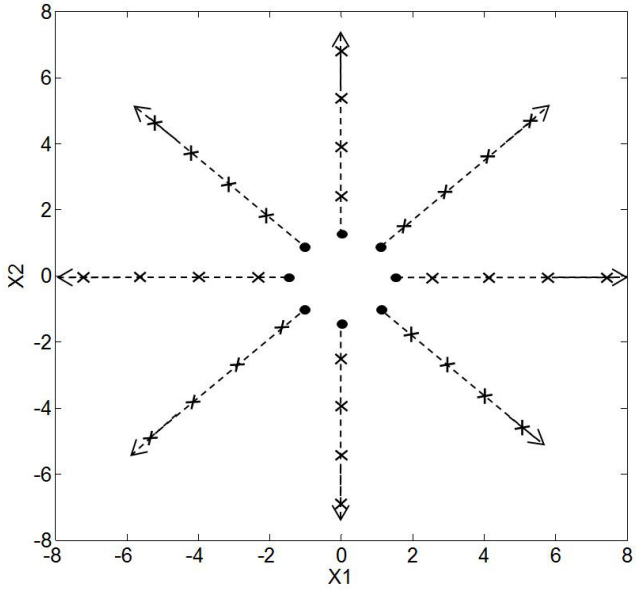

Figure 4: Radial motions are simulated with starting positions (shown as dots) initialised on a circle surrounding the origin, and targets (shown as crosses) placed at fixed distances up to the limit of the arms reach. Each start point/target pair represents a different orientation of movement (θ). The LIs of the resulting trajectories are then calculated and drawn onto the target point of each corresponding movement, producing a heatmap.

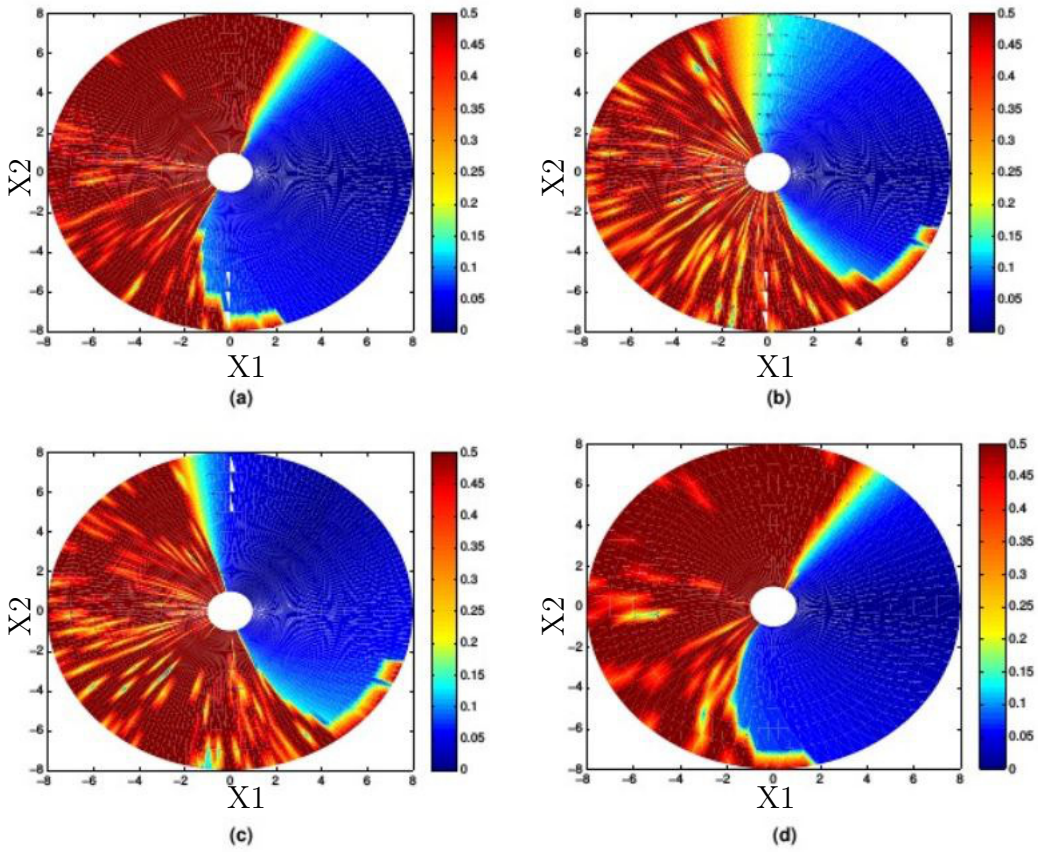

Figure 5: Comparison of four matrices optimised for movements with an orientation of 0 radians. The LI of outward reaching movements is visible as a heat map in the arm's workspace, with the LI values mapped to the target of each movement. LI is saturated at higher values as these correspond to non-convergent trajectories where the measure becomes unreliable. (a) $\boldsymbol{M} = \left(\begin{smallmatrix} 0.9808 & 0.9909 \\ -1 & 0.7828 \end{smallmatrix}\right)$, arrived at using simplex optimisation. (b) $\boldsymbol{M} = \left(\begin{smallmatrix} 0.6585 & 1 \\ -0.6572 & -0.174 \end{smallmatrix}\right)$, arrived at using simplex optimisation. (c) $\boldsymbol{M} = \left(\begin{smallmatrix} 0.4714 & 0.5744 \\ -1 & -0.1705 \end{smallmatrix}\right)$, arrived at using simplex optimisation. (d) $\boldsymbol{M} = \left(\begin{smallmatrix} 1 & 1 \\ -1 & 1 \end{smallmatrix}\right)$, the hypothesised optimum (lowest LI) value for movements with an orientation of 0 radians.

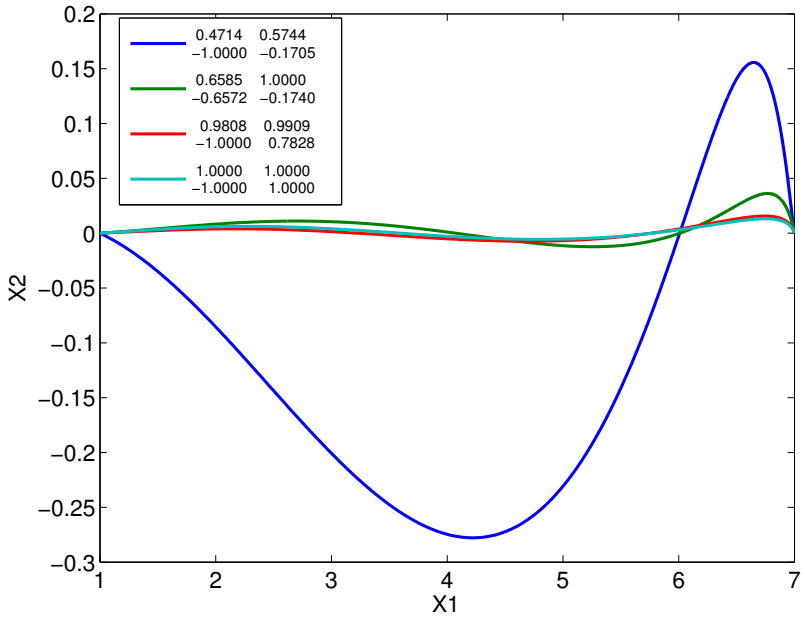

Figure 6: Paths taken by the end effector between the points (1,0) and (7,0), where $\boldsymbol{M}$ is set to a number of values. The first three matrices are the result of simplex optimisation, with each normalised by its largest value. The final matrix is the normalised 2D rotation matrix for $-\pi/4$ radians.

The considerations above lead to the hypothesis that the linear behaviour was not purely the property of a rotational transformation, and that the optimum $\boldsymbol{M}$ for a given radial motion could be factored into a rotational transformation and an invariant underlying matrix. These were denoted as a constant joint relationship matrix ($\boldsymbol{M}_{JRM}$), encoding the relationships between the motion of each joint in the arm and a 2D rotation matrix ($\boldsymbol{T}(-\theta)$) that aligns the coordinates of the target radial trajectory with the X_1 axis of the work space:

$$\boldsymbol{M} = \boldsymbol{M}_{JRM} \cdot \boldsymbol{T}(-\theta), \tag{3}$$

Thus, for the optimum $\boldsymbol{M}$ for any given orientation of movement, it was possible to post-multiply the final value by $\boldsymbol{T}(-\theta)$ to find if the value of $\boldsymbol{M}_{JRM}$ was invariant.

Properties of Analytically-Derived Transformation Matrix

In order to confirm that $\boldsymbol{M}$ could be decomposed into the components $\boldsymbol{M}_{JRM}$ and $\boldsymbol{T}(-\theta)$, the path generation procedure in Fig.4 was again used. The value of $\boldsymbol{M}_{JRM}$ was set to $\left(\begin{smallmatrix} 1 & 1 \\ -1 & 1 \end{smallmatrix}\right)$, corresponding to the optimal value at 0 degrees and this was post-multiplied by a rotation matrix $\boldsymbol{T}(\theta)$. If our hypothesis was correct, the combination of these two matrices would be the optimum $\boldsymbol{M}$ matrix for movements with the radial coordinate θ.

The test results are shown in Fig. 7, where it can be seen that there is a region of very low LI values (representing straight movements) occupying over a quarter of the work space. It can also be seen that multiplying the $\boldsymbol{M}_{JRM}$ by a rotation matrix rotates this region by the specified number of radians in the opposite direction, as hypothesised.

Figure 7 shows LI values up to 0.5, as higher values represent undesirable trajectories that have not converged on the target, making the calculation of LI unreliable. The transition between the convergent and non-convergent regions is very abrupt, with only a few degrees of moderately high LI separating them.

In order to see whether the 'convergent region' of the control law would be widened or constricted by the inclusion of joint space feedback, Eq. 1 was altered to include joint space feedback using a target calculated with the arm's inverse kinematics:

$$\boldsymbol{\tau} = k\boldsymbol{M}(\boldsymbol{K_p}(\boldsymbol{x_d} - \boldsymbol{x}) - \boldsymbol{K_v}\dot{\boldsymbol{x}}) + (1-k)(\boldsymbol{G_p}(\boldsymbol{q_d} - \boldsymbol{q}) - \boldsymbol{G_v}\dot{\boldsymbol{q}}), \qquad (4)$$

where $\boldsymbol{q}$ is the vector of joint rotations and $\boldsymbol{q}_d$ is the joint space target calculated using the arm's inverse kinematics ($\boldsymbol{q}_d = f^{-1}(\boldsymbol{x}_d)$). The variable k is a dimensionless scalar in the range $0 \leq k \leq 1$ controlling the proportion of kinematic feedback used by the control law. The effect of including kinematic feedback can be seen by comparing Fig. 8 with Fig. 7, which shows that including kinematic feedback does not qualitatively affect the results, but does slightly expand the area in which the arm is stable. Adding the joint space feedback thus appears to have a stabilising influence, but only when sufficiently near the stable region for the work space terms.

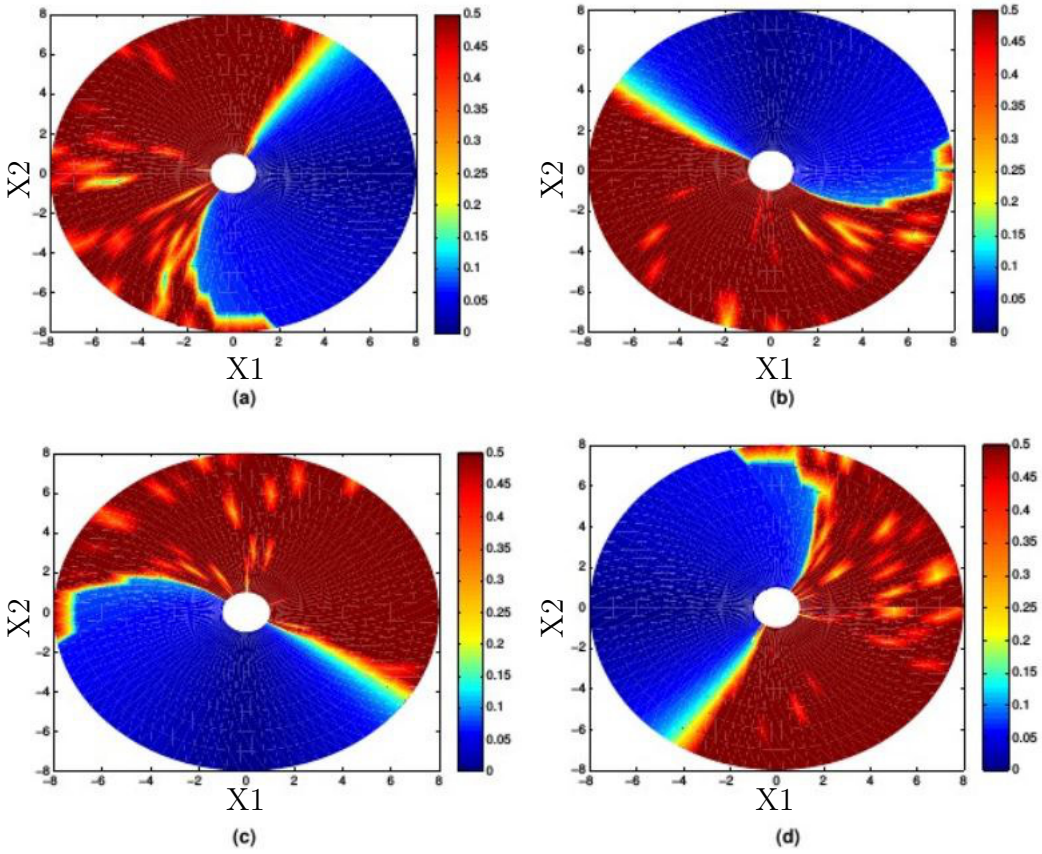

Figure 7: LI values for different $\boldsymbol{M}$ matrices where the $\boldsymbol{M}_{JRM}$ is kept constant at $\left(\begin{smallmatrix}1 & 1\\ -1 & 1\end{smallmatrix}\right)$ and the angle of $\boldsymbol{T}(-\theta)$ varies by $\pi/2$ radians, $\boldsymbol{K_p} = \left(\begin{smallmatrix}100 & 0\\ 0 & 100\end{smallmatrix}\right)$, $\boldsymbol{K_v} = \left(\begin{smallmatrix}150 & 0\\ 0 & 150\end{smallmatrix}\right)$, $k = 1$, link lengths = [4,4]. (a) $\theta = 0$, $\boldsymbol{M} = \left(\begin{smallmatrix}1 & 1\\ -1 & 1\end{smallmatrix}\right)$. (b) $\theta = \pi/2$, $\boldsymbol{M} = \left(\begin{smallmatrix}-1 & 1\\ -1 & -1\end{smallmatrix}\right)$. (c) $\theta = 3\pi/2$, $\boldsymbol{M} = \left(\begin{smallmatrix}1 & -1\\ 1 & 1\end{smallmatrix}\right)$. (d) $\theta = \pi$, $\boldsymbol{M} = \left(\begin{smallmatrix}-1 & -1\\ 1 & -1\end{smallmatrix}\right)$.

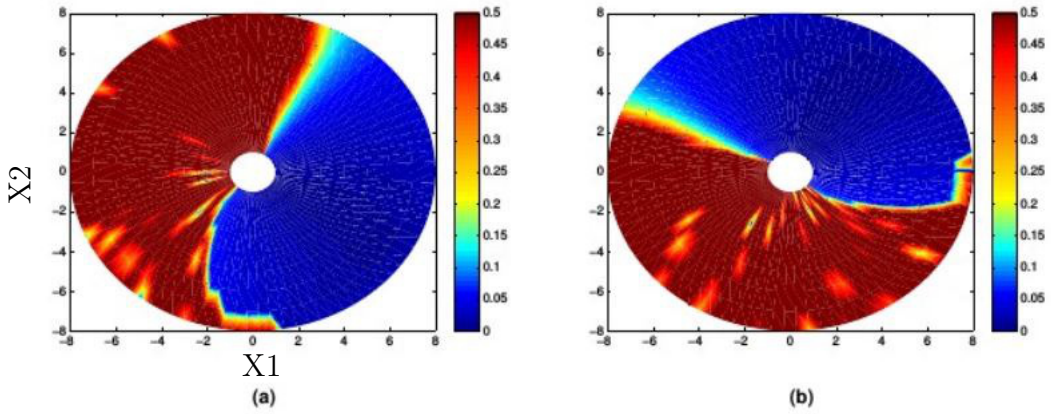

Figure 8: LI values produced where both visual and kinematic feedback is used. The $\boldsymbol{M}_{JRM}$ remains constant at $\left(\begin{smallmatrix}1 & 1\\ -1 & 1\end{smallmatrix}\right)$ and the angle of $\boldsymbol{T}(-\theta)$ varies by $\pi/2$ radians, $\boldsymbol{G_p} = \left(\begin{smallmatrix}200 & 0\\ 0 & 200\end{smallmatrix}\right)$, $\boldsymbol{G_v} = \left(\begin{smallmatrix}300 & 0\\ 0 & 300\end{smallmatrix}\right)$, $k = 0.5$, link lengths = [4,4]. (a) $\theta = 0$, $\boldsymbol{M} = \left(\begin{smallmatrix}1 & 1\\ -1 & 1\end{smallmatrix}\right)$. (b) $\theta = \pi/2$, $\boldsymbol{M} = \left(\begin{smallmatrix}-1 & 1\\ -1 & -1\end{smallmatrix}\right)$.

Mechanism of Joint Relationship Matrix

The fact that the control law defined in Eq. 1 produces near-straight trajectories (with the optimal $\boldsymbol{M}_{JRM}$) can be understood in terms of the arm's geometry and dynamics, instead of a coordinate transformation. Any movement of a revolute joint causes a curve in the trajectory of the end effector, deviating from the desired straight path. The $\boldsymbol{JRM}$ connects the torque at the joints to the motion of the end effector such that any deviation caused by one joint is compensated by the other. In this way, the motions of the two joints coordinate and the end effector remains on a straight trajectory.

This section considers the simplest case of an arm with links of equal length where the end effector approaches a target on the positive X_1 axis, with the second joint below it as pictured in Fig. 9. Because of this, there is no need to transform the coordinate system and $\boldsymbol{M}$ is equal to the $\boldsymbol{M}_{JRM}$. The optimal $\boldsymbol{M}_{JRM}$ matrix in this case has the form $\left(\begin{smallmatrix}1 & 1\\ -1 & 1\end{smallmatrix}\right)$. This form of matrix produces a motion of the end effector represented by the thick line in Fig. 10, indicating that the movements of the two joints are coordinated.

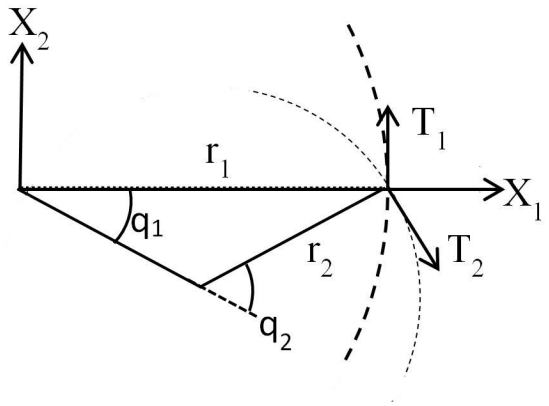

Figure 9: Instantaneous movement of a 2-joint planar arm: $\boldsymbol{q} = [q_1, q_2]$ represents the angles of the arm's two joints. r_1 and r_2 represent the radii of the sub-movements caused by joints 1 and 2, respectively while $\boldsymbol{T} = [T_1, T_2]$ represents the magnitudes of the resulting tangential displacements of the end effector. For this example the $\boldsymbol{M}_{JRM}$ is set to the identity matrix $\boldsymbol{I}$.

In order to understand the effect of the optimal $\boldsymbol{M}_{JRM}$, it is useful to decompose the movement of the end effector into two superimposed movements, as illustrated in Fig. 9. The first is the rotation of the entire arm around the base joint of the first link, giving a circular trajectory of the end effector with radius equal to the distance between the base joint and the end effector (r_1 in Fig. 9). The second movement is the rotation of the end effector around the second joint. This follows a circular path with a constant radius equal to the length of the second joint (r_2 in Fig. 9), but also causes a change in the radius of the first sub-movement (r_1). These two sub-movements are governed by the first and second rows of $\boldsymbol{M}_{JRM}$, respectively.

Here we consider the tangential displacements T_1 and T_2 caused by the first and second sub-movements, respectively, in order to explain how the control law described by Eq. 1 maintains a straight path.

In order for the end effector to remain on a straight path, the vertical components of the tangents T_1 and T_2 must cancel, leaving a net horizontal movement of the end effector. Because the angle between T_1 and T_2 changes as the arm extends, in order to follow the X_1 axis the velocity of joint 2 must change over time in order to maintain this balance. If it does not, the

end effector will diverge from the straight path as seen in the solid line in Fig. 10. In practice, the control law described by Eq.1 does not calculate the exact velocities needed, but relies on the fact that so long as the signs of the elements of $\boldsymbol{M}_{JRM}$) are correct, the end effector will eventually be drawn onto the line connecting the arm origin to the target. As the first joint 'extends' the arm by accelerating in a positive direction, it causes the vertical component of T_1 to grow, meaning that joint 2 must respond by accelerating in a negative direction to maintain balance. This is also why the transformation $\boldsymbol{T(-\theta)}$ is required in Eq.3, as the necessary signs will differ with the orientation of the radial movement. The fact that all elements of the optimum $\boldsymbol{M}_{JRM}$ have the same magnitude is a reflection of the fact that the links have the same length; the optimal $\boldsymbol{M}_{JRM}$ gives the closest match in joint velocities over the course of the movement, requiring smaller reactive corrections.

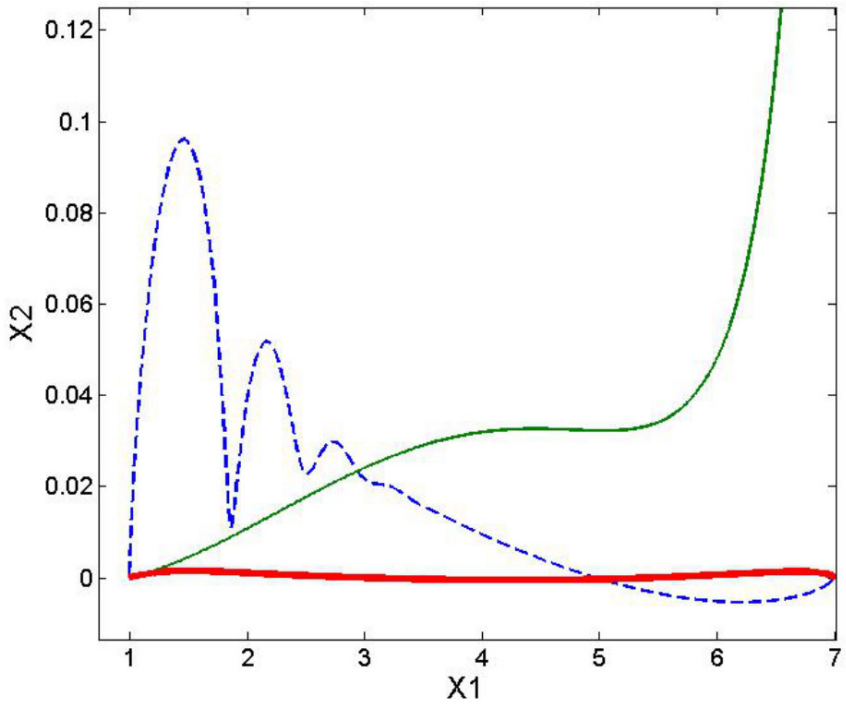

Figure 10: Trajectories between [1,0] and [7,0] where $\boldsymbol{M}_{JRM}$ equals $\left(\begin{smallmatrix}1 & 0\\ -1 & 0\end{smallmatrix}\right)$ (solid line), $\left(\begin{smallmatrix}1 & 0\\ 0 & 1\end{smallmatrix}\right)$ (dashed line) and $\left(\begin{smallmatrix}1 & 1\\ -1 & 1\end{smallmatrix}\right)$ (thick line). $\boldsymbol{K_p} = \left(\begin{smallmatrix}100 & 0\\ 0 & 100\end{smallmatrix}\right)$, $\boldsymbol{K_v} = \left(\begin{smallmatrix}150 & 0\\ 0 & 150\end{smallmatrix}\right)$, $k = 0$, link lengths = [4,4].

The dashed line in Fig. 10 demonstrates how errors caused by one joint are corrected by the other when $\boldsymbol{M}_{JRM}$ is set to the 2x2 identity matrix. In this case, the second joint reacts to the deviations caused by the first, but the speed of this correction is fundamentally limited by the response time of the joints (this can be seen in Fig. 11). In effect the problem of kinematic error has been replaced by one of temporal error; a failure of the joints to coordinate. The antidiagonal terms of the optimal $\boldsymbol{M}_{JRM}$ counteract this effect with a basic form of forward modeling: feedback of opposing sign is fed into the two joints, relying on their similar dynamic responses to create the similar movements. The deviations that must be corrected are thus rendered smaller and the instability associated with delay in the sensory-motor loop is reduced.

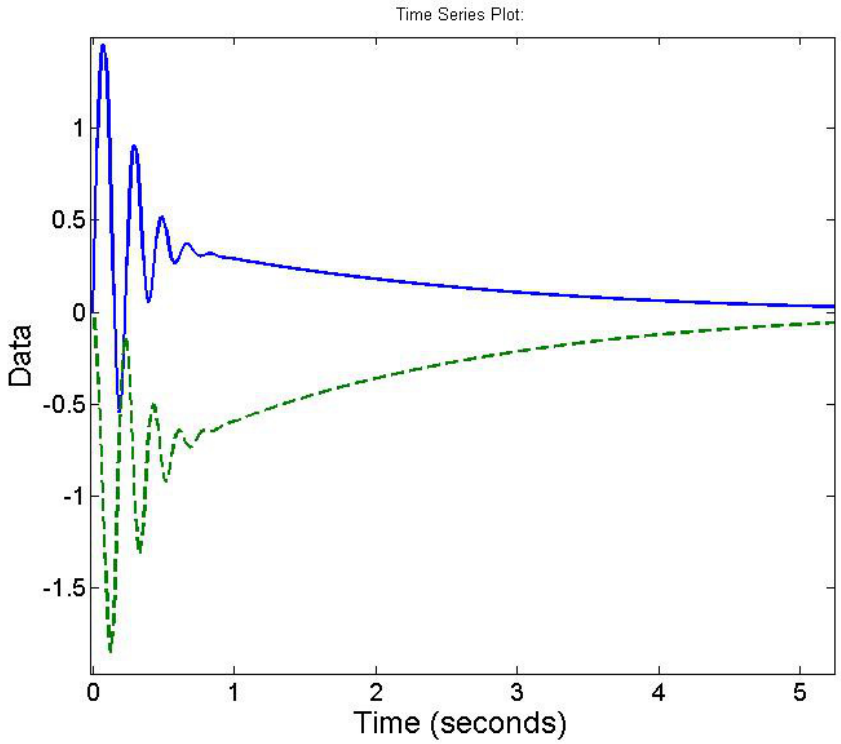

Figure 11: Velocities of joint q_1 (solid line) and q_2 (dashed line) where $\boldsymbol{M}_{JRM}$ equals $\left(\begin{smallmatrix} 1 & 0 \\ 0 & 1 \end{smallmatrix}\right)$

Energy Efficiency

The $\boldsymbol{M}_{JRM}$ matrix utilised in this control law operates by extending the arm, while simultaneously correcting any deviations from a straight line. We investigated whether this corrective method could execute a straight path while using relatively little energy, as opposed to if the torques were set directly by kinematic calculation. To that end this section measures the sum of squared torque (proportional to energy used for a DC motor) used by the $\boldsymbol{M}_{JRM}$ (set at $\left(\begin{smallmatrix} 1 & 1 \\ -1 & 1 \end{smallmatrix}\right)$) and the transpose of the arm Jacobian, when substituted into the control law (Eq. 1). Our paper does not distinguish between motor and braking torques because it is attempting to characterise an upper estimate in the absence of any mechanism for energy storage or restoration. It is intended to be a comparison between the velocity profiles produced by each control strategy, each of which requires the motors to exert a different amount of torque.

The Jacobian transpose is often used in closed loop control of robot manipulators as a means of transforming desired end effector forces into joint torques ($\boldsymbol{J}^T\boldsymbol{F} = \boldsymbol{\tau}$). The justification for this use is based on the relationship between end effector forces and joint torques defined by the virtual work principle:

$$\delta w = \boldsymbol{F}^T \delta \boldsymbol{x} - \boldsymbol{\tau}^T \delta \boldsymbol{q}, \tag{5}$$

Where δw is the change in the work performed by the arm, $\boldsymbol{F}$ is the vector of forces at the end effector, $\boldsymbol{\tau}$ is the vector of joint torques, $\delta \boldsymbol{x}$ is change in the Cartesian coordinates of the end effector and $\delta \boldsymbol{q}$ is the change in joint coordinates. This states that end effector forces can be directly transformed into joint torques where the arm is in equilibrium.

As can be seen in Fig. 12 and Fig. 13, respectively, the $\boldsymbol{M}_{JRM}$ method is considerably more efficient than the Jacobian transpose at simple point-to-point movements, but the difference is much less marked where the arm is tracking a moving equilibrium point. However, while the Jacobian transpose uses more energy to track at lower control gains, the energy used by the $\boldsymbol{M}_{JRM}$ method slightly decreases.

We postulate that this is because the Jacobian transpose's use as a transformation comes from the arm's statics, while the act of reaching requires the arm to perform work. This renders the direct relationship between forces

and torques invalid and leaves the Jacobian transpose as an inappropriate transformation so long as the arm is out of equilibrium. In contrast, our method's assumptions are not violated if the arm is in motion.

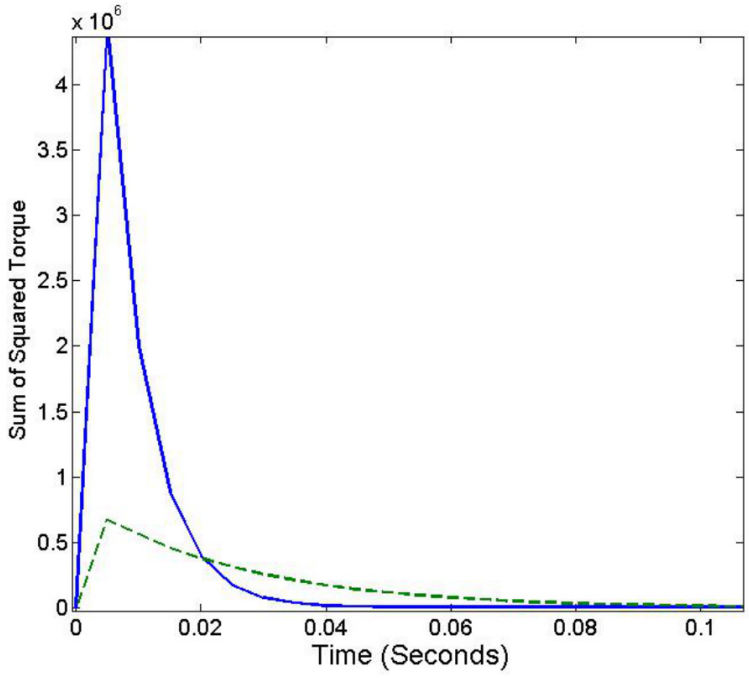

Figure 12: Comparison of torque applied during a point to point motion from [1,0] to [7,0] using the $\boldsymbol{M}_{JRM}$ $\left(\begin{smallmatrix} 1 & 1 \\ -1 & 1 \end{smallmatrix}\right)$ (dashed line) and the Jacobian transpose (solid line) as the transformation matrix.

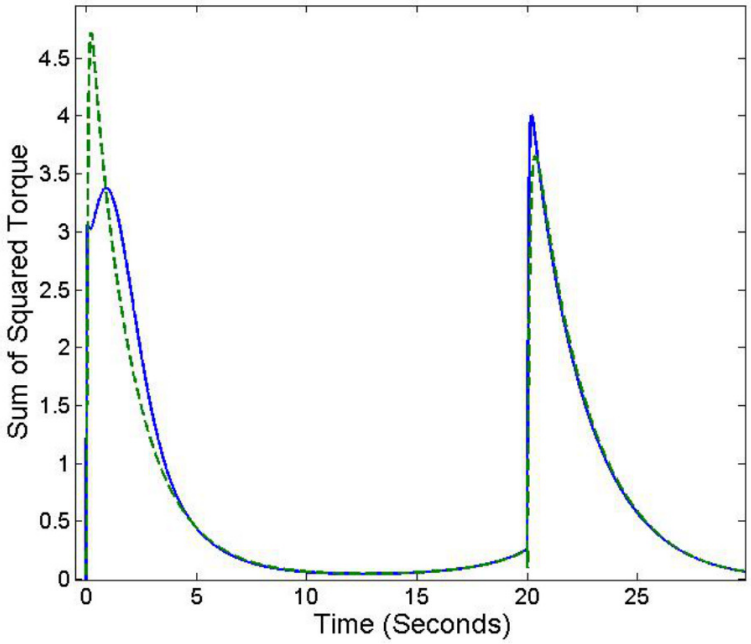

Figure 13: Comparison of torque applied tracking a point moving from [1,0] to [7,0] at a speed of 0.05 per second using the $\boldsymbol{M}_{JRM}\ \left(\begin{smallmatrix}1 & 1\\ -1 & 1\end{smallmatrix}\right)$ (dashed line) and the Jacobian transpose (solid line) as the transformation matrix.

Stability Analysis

Lyapunov's direct method was employed to prove the stability of the control law described by Eq. 1 when applied to a simulated robot arm with dynamics described by Eq. 19. Firstly, a Lyapunov candidate was defined:

$$V = \frac{1}{2}\dot{\boldsymbol{q}}^T \boldsymbol{R}\dot{\boldsymbol{q}} + \frac{1}{2}(\boldsymbol{x_d} - \boldsymbol{x})^T \boldsymbol{K_v}(\boldsymbol{x_d} - \boldsymbol{x}) - (\boldsymbol{x_d} - \boldsymbol{x})^T \boldsymbol{R}\boldsymbol{M}^{-1}\dot{\boldsymbol{q}} \tag{6}$$

In order to prove V is positive-definite, we rewrite the expression in matrix form:

$$V = \frac{1}{2}\boldsymbol{x}'^T A \boldsymbol{x}' \tag{7}$$

where:

$$\boldsymbol{x}' = \begin{bmatrix}\dot{\boldsymbol{x}}^T & (\boldsymbol{x_d} - \boldsymbol{x})^T\end{bmatrix}^T \tag{8}$$

and

$$\boldsymbol{A} = \begin{bmatrix} \boldsymbol{J}^{-T}\boldsymbol{R}\boldsymbol{J}^{-1} & -\boldsymbol{J}^{-T}\boldsymbol{R}\boldsymbol{M}^{-1} \\ -(\boldsymbol{J}^{-T}\boldsymbol{R}\boldsymbol{M}^{-1})^T & \boldsymbol{K_v} \end{bmatrix} \tag{9}$$

where $\boldsymbol{J}$ is the Jacobian $\boldsymbol{J} = \frac{\partial x}{\partial q}$. As $\boldsymbol{A}$ is a symmetric 2x2 block matrix; its Schur complement can be used to prove that it is positive definite. Thus $\boldsymbol{A} > 0$ (and thus $V > 0$) iff:

1. $\boldsymbol{K_v} > 0$

2. $\boldsymbol{J}^{-T}\boldsymbol{R}\boldsymbol{J}^{-1} - \boldsymbol{J}^{-T}\boldsymbol{R}\boldsymbol{M}^{-1}{\boldsymbol{K_v}}^{-1}\boldsymbol{M}^{-T}\boldsymbol{R}\boldsymbol{J}^{-1} > 0$

The first inequality is always true, as $\boldsymbol{K_v}$ is a positive diagonal matrix. Simplifying, and using the knowledge that $\boldsymbol{K_v} = k_v\boldsymbol{I}$, the second inequality becomes:

$$\boldsymbol{K_v} > \boldsymbol{M}^{-1}\boldsymbol{M}^{-T}\boldsymbol{R} \tag{10}$$

Thus, setting $\boldsymbol{K_v}$ to a sufficiently large positive value will ensure that V is positive definite.

Differentiating V with respect to time gives:

$$\dot{V} = \dot{\boldsymbol{q}}^T\boldsymbol{K_p}\boldsymbol{M}(\boldsymbol{x_d} - \boldsymbol{x}) - \dot{\boldsymbol{q}}^T\boldsymbol{K_v}\boldsymbol{M}\dot{\boldsymbol{x}} - \dot{\boldsymbol{q}}^T S\dot{\boldsymbol{q}} + \frac{1}{2}\dot{\boldsymbol{q}}^T\dot{\boldsymbol{R}}\dot{\boldsymbol{q}} - \dot{\boldsymbol{q}}^T\boldsymbol{J}^T\boldsymbol{K_v}(\boldsymbol{x_d} - \boldsymbol{x}) + \dot{\boldsymbol{q}}^T\boldsymbol{J}^T\boldsymbol{R}\boldsymbol{M}^{-1}\dot{\boldsymbol{q}} - (\boldsymbol{x} \tag{11}$$

$$- (\boldsymbol{x_d} - \boldsymbol{x})^T\boldsymbol{K_p}(\boldsymbol{x_d} - \boldsymbol{x}) + (\boldsymbol{x_d} - \boldsymbol{x})^T\boldsymbol{K_v}\dot{\boldsymbol{x}} + (\boldsymbol{x_d} - \boldsymbol{x})^T\boldsymbol{M}^{-1}\boldsymbol{S}\dot{\boldsymbol{q}}$$

Where $\boldsymbol{R}$ is the positive-definite, symmetric inertial matrix and $\boldsymbol{S}$ is a matrix of Coriolis forces. $\dot{\boldsymbol{R}} - 2\boldsymbol{S}$ is a skew-symmetric matrix, which means that:

$$\dot{\boldsymbol{q}}^T\boldsymbol{S}\dot{\boldsymbol{q}} + \frac{1}{2}\dot{\boldsymbol{q}}^T\dot{\boldsymbol{R}}\dot{\boldsymbol{q}} = 0 \tag{12}$$

and thus in matrix form:

$$\dot{V} = -\frac{1}{2}\boldsymbol{x'}^T\boldsymbol{B}\boldsymbol{x'} \tag{13}$$

where:

$$\boldsymbol{B} = \begin{bmatrix} c\boldsymbol{J}^{-T}(\boldsymbol{K_v}\boldsymbol{M}\boldsymbol{J} - \boldsymbol{J}^T\boldsymbol{R}\boldsymbol{M}^{-1})J^{-1} & \frac{1}{2}\boldsymbol{J}^{-T}(\dot{\boldsymbol{R}}\boldsymbol{M}^{-1} - \boldsymbol{M}^{-1}\boldsymbol{S} - \boldsymbol{K_p}\boldsymbol{M}) \\ \frac{1}{2}(\boldsymbol{J}^{-T}(\dot{\boldsymbol{R}}\boldsymbol{M}^{-1} - \boldsymbol{M}^{-1}\boldsymbol{S} - \boldsymbol{K_p}\boldsymbol{M}))^T & \boldsymbol{K_p} \end{bmatrix} \tag{14}$$

$\boldsymbol{B}$ is not a symmetric matrix, but the Schur complement of its Hermitian part can be calculated yielding $\dot{V}$ negative definite (and Eq. 1 asymptotically stable) iff:

1. $\boldsymbol{K_p} > 0$

2. $(\boldsymbol{K_v M J} + \boldsymbol{J}^T \boldsymbol{M}^T \boldsymbol{K_v}) > \boldsymbol{J}^T \boldsymbol{R} \boldsymbol{M}^{-1} + \boldsymbol{M}^{-T} \boldsymbol{R} \boldsymbol{J}^T + ((\dot{\boldsymbol{R}} \boldsymbol{M}^{-1} - \boldsymbol{M}^{-1} \boldsymbol{S} - \boldsymbol{K_p M}) \boldsymbol{J} + \boldsymbol{J}^T (\dot{\boldsymbol{R}} \boldsymbol{M}^{-1} - \boldsymbol{M}^{-1} \boldsymbol{S} - \boldsymbol{K_p M})) \boldsymbol{K_p}^{-1} ((\dot{\boldsymbol{R}} \boldsymbol{M}^{-1} - \boldsymbol{M}^{-1} \boldsymbol{S} - \boldsymbol{K_p M}) \boldsymbol{J} + \boldsymbol{J}^T (\dot{\boldsymbol{R}} \boldsymbol{M}^{-1} - \boldsymbol{M}^{-1} \boldsymbol{S} - \boldsymbol{K_p M}))^T$

The first inequality is true for all $\boldsymbol{K_p} > 0$ and thus applies to any diagonal gain matrix of the form $\boldsymbol{K_v} = k_v \boldsymbol{I}$. The second inequality holds if $(\boldsymbol{K_v M J} + \boldsymbol{J}^T \boldsymbol{M}^T \boldsymbol{K_v}) > 0$, both $\boldsymbol{K_v}$ and $\boldsymbol{K_p}$ are sufficiently large and $\boldsymbol{K_v}$ is sufficiently larger than $\boldsymbol{K_p}$. In particular, since $\boldsymbol{S}$ and $\dot{\boldsymbol{R}}$ are unbounded in $\dot{\boldsymbol{q}}$, the control gains set an effective constraint on the arm velocity, in that the gains must be large enough to counteract the Coriolis and other forces that act on the moving arm. Beyond the geometric constraints related to the end effector's location in the work space, these stability conditions are very similar to those of a traditional kinematics-based control law with a proportional-derivative control loop.

Discussion

This study demonstrates that the otherwise complex task of planning a straight path for an end effector can be solved without explicitly defining the path itself. This is achieved by exploiting the dynamic relationship between an open chain robot's components. The fact that the movement of any link affects all others further down the chain allows the implementation of a visual-motor loop that continuously corrects deviations from the desired path without relying on accurate kinematics, which are not available for all robotic systems.

A consequence of this is that not all standard means of comparison can be used in this case, as the tests rely on assumptions that are not applicable to our study. Tracking tests, for example, cannot be properly applied because the control is optimised for a cost function calculated over an unconstrained trajectory as no true reference trajectory exists, only a start point and target.

The simplicity of the $\boldsymbol{M}_{JRM}$ matrix and the wide area rendered stable by any given value also allow stable reaching motions to be achieved much more simply than in the classical robot model. The transformation matrix can easily be generalised over the entire work space by applying a rotational transformation. This transformed visual feedback can be linearly combined with conventional inverse-kinematics based error to add more reliability to the control, but if accurate encoder or visual sensors are available it is unlikely to be necessary.

Furthermore, the $\boldsymbol{M}_{JRM}$ method exerts less torque (and thus uses less energy) to move when in a non-equilibrium state than the Jacobian transpose. This could render it useful in situations where sufficient control gain to rigidly track a moving equilibrium point is not possible.

Because the $\boldsymbol{M}_{JRM}$ method has no assumptions about the kinematics beyond their basic geometry, there are few barriers to extending it to more complex robots. All this requires is that the elements of the $\boldsymbol{M}_{JRM}$ matrix must retain the same sign over the whole movement, which necessitates joint limits in a more complex redundant arm. Similarly, an extension to a three-dimensional workspace can be easily envisioned, although this would require two independent rotations of the matrix, and the area in which one rotation is valid would be smaller as a fraction of the total workspace.

In future work we hope to apply the same self-correcting behaviour to arbitrary motions within the work space, allowing true global stability to be achieved. The degree to which this method can be extended to systems with many degrees of freedom is a matter of continued investigation. There is preliminary evidence that redundant arms controlled using this method experience continual self-motion unless appropriate joint limits are imposed.

Methods

Numerical Simulation of a Planar Arm

The control scheme developed in this study was tested using a numerical simulation of a two-joint planar robot arm. This is the simplest form of an

arm capable of executing the 'reaching' motions the study aims to optimise. This reduced to a minimum the number of parameters that had to optimised while retaining the classical robot arm form.

Figure 2 shows the arm model used in this study, along with its primary attributes. The model's sensors can be thought of as accurate encoders at the joints and an undistorted camera overlooking the arm in a bird's-eye view to detect the end-effector position. The block diagram of the overall system can be seen in Fig. 1.

The model was implemented in Simulink, using a third-order ordinary differential equation solver with a constant step size of 0.005s. The primary components of the simulation are the arm's dynamics and the control law described by Eq. 1. Due to their relative complexity these are both implemented as custom MATLAB functions embedded in Simulink blocks. The control law block produces a time series of torque values that are input into the dynamics block to calculate the arm's joint acceleration over time. This is integrated twice and used to determine the arm's joint state. The position of the arm's end effector and joints is calculated using the forward kinematics of the arm and treated as the visual feedback.

The reaching target is simply modeled as a constant Cartesian coordinate vector.

Dynamics

The links of the arm are modeled as thin, uniform rods with the moment of inertia $j = ml^2/3$ (where m is the link mass and l is the link length) and their centre of mass halfway along their length. In the case we are modeling, the links have the same mass ($m_1 = m_2$) and equal length ($l_1 = l_2$). The arm is considered to be supported by a parallel plane, reducing the gravity term to 0. This restriction to a fixed plane replicates the constraints placed upon human subjects in many reaching experiments [8] [9] .

The dynamics of the simulation are derived by solving the Lagrange equation for a driven robotic system:

$$\frac{d}{dt}\left(\frac{\partial L}{\partial \dot{\boldsymbol{q}}}\right) - \frac{\partial L}{\partial \boldsymbol{q}} = \boldsymbol{\tau} \tag{15}$$

where $\boldsymbol{\tau}$ is the vector of joint torques, $\boldsymbol{q}$ is the vector of joint angles and $L = V - U$ where V and U are the kinetic and potential energy, respectively. Because no gravity is experienced by the arm, U is set to 0.

$$V = V_1 + V_2 \tag{16}$$

$$V_1 = \frac{1}{2} m_1 \dot{x}_{1,c1}^2 + \frac{1}{2} m_1 \dot{x}_{2,c1}^2 + \frac{1}{2} j_1 \dot{q}_1^2 \tag{17}$$

$$V_2 = \frac{1}{2} m_1 \dot{x}_{1,c2}^2 + \frac{1}{2} m_1 \dot{x}_{2,c2}^2 + \frac{1}{2} j_2 (\dot{q}_1^2 + \dot{q}_2^2) \tag{18}$$

Where $x_{1,cn}$ and $x_{2,cn}$ are the x_1 and x_2 coordinates of the nth joint's centre of mass, respectively.

Solving Eq.15 gives the final dynamics equation:

$$\ddot{\boldsymbol{q}} = \boldsymbol{R}(\boldsymbol{q})^{-1}(\boldsymbol{\tau} - \boldsymbol{S}(\boldsymbol{q}, \dot{\boldsymbol{q}})\dot{\boldsymbol{q}}) \tag{19}$$

with the inertial matrix:

$$\boldsymbol{R}(\boldsymbol{q}) = \begin{bmatrix} j_1 + j_2 + 2m_2 l_1 l_{c2} C_2 + m_2 l_1^2 + m_1 l_{c1}^2 + m_2 l_{c2}^2 & j_2 + m_2 l_1 l_{c2} C_2 + m_2 l_{c2}^2 \\ j_2 + m_2 l_1 l_{c2} C_2 + m_2 l_{c2}^2 & j_2 + m_2 l_{c2}^2 \end{bmatrix} \tag{20}$$

and a Coriolis force vector with the form below.

$$\boldsymbol{S}(\boldsymbol{q}, \dot{\boldsymbol{q}}) = \begin{bmatrix} -m_2 l_2 l_{c2} (2\dot{q}_1 + \dot{q}_2)\dot{q}_2 S_2 \\ m_2 l_1 l_{c2} \dot{q}_1^2 S_2 \end{bmatrix} \tag{21}$$

$C_n = \cos q_n$ and $S_n = \sin q_n$. Equation 19 is used to calculate the acceleration of the arm joints given the control torques. No friction is modelled at the joints (this is understood not to weaken the stability conditions for robotic control).

Simplex Optimisation

In order to optimise the transformation matrix M_{JRM} we used the widely-known simplex algorithm defined by Nelder and Mead [19] . Each element of the simplex is a value for the transformation matrix M in Eq. 1 (each with 4 elements, giving a 5-point simplex). The error for each matrix was acquired by substituting it into Eq. 1 and simulating a point-to-point movement of the robot in which all other parameters were fixed, before calculating the LI (defined in Eq. 2). By using this algorithm to continuously generate new matrices, it was possible to find the optimal value of M_{JRM} for a specific start/endpoint pair. Unlike the original formulation of the simplex algorithm, the algorithm used here does not include the 'contraction' step that reduces the simplex's deviation around the mean if the projected new value has a sufficiently high error. Not including this step improved the algorithms likelihood of finding a good solution in all the experiments performed.

The initial simplex to be optimised was generated by pseudo-randomly perturbing a 'seed' matrix. When performing individual 'runs' of experiments optimising for radial movements at a series of angles, this matrix was randomly chosen and kept constant throughout.

Because the end effector position is based on the angle of both joints, it was assumed that the components of $\boldsymbol{M}$ are inter-related, but without knowing this relationship, it was not possible to design a problem-specific algorithm. This limited the choice of algorithms to general optimisers. The simplex optimisation algorithm created by Nelder and Mead [19] was a good fit in that it is often used to optimise sets of variables with unclear relationships. Additionally, algorithms of this form do not require the derivative of the problem, which could not practically be found due to the sheer number of simulations that would be required.

References

[1] Hashimoto, K. A review on vision-based control of robot manipulators. *Advanced Robotics* **17**, 969–991 (2003).

[2] Shadmehr, R. *The computational neurobiology of reaching and pointing: a foundation for motor learning* (MIT press, 2005).

[3] Macfarlane, S. & Croft, E. A. Jerk-bounded manipulator trajectory planning: design for real-time applications. *Robotics and Automation, IEEE Transactions on* **19**, 42–52 (2003).

[4] Nakanishi, J., Cory, R., Mistry, M., Peters, J. & Schaal, S. Operational space control: A theoretical and empirical comparison. *The International Journal of Robotics Research* **27**, 737–757 (2008).

[5] Morasso, P. Spatial control of arm movements. *Experimental brain research* **42**, 223–227 (1981).

[6] Wolpert, D. M. & Ghahramani, Z. Computational principles of movement neuroscience. *nature neuroscience* **3**, 1212–1217 (2000).

[7] Feldman, A. G. & Latash, M. L. Testing hypotheses and the advancement of science: recent attempts to falsify the equilibrium point hypothesis. *Experimental Brain Research* **161**, 91–103 (2005).

[8] Wolpert, D. M., Ghahramani, Z. & Jordan, M. I. Perceptual distortion contributes to the curvature of human reaching movements. *Experimental brain research* **98**, 153–156 (1994).

[9] Flanagan, J. R. & Rao, A. K. Trajectory adaptation to a nonlinear visuomotor transformation: evidence of motion planning in visually perceived space. *Journal of neurophysiology* **74**, 2174–2178 (1995).

[10] Kawato, M., Furukawa, K. & Suzuki, R. A hierarchical neural-network model for control and learning of voluntary movement. *Biological cybernetics* **57**, 169–185 (1987).

[11] Wolpert, D. M., Miall, R. C. & Kawato, M. Internal models in the cerebellum. *Trends in cognitive sciences* **2**, 338–347 (1998).

[12] Wilson, W. J., Williams Hulls, C. & Bell, G. S. Relative end-effector control using cartesian position based visual servoing. *Robotics and Automation, IEEE Transactions on* **12**, 684–696 (1996).

[13] Corke, P. I. Visual control of robot manipulators-a review. *Visual servoing* **7**, 1–31 (1993).

[14] Nishida, R. & Kawamura, S. A new feedback robot control method based on position/image sensor integration. In *Intelligent Robots and Systems (IROS), 2012 IEEE/RSJ International Conference on*, 5012–5017 (IEEE, 2012).

[15] Mitsuda, T., Maru, N., Fujikawa, K. & Miyazaki, F. Binocular visual servoing based on linear time-invariant mapping. *Advanced robotics* **11**, 429–443 (1996).

[16] Giummarra, M. J., Gibson, S. J., Georgiou-Karistianis, N. & Bradshaw, J. L. Central mechanisms in phantom limb perception: the past, present and future. *Brain research reviews* **54**, 219–232 (2007).

[17] Holmes, N. P. & Spence, C. The body schema and multisensory representation (s) of peripersonal space. *Cognitive processing* **5**, 94–105 (2004).

[18] Desmurget, M., Jordan, M., Prablanc, C., Jeannerod, M. *et al.* Constrained and unconstrained movements involve different control strategies. *Journal of Neurophysiology* **77**, 1644–1650 (1997).

[19] Nelder, J. A. & Mead, R. A simplex method for function minimization. *Computer journal* **7**, 308–313 (1965).

Author contributions statement

H.E. developed/performed the simulations, and analysed the data. H.E., S.N., and Y.H. discussed the results, and all contributed to writing and editing the manuscript of the paper.

Acknowledgments

This research was in part made possible by a generous studentship from the University of Reading.

Additional information

The authors have no competing financial interests to declare.

Renormalized time scale for anticipating and lagging synchronization

Abstract

Anticipating synchronization has been recently proposed as a mechanism of interaction in dynamical systems which are able to bring about predictions of future states of a driver system. We suggest that an interesting insight into the anticipating synchronization can be obtained by the renormalization of the time scale in the driven system. Our approach directly links the feedback delay of the driven system with the renormalized time scale of the driven system, identifying the main component in the anticipating synchronization paradigm and suggesting an alternative method to generate the anticipating and the lagging synchronization.

1 Introduction

Synchronization of oscillations is abundant in nature from physical, chemical to biological systems [1, 2]. The synchronization of chaotic systems is a surprising phenomenon considering the exponential divergence of the trajectories, and chaotic synchronization as a new subfield of nonlinear systems has been increasingly investigated in the past two decades [3].

Anticipating synchronization has been recently proposed as a mechanism of interaction in dynamical systems able to bring about predictions of future states of a driver system by a driven system. A general framework was identified for anticipation by the driven system with delay [4]:

$$\dot{x}(t) = f[x(t)] \quad (1)$$

$$\dot{y}(t) = f[y(t)] + K[x(t) - y(t-\tau)], \quad (2)$$

where $f(\cdot)$ describes the internal dynamics of the state variables of both the driver system, x, and the driven system, y. Note here that the state variables can be extended to the multidimensional state variables. The second term in the driven system is a coupling term which drives it to be synchronized with the driver system. The term $y(t-\tau)$ takes into account the feedback delay in the driven system referring to its own state.

The anticipating synchronization is simply identified by the condition that manifold, $y(t) = x(t+\tau)$ be stable, hereafter, it will be called anticipating manifold. This implies that the driven system is anticipating the future state of the driver system.

This paradigm of anticipating synchronization in a uni-directional coupling configuration has been investigated in a variety of systems, chaotic lasers [5], autonomous chaotic systems [6], and excitable systems in the noisy environment [7, 8] numerically and experimentally. The paradigm was also extended to excitable systems in order to develop a control method to predict the driver's behavior, and to prevent the driver from firing [9]. Interestingly, it is the presence of a delay in the coupling that is a necessary condition to achieve the driven system's anticipation of the driver's dynamics. Pointing out the mechanism of the anticipating synchronization, the lowering of the excitability threshold of the slave in a delayed coupling scheme was shown to be a general mechanism for anticipating synchronization in excitable systems [8], and the linear stability analysis of the simple linear systems has been performed [10], and the effectiveness of the first order expansion was explored as a proof of concept [11].

In this paper, the paradigm of the anticipating synchronization is explored, leading to essential understanding of how the time delay gives rise to anticipating synchronization of the driven system, and we propose an alternative method of renormalized time step to generate the anticipating synchronization. The positive status of the delayed feedback is shown in a straightforward manner, i.e., the first order approximation of the coupling term of the driven system leads to the renormalization of time, amounting to speeding up the evolution of the driven system. On the other hand, the renormalization of time can also lead to the lagging synchronization by slowing down the evolution of the driven system. The chaotic system and the excitable systems were used to numerically validate the anticipating and lagging synchronization based on the renormalization of time.
Anticipating synchronization is still in many ways an unintuitive phenomenon. Although the final result is easily understood, the mechanism rarely is out-

side the field of dynamics. Possibly as a result of this, it is yet to be exploited in other fields where it could have useful applications, particularly in engineering. In addition to deepening our understanding of the phenomenon, it is hoped that reformulating anticipating synchronization in terms of renormalized time may make it more palatable to researchers in other areas of study.

2 Analytical solutions for one dimensional linear case

2.1 First order expansion of the time delay term

Consider a linear stability analysis for the anticipating manifold, taking a linear system, $f(x) = \alpha x$. First, we shift the time of the driver system by τ in Eq. (1). Subtracting Eq. (1) from Eq. (2), we have

$$\dot{z}(t) = \alpha z(t) - K z(t-\tau), \tag{3}$$

defining the transversal system, $z(t) = x(t+\tau) - y(t)$. As a next step, we expand the delay term, $z(t-\tau)$ in τ to the first order. After rearranging of the terms, the equation (3) becomes

$$\dot{z}(t) = -\frac{K-\alpha}{1-K\tau} z(t). \tag{4}$$

Equation (4) specifies two conditions for the presence of anticipating manifold as follows;

$$K > \alpha, \tag{5}$$

$$K\tau < 1. \tag{6}$$

These two conditions also indicate that the anticipatory horizon, the maximum τ value in the τ-K plane should be given by the intersection of $K\tau = 1$ and $K = \alpha$.

On the other hand, when $\tau < 0$, Equation (4) specifies one condition for the presence of anticipating manifold as follows;

$$K > \alpha \tag{7}$$

2.2 Solution for the delay differential equation

The stability conditions for the linear systems with the delay term can be obtained by calculating complex Lyapunov exponent. Extending the state variable to the complex plane, the stability conditions for the anticipating manifold can be calculated for the explicit time delay. In contrast to the section II A. where the solution for the driver dynamics is given by $x = Ae^{\alpha t}$, the solution should be given by $x = Ae^{(\alpha+i\omega)t}$. Thus, the driver dynamics follows $\dot{x}(t) = (\alpha + i\omega)x(t)$. The corresponding driven dynamics is given by $\dot{y}(t) = (\alpha + iw)y(t) + Ke^{i\beta}[x(t) - y(t-\tau)]$ where the coupling constant is also given by the complex number, $Ke^{i\beta}$. The transversal system, $z(t) = x(t+\tau) - y(t)$ evolves as

$$\dot{z}(t) = (\alpha + iw)z(t) - Ke^{i\beta}z(t-\tau). \tag{8}$$

The solution of the Eq.(8) should be given by $z(t) = Be^{(\lambda+i\omega)t}$ where λ is a Lyapunov exponent. By substituting the solution into Eq.(8), we have

$$\lambda = \alpha - Ke^{i(\beta-\omega\tau)}e^{-\lambda\tau}. \tag{9}$$

Here, let β compensate the time delay, τ on the imaginary axis by setting $\beta = \omega\tau$ [6]. The equation (9) can be rewritten as

$$\lambda = \alpha + \frac{1}{\tau}W(-\tau Ke^{-\alpha\tau}) \tag{10}$$

where $W(x)$ is the Lambert W function, $x = W(x)e^{W(x)}$. As a multivalued function, $W(x)$ has two values in the region $-1/e < x < 0$. For $\lambda = 0$, $-\alpha\tau = W(-\tau Ke^{-\alpha\tau})$ should have solution for $W_0(x)$. This condition imposes $-\alpha\tau = W(-1/e)(= -1)$ which is the extreme value of $W(x)$ function. Thus, the maximum τ is determined by $\tau > -1/\alpha$, and $K = \alpha$ is obtained from $x = -1/e$. The anticipation horizon coincides with the one based on the first order expansion (Fig. 1).

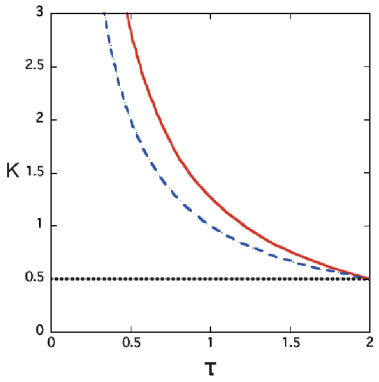

Figure 1: Stability diagram of the anticipating synchronization for the linear system. The solid line represents the case when the delay term, $y(t-\tau)$ is treated exactly. The dashed line represents the case when $y(t-\tau)$ is expanded to the first order. The dotted line $K = \alpha$ represents the stability boundary for both cases ($\alpha = 0.5$). The stability regions are determined by the area surrounded by the solid line and dotted lines for the non-expansion case and by the dashed and doted lines for the case of the first order expansion.

The stability conditions for Lyapunov exponent, $\lambda < 0$ determines the stability region in $\tau - K$ plane for a given α. The solution of Eq. (10) when $\lambda = 0$ gives the necessary condition for stability to be $\alpha < K$. For the condition when $Re(\lambda) = 0$, substituting $\lambda = i\theta \quad (\theta \in [0, \infty])$ into Eq. (10) leads to $K = (\alpha^2 + \lambda^2)^{1/2}$ and $\tau = \tan^{-1}(\theta/\alpha)/\theta$. The stability region of the system is then determined by the region shown in Fig. 1. Note here that the τ can only give the positive value as a function of θ. Thus, there is no analytical solution for the region $\tau < 0$, confirming that Equation (2) cannot refer to the future state of itself.

In contrast to the statement that $x(t+\tau) - y(t)$ is a fixed point of this system for any time delay τ (the anticipation horizon) [4], the maximum τ value is given by the intersection of two functions, namely, $K\tau = 1$ and $K = \alpha$. This is the same as in the case of stability analysis for the first order expansion, even though the stable area is larger for the driven system on the time delay term.

Thus, from the above analysis, it follows that even explicit account of the feedback delay does not increase the anticipatory horizon compared to the one obtained from the first order expansion. The analytical calculations in this section are restricted to the one dimensional and linear case. We will

validate the outcome of the first order expansion of the time delay term by numerical calculations in the following sections.

3 Renormalization of time

Let us further consider the outcome of the first order expansion of the time delay term. The expansion of $z(t-\tau)$ up to the first order is equivalent to the expansion of $y(t-\tau)$ in Eq. (2) to the first order, which gives

$$\frac{dy(t)}{dt^*} = f[y(t)] + k[x(t) - y(t)] \tag{11}$$

where $t^* = t/(1-k\tau)$ is a renormalized time in the driven system. From $K > 0$ and $\tau > 0$ and from Eq. (6), we can obtain $0 < 1 - K\tau < 1$, which leads to $t < t^*$. For the case of $\tau < 0$, we have $1 - k\tau > 1$, which leads to $t^* < t$. This outcome suggests that the time scale of the driven system should be larger or smaller than that of the driver system, depending on the sign of τ. Thus, with respect to the first order expansion, the time delay in the coupling term in Eq. (2) can be equivalently replaced by the renormalized time in the driven system.

4 Numerical calculations for multidimensional and nonlinear cases

4.1 Rössler chaotic system

Even though the analytical characterization was obtained only for the one dimensional linear dynamics, the anticipating synchronization based on the renormalized time should be applied to more complex hyperbolic systems. As a test model, we numerically examine the coupled dynamics of a driver and driven system using a Rössler chaotic system. The chaotic oscillator model for the driver system is given,

$$\frac{dx_1}{dt} = -x_2 - x_3 \tag{12}$$

$$\frac{dx_2}{dt} = x_1 - ax_2, \tag{13}$$

$$\frac{dx_3}{dt} = b - x_3(x_2 - c), \tag{14}$$

where x_1, x_2 and x_3 are state variables. For the driven system based on Eq. (11), we have similarly,

$$\frac{dy_1}{dt^*} = -y_2 - y_3 + K(x_1 - y_1) \quad (15)$$

$$\frac{dy_2}{dt^*} = y_1 - ay_2, \quad (16)$$

$$\frac{dy_3}{dt^*} = b - y_3(y_2 - c), \quad (17)$$

where y_1, y_2 and y_3 are state variables of the driven system and $K(x_1 - y_1)$ represents a coupling between the driver and driven systems. Note that the driven system incorporates the renormalized time scale, $t^* = t/(1 - k\tau)$ in the time derivative.

Figure 2 shows the numerical results of the Rössler chaotic system when $\tau = 0.4$. It is interesting to note that the driven system on the renormalized time scale can show the precedence of phase, even though its amplitude differs more from that of the driver system. Also, shifting the renormalized time for the condition, $t^* < t$ when $\tau = -0.4$, the driven system showed the lagging synchronization (Fig. 2). With respect to the first order approximation, we found that the reference to its own future state in the feedback loop actually lead to the delay in response to the driver system. It is intriguing, the the lagging synchronization cannot be achieved by the explicit term in Eq. (2).

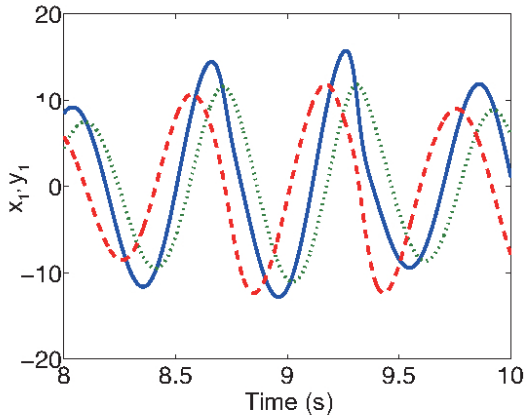

Figure 2: Time series of Rössler chaotic system, $x_1(t)$ and $y_1(t)$. The solid line represents the driver system with the time step, $\triangle t_{step} = 0.0005$, the dashed line represents the driven system on the renormalized time step, corresponding to $\tau = 0.4$, and the dotted line represents the driven system on the renormalized time step, corresponding to $\tau = -0.4$. The values for parameters were $a = 0.15, b = 0.20, c = 10.0, K = 1.0$.

Figure 3 shows the stability diagram of the cross-correlation coefficient with respect to the driver system. The maximum values of the cross-correlation coefficients in the cross-correlation functions were calculated, and the individual values were plotted in τ-K plane. Stability is determined experimentally using the cross-correlation coefficient - as the anticipation manifold becomes unstable there is an abrupt transition from high (close to 1) to very low correlation coefficient. This manifests as a highly visible discontinuity in the figures. In the case of the renormalised timescale, the cross-correlation is undefined for an unstable manifold and the region is left blank as a result.

For the region $\tau < 0.4$ in Fig. 3 (b), the cross-correlation coefficients are close to 1, therefore, there is a good agreement between the driver and driven systems in terms of the amplitudes of the curve profiles. However, the cross-correlation coefficients with respect to the driver system decrease gradually as τ increases more than 0.4 and the area of the good agreement in terms of the amplitude of the curve profile is smaller than the one calculated from the original case of the delay differential equation (Fig. 3 (a)).

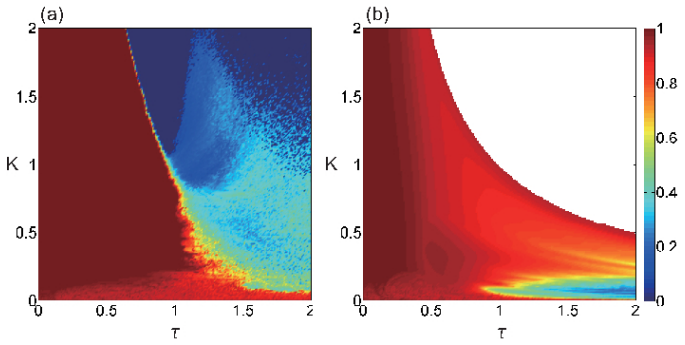

Figure 3: Stability diagram of the cross-correlation coefficient with respect to the driver system (Rössler system). The maximum values of the coefficient in the cross-correlation functions were plotted in τ-K plane. The driven systems were based on (a) time delay term (b) renormalized time step. The values of parameters were $a = 0.15, b = 0.20, c = 10.0$.

Figure 4 shows the stability diagram of the time shift of the driven system, $\triangle t$ with respect to the driver system. The time shift is defined by the time lag in the cross-correlation functions at which the maximum values of the coefficient are to be found. Ideally, the anticipating manifold should be fulfilled as $\triangle t = \tau$ where τ is a self-feedback delay of the driven system.

However, the driven system based on the renormalized time step shows the larger time shift, $\triangle t > \tau$ for the region of $\tau > 0.4$. In this region of $\tau > 0.4$, even though the deviation from the driver system becomes larger in terms of amplitude correlation of the functions (Fig. 3), we found the the tendency of the driven system for larger precedence of the driver in the case of the renormalized time step compared to the driven system with the time delay (Fig. 4 (b)). Additionally, in the renormalized case, anticipation is highest at the stability boundary $K\tau = 1$, as this maximizes $t^* = t/(1 - k\tau)$. The anticipation period in the delay coupled case is dependent only on the delay τ, above a minimum value of K (see the area below $K = 0.1$ in Fig. 4), and thus doesn't exhibit this effect.

Note here that the stability diagram obtained by the one dimensional case (Fig. 1) showed a qualitative agreement with the stability diagram of the chaotic system (Fig. 3 and Fig. 4).

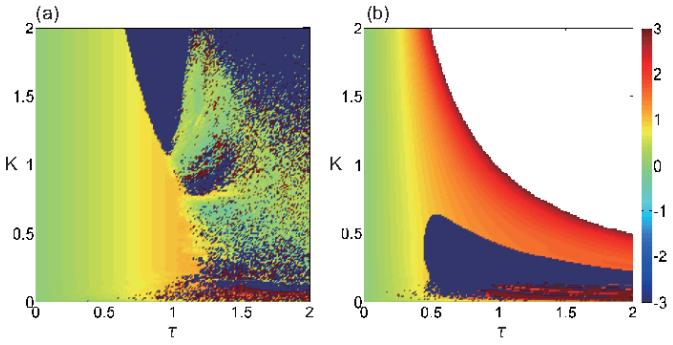

Figure 4: Stability diagram of the time shift with respect to the driver system (Rössler system), which gives the maximum value of the coefficient in the cross-correlation functions. The driven systems were based on (a) Time delay term (b) Renormalized time step. The values of parameters were $a = 0.15, b = 0.20, c = 10.0$.

Figure 5 shows the stability diagram of the lagging synchronization with the positive τ region. We found that stability region for the negative τ is consistent with the stability regions derived for the linear case ($K > \alpha$), and also the smooth transition was found from the lagging to anticipating synchronization as τ increases from the negative to positive value.

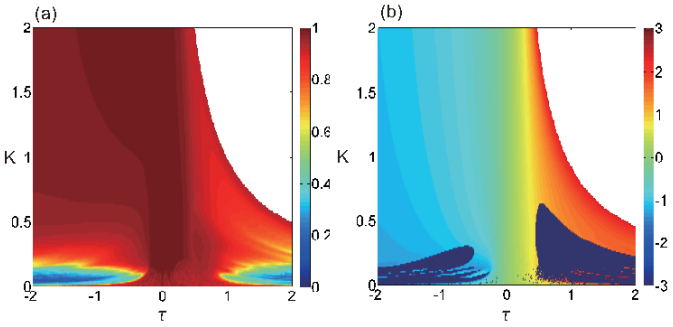

Figure 5: Stability diagram of the lagging synchronization with respect to the driver system (Rössler system). The driven systems were based on the renormalized time step. (a) Stability diagram of the maximum cross-correlation coefficient. (b) Stability diagram of the time shift. The values of parameters were $a = 0.15, b = 0.20, c = 10.0$.

4.2 Excitable systems

4.2.1 Adler system

As a next step, we numerically validate that the renormalization of the time step can also work for an excitable system. Adler system is used to study the excitable behavior responding to the same external forcing of the driver and driven system. We consider two identical Adler's systems in unidirectional coupling under the simultaneous external perturbation $I(t)$ on both systems,

$$\frac{dx}{dt} = \mu - \cos x + I(t) \tag{18}$$

$$\frac{dy}{dt^*} = \mu - \cos y + I(t) + K(x - y) \tag{19}$$

where state variable x (driver system) and y (driven system) are angular variables, μ is the bifurcation parameter. When $|\mu| > 0$, the system exhibits the excitable behavior. For the driven system, the time scale is renormalized as $t^* = t/(1 - K\tau)$.

The excitable systems possess a single stable rest state, corresponding to a fixed point. The small perturbation of the system, for example, the environmental noise pushes the state variable out of the fixed point, and the large excursions of the state variables follow, which are called spikes. Since many biological systems, e.g., neurons, are essentially the excitable systems with a few feedback pathways, it is important to consider the excitable system triggered by the random noise to test our hypothesis of the renormalized time. Figure 6 shows that the renormalization of the time step can work in good agreement in terms of amplitude with the driver system for the anticipating synchronization as well as the lagging synchronization.

The driven system based on the renormalized time step showed a wide range of maximum amplitude correlation values with the driven system (Fig.7 (b)), and the degrees of the correlation were almost identical with to those of the driven system based on the time delay feedback (Fig. 7 (a)).

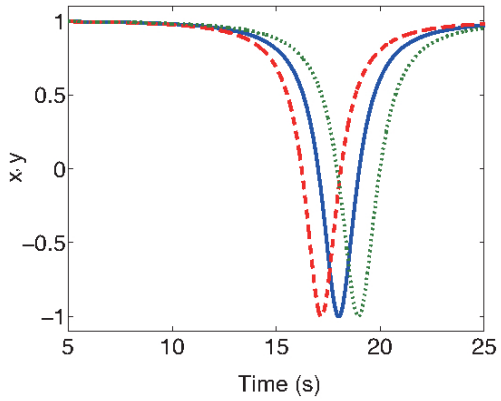

Figure 6: Time series of Adler system, $x(t)$ and $y(t)$. The solid line represents the driver system with the time step, $\triangle t_{step} = 0.0005$, the dashed line represents the driven system on the renormalized time step, corresponding to $\tau = 5.0$, and the dotted line represents the driven system on the renormalized time step, corresponding to $\tau = -5.0$. The values of parameters were $\mu = 0.95, K = 0.01$.

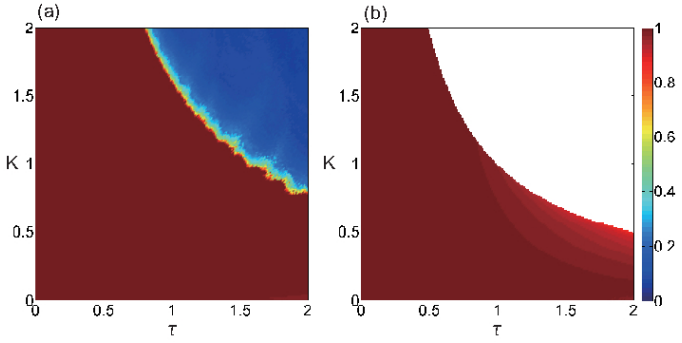

Figure 7: Stability diagram of the cross-correlation coefficient with respect to the driver system (Adler system). The maximum values of the coefficient in the cross-correlation functions were calculated in τ-K plane. The driven systems were based on (a) Time delay term (b) Renormalized time step. The value of parameter was $\mu = 0.95$.

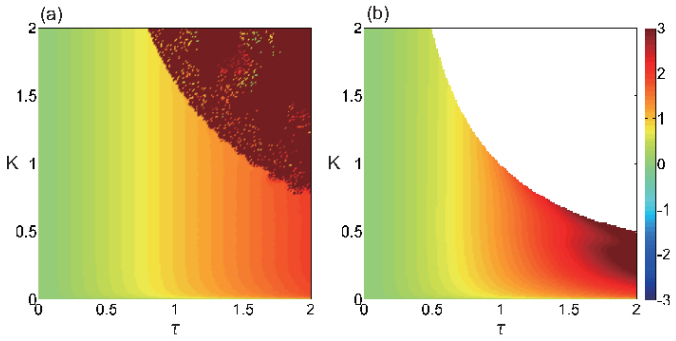

Figure 8: Stability diagram of the time shift with respect to the driver system (Adler system), which gives the maximum value of the coefficient in the cross-correlation functions. The driven systems were based on (a) Time delay term (b) Renormalized time step. The value of parameter was $\mu = 0.95$.

Figure 8 shows the stability diagram of the time shift of the driven system, $\triangle t$ with respect to the driver system. The anticipating manifold should be fulfilled, $\triangle t = \tau$. In the excitable system, the driven system based on the renormalized time step showed the wider stable region fulfilling the anticipating manifold, compared to the chaotic system (Fig. 3 and Fig. 4). Note here that when $\tau > 1.5$, the stronger tendency of the time shift was found towards the future state of the driver system, $\triangle t > \tau$.

It is straightforward to understand that the larger time step leads to the higher frequency of the angular state variable. Since the state variable of excitable system, once perturbed to be out of the fixed point, travels the orbit which follows the connection of the saddle and the node. The amplitude of the state variable is well preserved as the state variable travels the orbit. According to the study by Cizak et. Al., the coupling term in the driven system (Eq. (2)) gives rise to the effective μ_{eff} ($\mu_{eff} > \mu$) [8], They explained the dynamical mechanism of anticipating synchronization based on the fact that μ_{eff} decreases the response time from the onset of perturbation to the time at which the pulse reaches its maximum amplitude. Regarding the first order expansion, substituting $y(t-\tau)$ by $y(t) - \frac{dy}{dt}\tau$ in the coupling term would also lead to the increase of μ_{eff} on the onset of perturbation, resulting into the decrease in the response time. Thus, for this Adler system, two explanation, namely, the faster evolution and the effect of μ_{eff} on the decrease in the response time would be plausible.

Figure 9 shows the stability diagram of the lagging synchronization with

the positive τ region. We found that the degrees of the correlation were close to one with those of the driver system (Fig. 9 (a)) and that the gradual time shift for the lagging synchronization was also found in the negative τ region (Fig. 9 (b)).

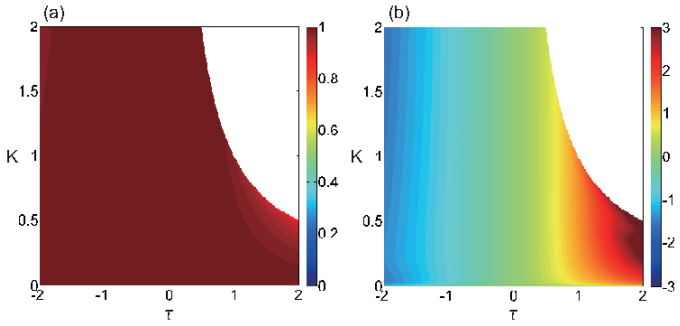

Figure 9: Stability diagram of the lagging synchronization with respect to the driver system (Adler system). The driven systems were based on the renormalized time step. (a) Stability diagram of the maximum cross-correlation coefficient. (b) Stability diagram of the time shift. The values of parameters were $a = 0.15, b = 0.2, c = 10.0$.

4.2.2 FitzHugh-Nagumo system

The FitzHugh-Nagumo system is another example of a excitable oscillator, a simplified version of the Hodgkin-Huxley model which models activation and deactivation dynamics of a spiking neuron. This behavior is typical for spike generations in a neuron after stimulation by an external input current. The equations for this dynamical system are given by

$$\frac{dv_1}{dt} = v_1 - \frac{1}{3}v_1^3 + I(t) \tag{20}$$

$$\frac{dw_1}{dt} = \epsilon(v_1 + a - bw_1) \tag{21}$$

where v_1 is a membrane voltage, and w_1 is a linear recovery variable. When the external stimulus exceeds a certain threshold value, the system will be kicked out from the fixed point, and exhibit a characteristic excursion in phase space. On the other hand, the driven system based on the renormalized time, t^* is described by

$$\frac{dv_2}{dt^*} = v_2 - \frac{1}{3}v_2^3 + I(t) + K(v_1 - v_2) \tag{22}$$

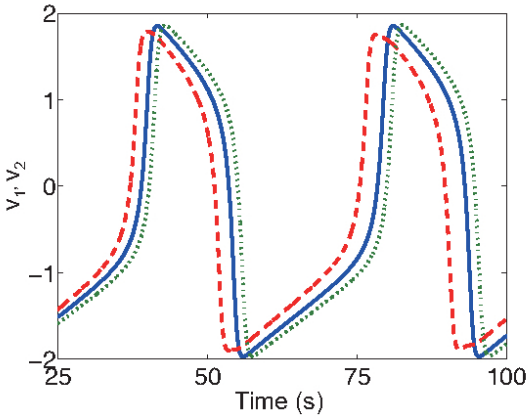

Figure 10: Time series of FitzHugh-Nagumo system, v_1 and v_2. The solid line represents the driver system with the time step, $\triangle t_{step} = 0.0005$, the dashed line represents the driven system on the renormalized time step, corresponding to $\tau = 0.75$, and the dotted line represents the driven system on the renormalized time step, corresponding to $\tau = -0.75$. The values of parameters were $\epsilon = 0.08, a = 0.70, b = 0.80, K = 0.10$.

$$\frac{dw_2}{dt^*} = \epsilon(v_2 + a - bw_2). \tag{23}$$

Figure 10 shows the numerical results of the FitzHugh-Nagumo system for $\tau = \pm 0.75$. We observe the steady phase shift for the anticipating and the lagging synchronization for the continuous firing. Figure 11 shows the stability diagram of the cross-correlation coefficient with respect to the driver system. When $\tau > 1.0$, the driven system starts to deteriorate from dynamics of the driver system. Regarding the stability diagram of the time shift of the driven system (Fig. 12), we found the stronger drive of $\triangle t$ in the region defined by $K < 0.2$ and $\tau > 0.5$ with respect to the driver system.

Figure 13 shows the stability diagram of the lagging synchronization. We found that the driven system on the renormalized time scale shows a good agreement with the driven system in terms of amplitude (Fig. 13 (a)) as well as the steady lagging shift (Fig. 13 (b)).

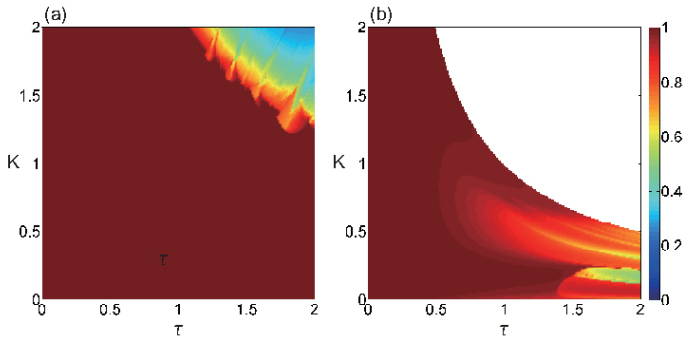

Figure 11: Stability diagram of the cross-correlation coefficient with respect to the driver system (FitzHugh-Nagumo system). The maximum values of the coefficient in the cross-correlation functions were calculated in τ-K plane. The driven systems were based on (a) Time delay term (b) Renormalized time step. The values of parameters were $\epsilon = 0.08, a = 0.70, b = 0.80$.

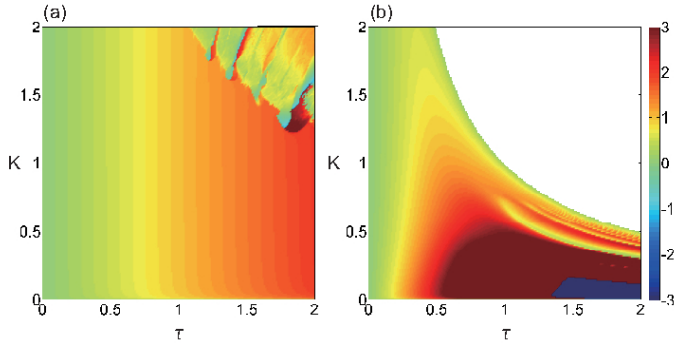

Figure 12: Stability diagram of the time shift with respect to the driver system (FitzHugh-Nagumo system), which gives the maximum value of the coefficient in the cross-correlation functions. The driven systems were based on (a) Time delay term (b) Renormalized time step. The values of parameters were $\epsilon = 0.08, a = 0.70, b = 0.80$.

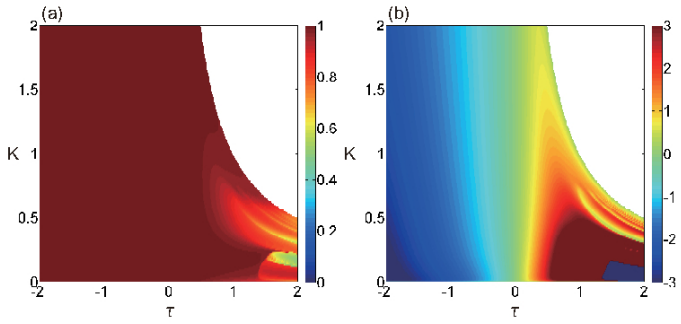

Figure 13: Stability diagram of the lagging synchronization with respect to the driver system (FitzHugh-Nagumo system). The driven systems were based on the renormalized time step. (a) Stability diagram of the maximum cross-correlation coefficient. (b) Stability diagram of the time shift. The values of parameters were $\epsilon = 0.08, a = 0.70, b = 0.80$.

5 General discussion

Our approach directly links the feedback delay of the driven system with the renormalized time scale of the driven system (Section III), identifying the main component in the anticipating synchronization paradigm, and suggesting an alternative method to generate the anticipating synchronization as well as lagging synchronization.

The following points summarize the method of renormalized time step, extending the paradigm of anticipating synchronization;

1. Larger time scale amounts to the faster evolution of the state variable of the driven system based on the internal dynamics.

2. Smaller time scale amounts to the slower evolution of the state variable of the driven system based on the internal dynamics.

3. Coupling term drives the state variable of the driven systems to be synchronized with the one of the driver system.

4. Interplay between internal dynamics and coupling term gives rise to the steady the anticipating or lagging synchronization of the driven system.

In this study, we proved the ability of anticipating synchronization based on the renormalized time steps in the one dimensional linear case, and systematically validated the outcomes of the renormalized time steps for the case of multidimensional nonlinear dynamics by the numerical calculations. The stability diagram showed that tuning of τ can induce the anticipating synchronization for $\tau > 0$ and the lagging synchronization for $\tau < 0$. It is intriguing that the lagging synchronization is only possible in the case of the renormalized time steps.

From the numerically obtained stability diagrams, the renormalized time scale of the driven system was proven to be the alternative method to induce the anticipating synchronization when the time delay term is not available to the driven system. Our results have an important implication that the different time scales of the dynamical systems can be considered as different clocks governing their temporal evolution of the dynamical systems, i.e., depending on the sign of τ, the time evolution of the driven system can be anticipating or lagging with respect to the driver system. When the dynamical systems running based on the different clocks interact uni-directionally, the anticipating synchronization can appear without any time delays. Therefore, our approach will further expand this interesting paradigm towards a wider range of dynamical scenarios.

In behavioural sciences, the feedforward model or the internal predictive model is motivated by the assumption that the feedback delays destabilize the controlled objects. Internal models have been a wide spread concept to explain the human motion overcoming the time-delay in the sensory-motor systems [12]. Kawato concluded that forward internal models can predict sensory consequences from efference copies of issued motor commands and that inverse internal models can calculate necessary feedforward motor commands from desired trajectory information. However, this approach ignores the dynamics of motion, and can be considered as the mapping between the positions in work space and the sequence of motor commands in a static manner.

On contrary to the internal model, Stepp performed tracking experiments in which the participants were given delayed visual feedback of their own movements, and found some characteristics of anticipating synchronization [13]. Even though his finding is at the empirical level, the attempt to emphasize the dynamical coupling with the changing environment should be appreciated to make a link between human behavior and dynamical systems [14, 15]. Also, in the interpersonal interactions, Hayashi and Kondo found

that humans follow the feedback control to tune the cycle time based on the synchronization errors, and that the gain parameters changes as a function of tapping frequency [16]. From the perspective of renormalization of time, we found that the tuning of the gain parameters can be attributed to the internal time scale to detect the cycle time of tapping motion. Therefore, the internal time scale functioning flexibly to anticipate the changing environment or lag behind it could be a fundamental mechanisms of the living systems for which 'orienting towards the future' is a crucial nature [17].

Using a biologically plausible neuronal model, Matias et. Al. showed that master-slave configuration with the inhibitory neuron can induce anticipating synchronization without the explicit time delay, rather, it was simply triggered by biological plausible delay of the inhibitory neuron to regulate the slave neuron [18]. Recently, identifying the neuronal populations in the cortical regions, the anticipating synchronization was presented as a plausible model for the observed phase shifts in a certain primate cortical circuit under a visual task [19]. This kind of studies can be also explored in terms of the different time scales involved in the individual dynamical systems.

The presence of any feedback delay is regarded as an unfortunate feature of biological and robotic systems. However, as shown in this paper, the positive, productive status of the delayed feedback should be emphasized in terms of the 'internal clock' of the biological systems, as it may have very important implications for our understanding of how neuronal and cognitive systems can predict future outcomes of the changing environment during many crucial tasks from neuronal systems to sensory-motor systems of humans [13, 15, 8, 20, 21].

References

[1] Y. Kuramoto, *Chemical Oscillations, Waves, and Turbulence* (Dover Publications, New York, United States, 2003).

[2] A. Pikovsky, M. Rosenblum and J. Kurths, *Synchronization: A universal concept in nonlinear sciences* (Cambridge University Press, Cambridge, England, 2001).

[3] L. M. Pecora and T. L. Carroll, Phys. Rev. Lett. **64**, 821 (1990).

[4] H. U. Voss, Phys. Rev. E, **61**, 5115 (2000).

[5] C. Masoller, Phys. Rev. Lett. **86**, 2782 (2001).

[6] K. Pyragas and T. Pyragiene, Phys. Rev. E **78**, 046217 (2008).

[7] M. Ciszak, O. Calvo, C. Masoller, C. Mirasso, and R. Toral, Phys. Rev. Lett. **90**, 204102 (2003).

[8] M. Ciszak, F. Marino, R. Toral, and S. Balle, Phys. Rev. Lett. **93**, 114102 (2004).

[9] M. Ciszak, C. R. Mirasso, R. Toral, and O. Calvo, Phys. Rev. E **79**, 046203 (2009).

[10] O. Calvo, D. R. Chialvo, V. M. Eguiluz, C. Mirasso, and R. Toral, Chaos, **14**, 7 (2004).

[11] N. Corron, J. N. Blakely, and S. D. Pethel, Chaos, **15**, 023110 (2005).

[12] M. Kawato, Current Opinion in Neurobiology, **9**, 718 (1999).

[13] N. Stepp, Experimental Brain Research, **198**, 521 (2009).

[14] N. Stepp and M. T. Turvey, Cogn. Syst. Res. **11**-2, 148 (2010).

[15] Y. Hayashi, J. Blake, and S. Nasuto, *Anticipation Across Disciplines, M. Nadin (Ed)* (Springer, New York, United States, 2015).

[16] Y. Hayashi and T. Kondo, Physical Review E, **88**-2, 022715 (2013).

[17] R. Rosen, *Anticipatory Systems: Philosophical, Mathematical, and Methodological Foundations* (Springer, New York, United States, 2012).

[18] F. S. Matias, P. V. Carelli, C. R. Mirasso, and M. Copelli, Physical Review E **84**, 021922 (2011).

[19] F. S. Matias, L. L. Gollo, P. Carelli, S. Bressler, M. Copelli M, C. R. Mirasso, Neuroimage, **99**, 411 (2014).

[20] Y. Hayashi and Y. Sawada, Phys. Rev. E, **88**, 022704 (2013).

[21] S. Nasuto, S. and Y. Hayashi, *Anticipation Across Disciplines, M. Nadin (Ed)* (Springer, New York, United States, 2015).

Anticipation from Sensation: Using Anticipating Synchronisation to Stabilise a System with Inherent Sensory Delay

Abstract

We present a novel way of using a dynamical model for predictive tracking control that can adapt to a wide range of delays without parameter update. This is achieved by incorporating the paradigm of anticipating synchronisation (AS), where a 'slave' system predicts a 'master' via delayed self-feedback. By treating the delayed output of the plant as one half of a 'sensory' AS coupling, the plant and an internal dynamical model can be synchronised such that the plant consistently leads the target's motion. We use two simulated robotic systems with differing arrangements of the plant and internal model ('parallel' and 'serial') to demonstrate that this form of control adapts to a wide range of delays without requiring the parameters of the controller to be changed.

1 Introduction

Closed-loop control is ubiquitous precisely because it is so useful - negative feedback allows a system to remain stable in the face of disturbance and continue functioning even in a changing environment. It is no surprise, then, that negative feedback loops are found so often in living organisms, which must cope with uncertain environmental conditions - the very concept of homeostasis is predicated upon them. However, some processes such as motor control are difficult to explain: closed-loop control is highly sensitive to feedback delay, and delays in the nervous system would not seem to support

the quick movements that animals like humans make routinely. Some theorists argue that this can be reconciled through 'strong anticipation' [1], where a continuous coupling between the controlling process within the nervous system and the body itself allows otherwise delayed feedback to be predicted. This suggests a useful paradigm for the control of artificial systems as well, but practical examples of how a strongly anticipating system could be constructed are lacking. We have designed a framework for using the paradigm of anticipating synchronisation (AS) to enable closed-loop control in the presence of uncertain or variable delays that we call the 'sensory coupling', which we believe displays the hallmarks of strong anticipation, and applied it to a classic control task of tracking a moving target with a simple robot arm.

AS is an extension of the phenomenon of synchronisation in dynamical systems , where a 'slave' system can be made to synchronise with the future, rather than the instantaneous, state of an identical (or similar, in terms of their vector fields) 'master'. The evidence for an AS-like phenomenon in human motor behaviour comes from delayed-feedback manual tracking experiments where human subjects attempted to synchronise the motion of their hands with a moving cursor. Stepp conducted one such study [2] in which subjects were instructed to track a chaotically oscillating target using a cursor that showed a delayed version of their movement. Subjects led (anticipated) the target in proportion to this delay until it reached a maximal value, rather than anticipating to the maximum degree immediately. This result is corroborated by multiple earlier studies that used similar methodology ([3], [4], [5]). Stepp found this consistent with a type of AS system identified by Voss [6], where anticipation is caused by a coupling term $K[x(t) - y(t - t_{delay})]$ added to the slave, as in Eq. 2 and Fig.1:

$$\dot{x}(t) = f(x(t)) \tag{1}$$

$$\dot{y}(t) = f(y(t)) + K[x(t) - y(t - \tau)] \tag{2}$$

but only if τ represents the feedback delay imposed by the experiment. A later collaboration between Stepp and Voss even indicated that so long as the continuous coupling with the body exists, the slave does not need to be similar to the master, and similar results can be achieved by a filter-like system that exhibits negative group delay [7].

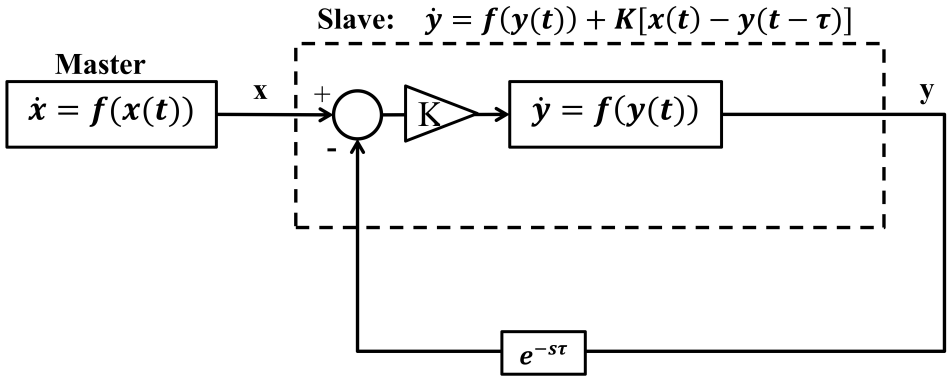

Figure 1: A generalised AS configuration based on delayed slave self-feedback, as described in [6]. The master (x) and slave (y) are governed by the same dynamics, save for the coupling term $K[x(t) - y(t - \tau)]$. This term effectively increases the time constant of the slave, causing it to evolve more quickly than the master until $y(t) = x(t + \tau)$, at which point the coupling term reduces to 0 and the slave is synchronised with the future value of the master. If the master and slave dynamics are merely similar, not identical, synchronisation can occur, but the coupling will never fully disappear.

This is in direct opposition to the theory postulating that motor control is dependent on a series of 'forward models' that fully replace the real, delayed sensory input with an estimate that is learned over time [8][9]. Miall and Wolpert [10] argued this explains how humans can perform fast movements that should be hindered by their physiological delays; the model is feed-forward, and does not need to wait for input from the body. This has not stopped AS potential for control theory applications from being recognised by some authors.

However, where AS has been applied to control it has been utilised within standard existing control frameworks rather than in an attempt to replicate strong anticipation. Oguchi and Nijmeijer [11] demonstrated that an AS slave system with a specified anticipation period could be inserted into a control loop, stabilising it analogously to a Smith predictor [12][13]. The delayed feedback is fully replaced by a predicted signal, allowing the controller to be designed as if the delay does not exist, but in principle the slave and its self-feedback could be replaced by a feed-forward model that estimates some n time steps ahead.

Although AS can be used within predictive control as shown by Oguchi and Nijmeijer, existing predictive controllers cannot be used to implement or replace a strongly anticipating AS controller. Firstly, there is no one element within the AS paradigm that can be replaced with a predictive model, as anticipation is a result of the continuous interaction between the master and slave. Secondly, and more importantly, there is no single predictive controller with fixed parameters that would exhibit equivalent behaviour to the strongly anticipating control proposed by Stepp and Voss, where the controller anticipates in proportion to the real feedback delay within the system.

We hypothesise that a control scheme based directly on the strong anticipation principle and utilising AS can be designed by coupling a correctly designed dynamical model to the real output of the plant through the sensors - a sensory coupling. Because the sensed output of the plant is subject to both, the delays introduced by the plant itself (feedback delay, τ_f), and those that result from sensory processing (sensory delay, τ), the anticipation period will always be equal to the true delay within the system. The logic of this principle is similar to that of 'signal bouncing' [14], which avoids modelling network delay by 'bouncing' the output of a predictive model through the delaying channel itself.

We test our hypothesis by using a simulated robot (modelled in Simulink) to perform a tracking task in the presence of delay. Because of the challenges specific to this application, namely that the plant can only be controlled by a torque signal that is defined in a different coordinate system to the target, there are restrictions on how this coupling can be applied. Nonetheless, we believe we identified the two most plausible systems.

The 'parallel' system couples the plant itself to an internal model that encodes the 'normal' response of the control loop without delays. With both the model and plant tracking the same target, the plant synchronises with the future state of the model, anticipating by a sufficient amount to counteract the delays in the real system.

The 'serial' system treats the moving target as the master, with an internal model predicting its motion. The control signal that corresponds to this predicted target is calculated and used to control the plant. The output of

the plant, subject to the real system delays, forms the 'slave' part of the sensory coupling and ensures the degree of anticipation is always appropriate. In both of these cases, anticipation cannot occur without continuous interaction with the real target and plant, fulfilling on a basic level the requirements of strong anticipation.

The stability and tracking accuracy of the parallel and serial systems are tested and discussed in sections 3 and 4, respectively. In addition to being compared with each other, comparisons are made with an unmodified control loop without anticipation 2 and one that does use AS, but without the new sensory coupling.

2 Common System Elements

2.1 Common Control Loop Dynamics

We present modifications to an underlying closed loop control system, seen in Fig.2. The plant is a simple two-link planar arm, modelled as two thin rods connected by frictionless revolute joints:

$$\ddot{\boldsymbol{q}} = \boldsymbol{R}(\boldsymbol{q})^{-1}(\boldsymbol{\tau} - \boldsymbol{S}(\boldsymbol{q}, \dot{\boldsymbol{q}})\dot{\boldsymbol{q}}) \tag{3}$$

Where $\boldsymbol{q}$, $\dot{\boldsymbol{q}}$ and $\ddot{\boldsymbol{q}}$ are the rotational joint position, velocity and acceleration respectively, $\boldsymbol{\tau}$ is the torque at the joints, $\boldsymbol{R}(\boldsymbol{q})$ is an inertia matrix and $\boldsymbol{S}(\boldsymbol{q}, \dot{\boldsymbol{q}})$ is a vector of Coriolis forces.

The Cartesian position of the arm's end effector ($\boldsymbol{x}_{effector}$) is related to the rotational position of its joints ($\boldsymbol{q}$) by the forward kinematic equation:

$$x_{effector1} = l_1 \cos(q_1) + l_2 \cos(q_1 + q_2) \tag{4}$$

$$x_{effector2} = l_1 \sin(q_1) + l_2 \sin(q_1 + q_2) \tag{5}$$

Where l_1 and l_2 are the lengths of the rods that compose the arm.

The target's motion follows the x and y terms of a chaotic Rössler system, governed by Eqs.6-8, such that $x_{target1} = x$ and $x_{target2} = y$.

$$\dot{x} = -y - z \tag{6}$$

$$\dot{y} = x - 0.15y \tag{7}$$

$$\dot{z} = 0.2 + z(x - 10) \tag{8}$$

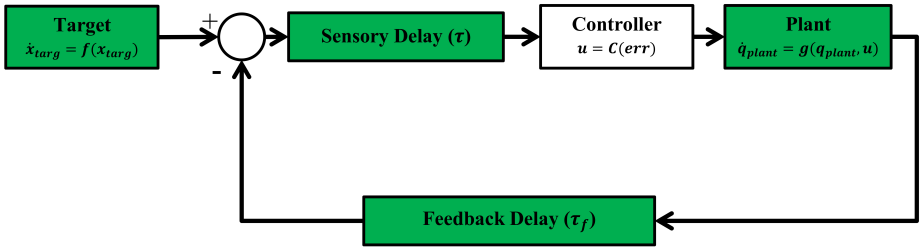

Figure 2: Block diagram of the basic control loop, without any form of anticipation applied. Green blocks represent unchangeable elements of the underlying system. The controller transforms the Cartesian difference between the position of the target and the end effector of the robotic arm plant into appropriate motor torques using Eq.9. The sensory delay term (τ) represents a delay in processing all sensory information, while the feedback delay term (τ_f) represents a delayed reaction from the plant.

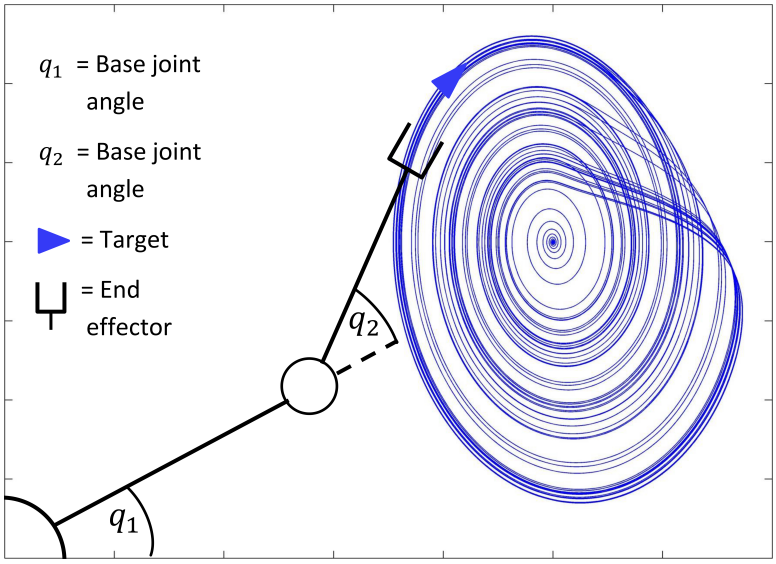

Figure 3: Illustration of the task performed by the simulated robot arm: the target, represented by a blue arrow, moves along a chaotic trajectory, while the controller changes the joint angles q_1 and q_2 of the arm in order to track it with the end effector. The length of each link is set at 4, while their masses are set at 5 (in arbitrary units).

The arm must track the target, meaning that the end-effector of the arm must maintain the target's position and velocity (Fig.3). This is achieved through the use of a simple proportional-derivative control law based on the Jacobian transpose method, which is a well-documented means of transforming a Cartesian error into appropriate torques at the joints [15]:

$$\boldsymbol{\tau} = \boldsymbol{J}^T(\boldsymbol{K_p}(\boldsymbol{x_{target}} - \boldsymbol{x_{effector}}) - \boldsymbol{K_v}\dot{\boldsymbol{x}}_{\boldsymbol{effector}}), \tag{9}$$

where $\boldsymbol{K_P}$ and $\boldsymbol{K_V}$ are the proportional and derivative gain terms, and $\boldsymbol{J}$ is the derivative of the arm's forward kinematics (Eq. 5) with respect to the joint angles $\boldsymbol{q}$.

2.2 Simulation Parameters

We simulate the control loop using MATLAB Simulink with a ode3 Bogacki-Shampine fixed-step solver at a time resolution of 0.001 s. The control loop performance is hindered by two distinct 'problematic' delays, both modelled by a Simulink variable-time transport delay block. Firstly, a delay (τ) is applied to output from both the target and plant, representing an unavoidable sensory processing delay. The feedback delay (τ_f) applies only to the feedback from the plant, and represents an additional delay between the plant receiving the control signal u and its observable response. These both represent delays in the controlled system that ordinarily prevent stability and must be overcome through the introduction of the AS paradigm in the form of the sensory coupling.

2.3 Predictive Tracking Problem

The aim for the two sensory coupling-based models is to effectively compensate for τ and τ_f through anticipation, ensuring that the robot neither lags the target nor loses tracking accuracy when subject to these delays. As such, their performance is compared against that of the original control loop (Fig.2) when τ and τ_f are both 0. Lag (or lead, when successfully anticipating the target) is measured in seconds and calculated by cross-correlating the X-axis positions of the target and end effector over 200 s of simulated tracking and finding the time lag (or lead) of the maximum correlation coefficient. The accuracy of the robot's tracking is treated separately from anticipation - the standard performance measure of root mean squared error between target

and end effector is calculated after time-shifting the end-effector's output to account for lag/lead (lag-adjusted RMS error):

$$E_{RMS} = \begin{cases} \sqrt{\frac{\sum_{t=|l|}^{T}(x_{targ}(t) - x_{effector}(t-|l|))}{T-2|l|}} & l >= 0 \\ \sqrt{\frac{\sum_{t=1}^{T-|l|}(x_{targ}(t-|l|) - x_{effector}(t))}{T-2|l|}} & l < 0 \end{cases}$$

Where T is the length of the simulation and l is the lag term. This is done because an accurate anticipation of the target with appreciable lead time would exhibit a high RMS error, despite being the desired outcome of the experiment. Performing the time shift allows both the accuracy of the prediction and the length of the anticipation period to be judged simultaneously.

this makes it possible to distinguish behaviour that is merely anticipatory with behaviour that is anticipatory and accurate, which is our stated goal.

Without delays, and with the gain values $\boldsymbol{K_P} = 70$ and $\boldsymbol{K_V} = 100$, the lag-adjusted root-mean-square error between the positions of the end-effector and target is 0.1024 (for comparison, the target's distance from the origin varies between 0 and 2) and the lag is 0.01 s. The basic control loop becomes increasingly unstable as delay is increased, with unstable oscillations masking any tracking behaviour at or above 0.045 s feedback or sensory delay.

3 Anticipation Using Plant Dynamics (Parallel System)

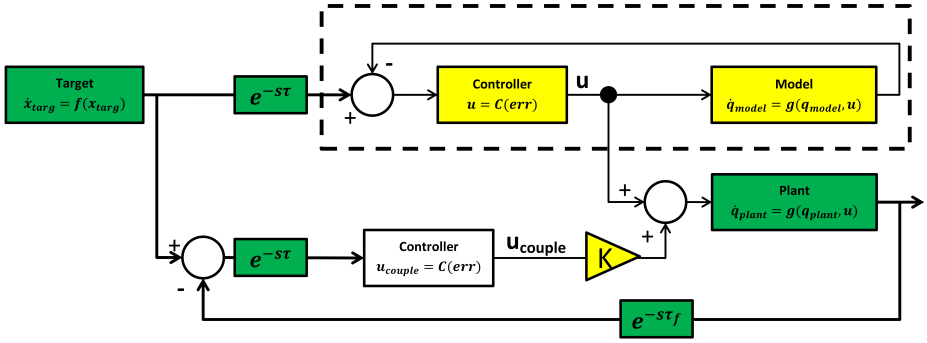

Figure 4: The parallel system. The dynamics of the plant ($g(\boldsymbol{q_{plant}}, \boldsymbol{u})$) and controller ($\boldsymbol{u} = C(\boldsymbol{err})$) are replicated in an internal model (delineated by a dashed box) that uses instantaneous feedback to produce the primary control signal $\boldsymbol{u}$. Green blocks represent unchangeable elements of the underlying system, while yellow blocks have been added to enable anticipation. The delayed feedback from the plant provides the 'slave' component for the coupling term, which is transformed by the controller into a secondary control signal (u_{couple}) that is scaled by the coupling constant K. This drives the plant itself to anticipate the target.

In order to anticipate the target while using only the plant dynamics the plant and an internal model with identical dynamics are coupled in what we call a 'parallel' configuration, which can be seen in Fig.4. This is based on the principle that anticipation can occur between non-autonomous dynamics that share a common driver [16] [17]. In the parallel system the plant anticipates the internal model, which is itself driven to follow the target - the result is that the plant anticipates the target by a small amount.

As stated in the introduction, information from the plant is affected by an associated sensory delay, τ and feedback delay, τ_f. However the internal model is not, and because of its instantaneous feedback it is used to calculate the control signal for both itself and the plant, and is treated as the AS master. The plant's state acts as the delayed self-feedback necessary for the AS coupling, designating it as the slave. Because the plant is a robot that must be controlled by applying torque at its joints, the control law in Eq.9

(with gains of $\boldsymbol{K}_p = 70$ and $\boldsymbol{K}_v = 100$) transforms the difference between the target and plant positions into an appropriate coupling torque that is added to the plant's control input. This coupling torque drives anticipation in the plant and compensates for discrepancies between the control signal based on the internal model and the actual state of the plant.

We expect the sensory coupling to increase the system's robustness to disturbance in the plant, as opposed to a controller based only on an internal model, so the relationship between coupling strength and stability is examined in addition to anticipation.

3.1 Testing

In order to find the limits of the parallel system's anticipation, the tracking task was simulated over a range of vaues for K and both τ and τ_f and the lag and lag-adjusted RMS error. This allows the region in which stable anticipation (and thus, accurate tracking) occurs to be plotted as a function of coupling strength and delay. The system was also exposed to a sensory delay that was abruptly doubled in length partway through a movement in order to test its robustness to non-constant delay.

Finally, the system was again simulated over a range of K and τ values, this time perturbing the plant with a large torque impulse and recording the RMS error immediately afterwards in order to determine the coupling's effect on robustness with respect to external disturbance.

3.2 Results

As the τ_f is increased in this system, the plant begins leading the target as hypothesised (this can be seen in Fig.6a). This is associated with a decrease in tracking accuracy however; once the feedback delay has reached 0.5 s the error has grown noticeably (Fig.6b).

When τ is increased, as seen in Fig. 5a, the lag changes very little over the stable area, which is the same as in the previous condition. This reflects that the plant's anticipation is near equal to the delay on the target information. This holds even if the delay increases during the movement. Fig.7 shows how

a mid-execution doubling of sensory delay does not affect the system's lag, although the increase in tracking error can be observed in specific peaks of the end effector's motion (insets a and b).

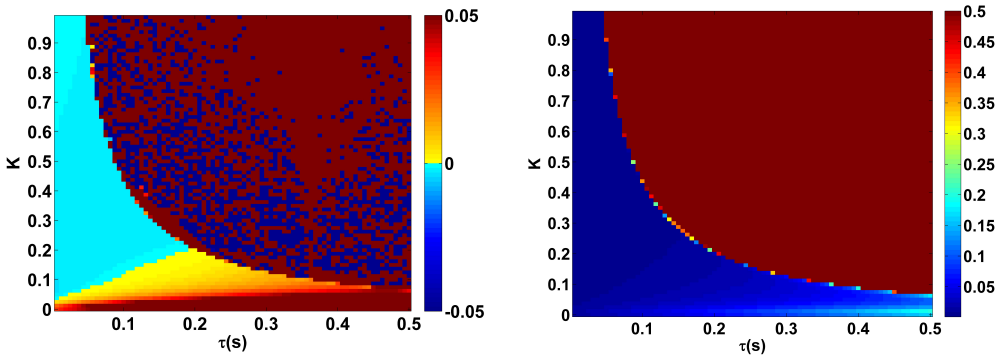

(a) Lag

(b) Lag-adjusted RMS error

Figure 5: Lag (a) and lag-adjusted RMS error (b) between x_{target} and $x_{effector}$, plotted as a heat map. τ_f is set to 0 s, while τ is varied between 0.01 and 0.5 s. Lag remains close to 0 to the left of the stability boundary (which can be approximated by $K\tau = 0.14$), beyond which error rises above acceptable levels and lag can no longer be accurately measured. For this reason, the error is saturated at 0.5.

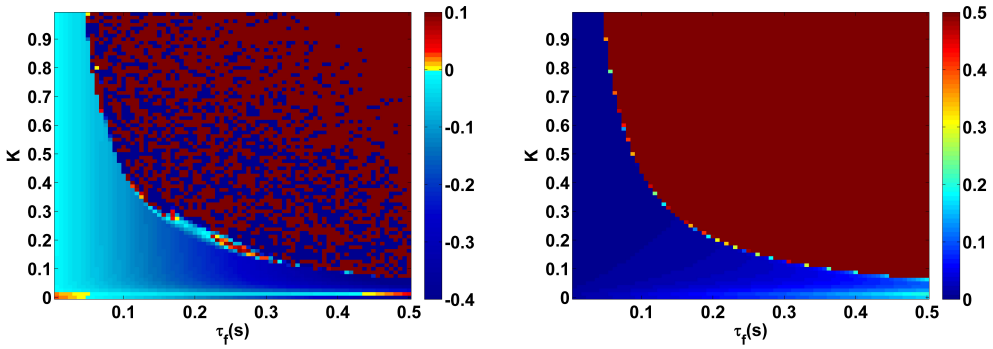

(a) Lag (b) Lag-adjusted RMS error

Figure 6: Lag (a) and lag-adjusted RMS error (b) between x_{target} and $x_{effector}$, plotted as a heat map. τ is set to 0 s, while τ_f is varied between 0.01 and 0.5 s. Anticipation (seen here as blue, negative lag values) increases with τ_f, reaching its maximum near the stability boundary (which can be approximated by $K\tau = 0.14$) beyond which error rises above acceptable levels and lag can no longer be accurately measured. For this reason, the error is saturated at 0.5.

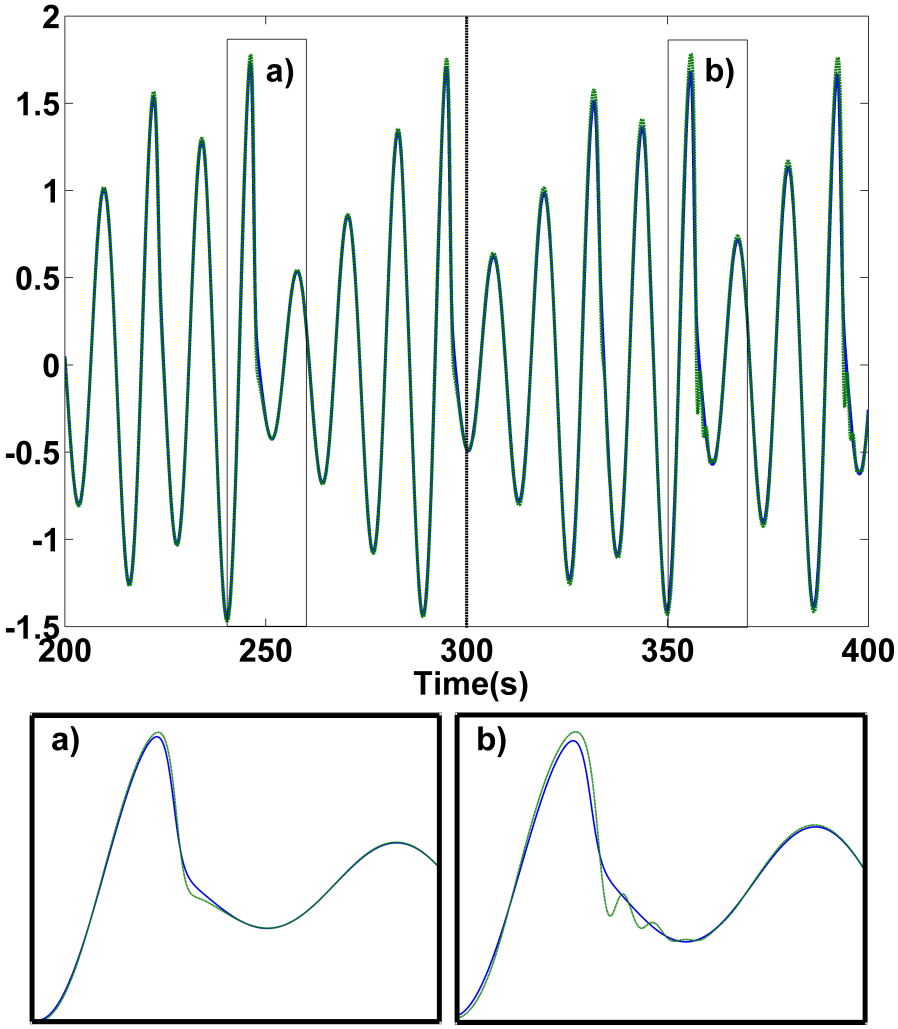

Figure 7: X-axis movement of the target (blue, solid line) and the end effector of the parallel system plant with $K = 0.3$ (green, dashed line), which must track it. $\tau = 0.1$ s before rising to 0.3 s at the 300 s point. The increase in τ causes the end effector to oscillate more after non-sinusoidal moments of the target (compare inset figures a and b), but does not cause a proportionate increase in lag.

Finally, the coupling has a beneficial effect on the system's ability to resist perturbation. As seen in Fig.8, an increased K value makes the system more robust to a large impulse disturbance, even at low delays, and more so than the original control loop. This is clearly displayed in Fig.9, where it can be

seen that the response of the parallel system to disturbance is much smaller in magnitude.

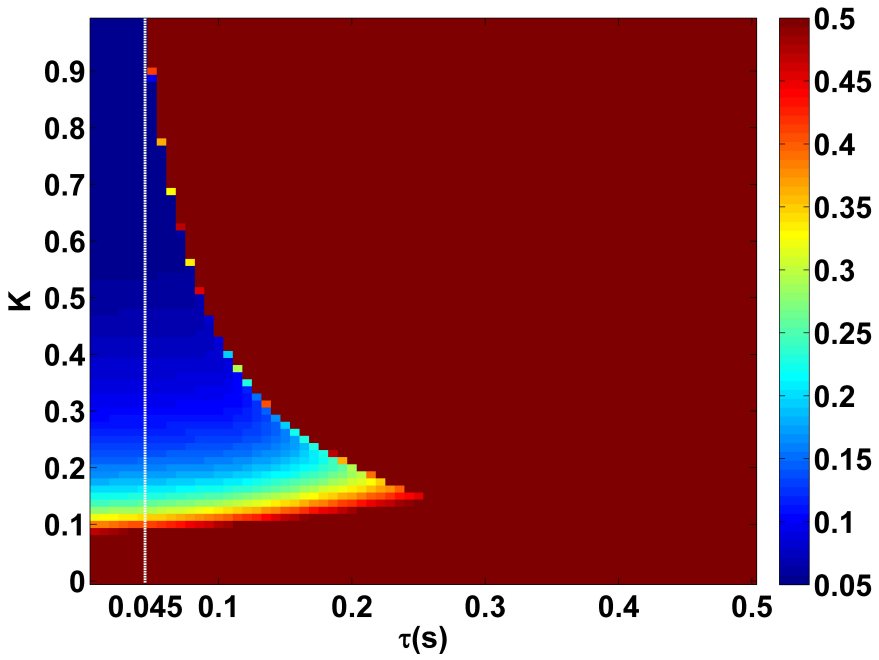

Figure 8: RMS error in the 100 s after an impulse torque disturbance of magnitude 700 is applied at both joints, plotted as a function of K and τ on a heat map. The heat map is saturated above an error of 0.5, representing a failure to track the target. Higher values of K reduce the effect of the disturbance, meaning that the stable region is bounded by the approximate $K\tau = 0.14$ stability boundary, as well as a lower limit in K of approximately 0.1. A white dotted line indicates the highest delay value (0.045 s) at which the original control loop is stable (subject to the same conditions).

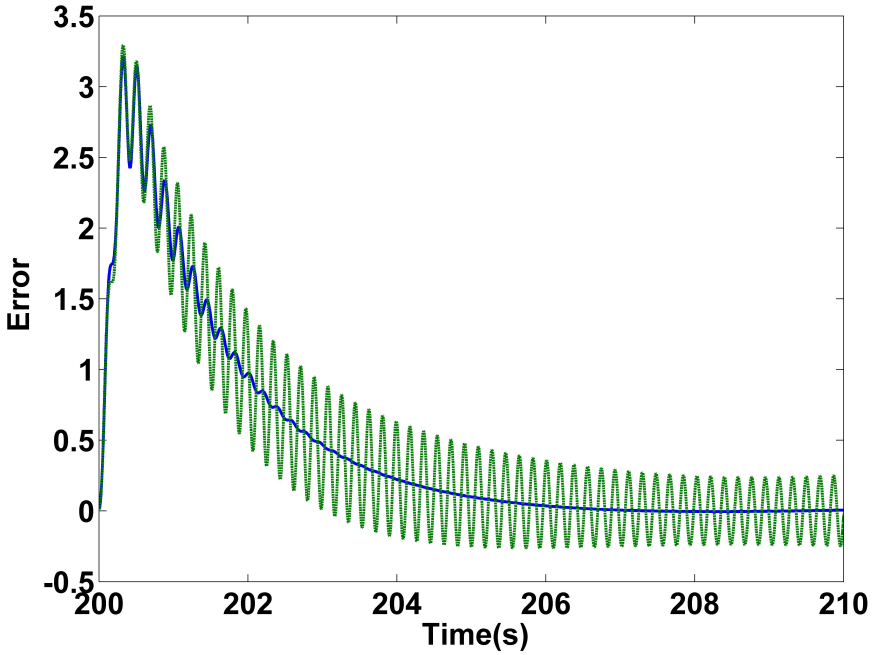

Figure 9: Instantaneous error between the positions of the target and the end effector ($x_{target} - x_{effector}$) for the parallel system with $K = 0.9$ (blue line) and the unmodified control loop (green dashed line) along the X-axis in response to a large impulse torque of magnitude 4000 and duration 0.3 s at both arm joints beginning at 200 seconds. Both systems are subject to the delay terms $\tau = 0$s and $\tau_f = 0.045$s. The parallel system exhibits a significantly reduced response, ceasing oscillation within 5 seconds.

3.3 Discussion of Parallel System Performance

In the parallel system, the plant itself is turned into a predictor by treating its coupling with the internal model as an additional control signal. Through this sensory coupling, the internal model becomes the master and the plant the slave, a reversal of the relationship seen in the work of Oguchi and Nijmeijer [11] and indeed the general expectation that a predictor would be a separable element from the system under control. This is reminiscent of the principle of morphological control [18]: in effect, since an AS-based predictor is being 'simulated' by altering the dynamical behaviour of the robot, the same results could theoretically be achieved by manufacturing a robot which

already exhibits the correct dynamics to anticipate the target. However, even in this scenario it is highly unlikely a single robot could act as an accurate predictor in multiple contexts, so the parallel control structure would still be necessary if the robot needed to perform a variety of tasks.

The parallel system is very stable both to feedback delay and disturbance at the plant, becoming more so as the coupling strength is increased. Where the delay is 0, this is nothing more than an increase in control gain, but the mechanism becomes distinct as the delay increases. Correcting a disturbance can be thought of as a form of initial-value problem. A sufficiently strong coupling allows a slave system to synchronise with the master, even if their current states differ, which is the situation created by a disturbance to the plant. However, the prediction loses accuracy at inflection points in the target's motion, corresponding to characteristic chaotic features of the Rössler dynamics governing it. These are the points where the dynamical behaviour of the target and robot diverge most strongly, causing a transient discrepancy that persists for a short period. This is a known consequence of a mismatch between AS master and slave dynamics, and could be limited in future by taking into account prior information on the target dynamics, rather than limiting ourselves to only replicating the dynamics of the plant in the parallel model.

4 Anticipation Using Environmental Dynamics (Serial System)

In our second, 'serial', system the internal slave contains both the dynamics of the both the target and the plant, in order to anticipate the visual error term err (the difference between the positions of the target and end effector). This term is fed directly into the controller, replacing the true delayed value of err, as seen in the block diagram shown in Fig.10a.

The target is treated as the master, while the slave has the same dynamics as the system described in section 2.1 and shown in Fig.2, minus the sensory and feedback delays. This constitutes an autonomous system that can be synchronised with the target's motion. The coupling term (Eq.10) is added directly to the $\dot{x}$ and $\dot{y}$ terms of the target dynamics within the slave

(Eq. 6, Eq. 7). The plant itself is treated as a delay between sensing the movement of the target and sensing the end effector's response. Theoretically, any sensory or actuation delays (within certain stability bounds) will be compensated by an equal period of anticipation.

$$K[\boldsymbol{x_{targ}}(t-\tau) - \boldsymbol{x_{plant}}(t-\tau-\tau_f)] \tag{10}$$

Since the target dynamics are incorporated in the slave, the serial system should be able to more accurately anticipate all features of the target's movement and thus achieve better prediction accuracy than the parallel system.

We compare this with an approach where the state of the slave is delayed within the slave model (τ_{model} and fed directly fed back in the coupling, as in Fig.10b, in order to demonstrate that our system is not vulnerable to applying anticipation that does not match the true system delay.

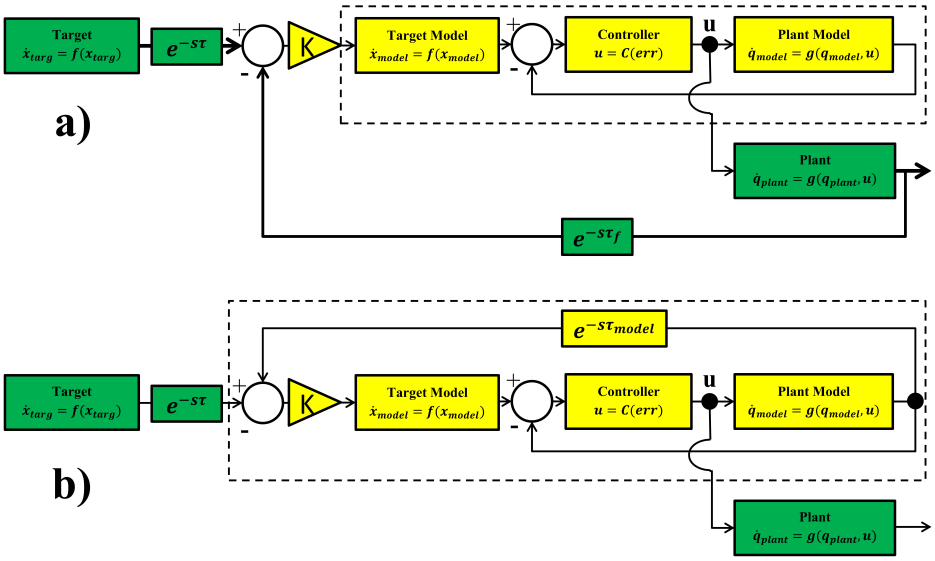

Figure 10: The serial system and an alternative system based on direct slave feedback. The internal slave model is delineated by a dashed box. Green blocks represent unchangeable elements of the underlying control loop, while yellow blocks have been added to enable anticipation.
a) The serial system. An internal model of the system's dynamics acts as the 'slave' in an anticipating synchronisation, while the output of the plant provides delayed self-feedback. The output of the model is a prediction of the future value of the *err* term, which is used to drive the controller without lag.
b) Alternative system where the delayed self-feedback is taken directly from the slave with an independent delay τ_{model} that must be tuned to closely match the sum of delays in the system. This entails the removal of feedback from the real slave.

4.1 Testing

In order to find the limits of the serial system's anticipation, the tracking task was simulated over a range of vaues for K and both τ and τ_f and the lag and lag-adjusted RMS error. This allows the region in which stable anticipation (and thus, accurate tracking) occurs to be plotted as a function of coupling strength and delay. The system was also exposed to a sensory delay that was abruptly doubled in length partway through a movement, and its response compared with that of the system described in Fig.10b.

The system was simulated over a range of K and τ values while subject to a torque disturbance at a fixed point in each movement. The system stability was also compared against that of the original control loop by exposing both to a step disturbance and recording their response.

4.2 Results

The relationship between anticipation time, coupling strength and feedback delay can be seen in Fig.11a. The lag between target and end effector decreases and is replaced by a significant degree of anticipation as the feedback delay τ_f is increased.Unlike the parallel system, the prediction accuracy barely decreases within the region of stable anticipation, as seen in Fig.11b.

Where the feedback delay is set to 0 s, the lag remains close to 0 for a range of values of τ, as can be seen in Fig.12a, indicating that the anticipation closely matches the delay. As shown in Fig.12b, the dependence of the tracking accuracy on τ is the same as its dependence on τ_f.

The serial system is very robust to changes in delay. Even if τ doubles mid-movement, the behaviour of the system does not change, while a system based on internal delay falls out of step with the target (Fig 13).

The serial system was found to be much less robust to disturbance than the parallel system when subject to the same tests, with even a small disturbance to the plant's torque causing major instability and divergence from the target trajectory.

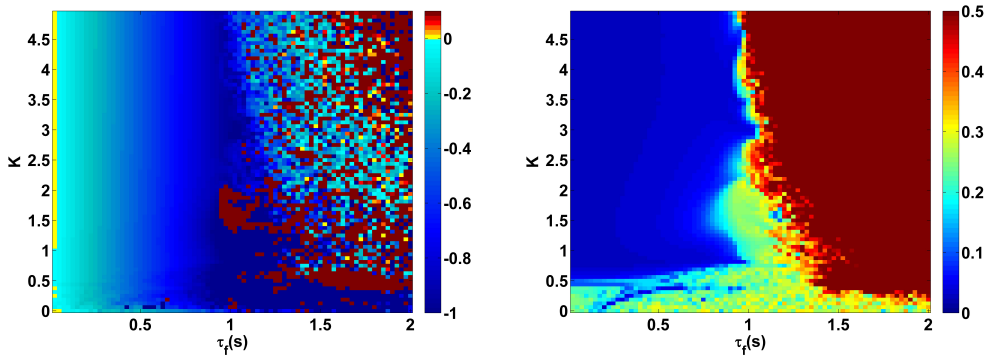

(a) Lag (b) Lag-adjusted RMS error

Figure 11: Lag (a) and lag-adjusted RMS error (b) between x_{target} and $x_{effector}$, plotted as a heat map. τ is set to 0 s, while τ_f is varied between 0.01 and 2 s. The anticipation (seen as negative lag) closely matches τ_f within a near-rectangular region bounded by $K > 1$ and $\tau_f < 1$s, while at higher delays tracking no longer occurs and lag cannot be accurately measured. For this reason, the error is saturated at 0.5.

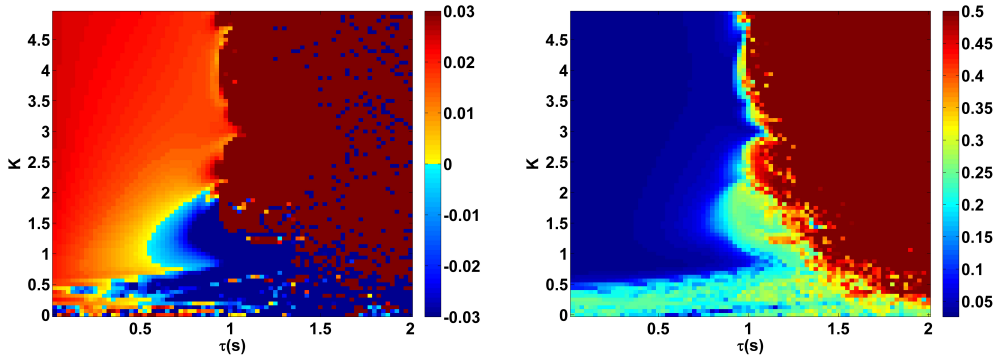

(a) Lag (b) Lag-adjusted RMS error

Figure 12: Lag (a) and lag-adjusted RMS error (b) between x_{target} and $x_{effector}$, plotted as a heat map. τ_f is set to 0 s, while τ is varied between 0.01 and 2 s. The lag remains close to 0 s within a near-rectangular region bounded by $K > 1$ and $\tau_f < 1$ s, while at higher delays tracking no longer occurs and lag cannot be accurately measured. For this reason, the error is saturated at 0.5.

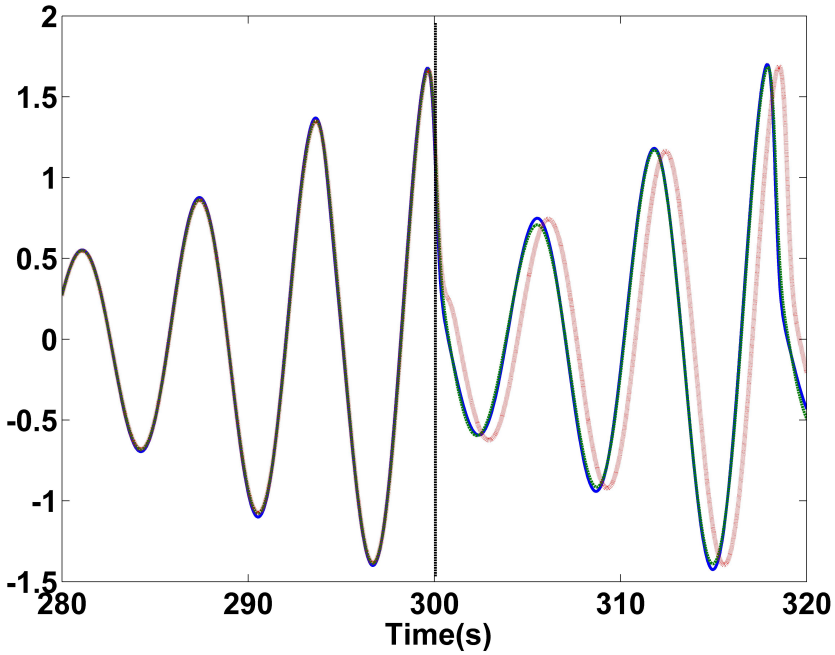

Figure 13: X-axis position of the target (blue, solid line), the end effector of the serial system (green, dashed line), and the end effector of the alternative system using direct slave feedback with $\tau_{model} = 0.3$ (red, dotted line). In both cases, $\tau = 0.1$ s before rising to 0.7 s at the 300 second point (black, dashed vertical line) and $K = 1$. To begin with, all three coincide in time, but after the increase in τ the system with direct slave feedback clearly lags (by the difference between τ and τ_{model}).

4.3 Discussion of Serial System Performance

The serial system achieves a long period of highly accurate anticipation by replicating the full dynamics of the target system in the internal slave, meaning that even a chaotic target can be tracked with very high accuracy (as seen in Fig. 13). Because the true plant is assumed to behave identically to the matching dynamics within the slave, its output is treated as simply a delayed version of the slave's state. Any disturbance to the plant will violate this assumption, and in practice the serial system becomes unstable when subject to much smaller disturbances than the parallel, to the point that a counterpart to Fig. 9 could not be made.

This limitation is linked to the sensitivity to initial conditions of the chaotic dynamics that represent the target in the slave. These diverge exponentially from the target's actual movement when the plant, and thus the sensory coupling, is disturbed. It would be possible to achieve anticipation using less-sensitive dynamics to represent the target within the slave, but these would no longer match the target dynamics and thus limit both the anticipation period and accuracy that can be achieved, resembling more the performance of the parallel system.

5 General Discussion

In this work we sought to find a 'middle ground' between two very different approaches to reconciling AS with the problem of controlling delayed systems. Oguchi and collaborators [11] [14] adapted well-understood predictive control frameworks such that a feed-forward predictive model could be replaced by an AS slave with delayed self-feedback. In contrast, the works of Voss and Stepp identified a strong correspondence between human subjects' ability to anticipate a moving target and the feedback delay they experienced and fitted a plausible high-level AS [2] (and later, anticipatory negative group delay [7]) model to this behaviour. With the parallel and serial systems based on the sensory coupling we aimed to apply the beneficial properties of the anticipatory systems designed in the latter approach (the ability to respond to a wide range of delays with the appropriate degree of anticipation) to a well-defined nonlinear control task - tracking a moving target with a planar two-joint robot arm.

Both the parallel and serial systems exhibited hallmarks of strong anticipation: no anticipation occurred unless there were delays present in the underlying control loop, and where it did occur it was proportional to that delay, as seen in Figs. 6, 5, 11 and 12. This is qualitatively the same behaviour that led Stepp to suggest AS as a principle employed in human motor control, and it is also uniquely useful for the control of artificial systems (such as robots), representing control that is both adaptable and robust. Continuous feedback from the plant allows compensation for multiple levels of delay without changing the gain of the controller or the parameters of the internal dynamical model (a concept outlined by the comparison in Fig. 13 between

the serial system and its counterpart without this feedback).

In performing a tracking task an additional criterion was imposed, that in addition to exhibiting stable anticipation the robot's motion must closely match that of the target. In this latter respect the serial system was more successful, showing low overall error over the majority of the parameter region in which it was stable, unlike the steady increase of error with delay shown by the parallel system (compare Fig. 5b with Fig.12b). This is unsurprising in that the serial system anticipates the target using a slave that contains identical dynamics, which previous studies on AS have suggested is a 'gold standard' for accurate prediction. However, in this case the chaotic Rössler dynamics of the target were highly sensitive to external disturbance, which was inevitably transmitted through the sensory coupling,causing instability. This suggests that for control tasks, where robustness to disturbance is at least as important as robustness to delay, there may be trade-offs for fully accurate prediction.

The parallel system exhibited much greater robustness to disturbance and a lesser accuracy than the serial system, as can be seen in Fig. 8. This suggests that while the near-perfect prediction of the serial system would be appropriate for tasks where unexpected events will not occur, it is the parallel system that is more suited for robots performing 'human-like' tasks in unstructured environments, particularly since it is not limited to anticipating a single type of target. Since many solutions exist for actuation in predictable environments, it would seem that the parallel system has a larger niche in the existing robotic control landscape.

6 Conclusions

We have introduced two closed loop control systems that represent early applications of the principles of strong anticipation to robotic control, utilising the paradigm of anticipating synchronisation. Thanks to a 'sensory coupling' between an internal model and the true dynamics of the plant, delays within the control loop are seamlessly counteracted by a matching degree of anticipation, ensuring that the robot's response neither lags nor becomes unstable. This holds true even if the delay changes mid-execution, with no need to change a corresponding parameter within the internal model. In the

'parallel' system, the sensory coupling is fed to the plant concurrently (or 'in parallel') with the primary control signal to enable anticipation while in the 'serial' system the same coupling drives the internal model to produce a primary control signal that anticipates the target.

Both of these proposed control schemes would be applicable to controlling a teleoperated robot, or one with slow actuation (such as a soft robot). In particular, the 'parallel' system exhibits robustness to both unpredictable delay and unmodelled disturbances, while its internal model's dynamics are not specific to the chaotic target in this tracking task, meaning it is not limited to tracking only one possible target. This fact, combined with the fact that the serial system's target-specific dynamics proved unstable in response to disturbances, indicates that strong anticipation through coupling with the body dynamics alone could be a useful paradigm for tasks in highly unstructured environments.

In addition to testing this new control methodology on a more complex robot model, this work could be greatly expanded by exploring the behaviour of these systems where their internal model does not match the dynamics of the plant or the target. Although counter-intuitive, there is evidence that this could have a beneficial effect on the robustness of the control, and would allow for a more generally applicable controller.

7 Data Availability

The Simulink models and MATLAB code used to generate the results seen in this manuscript are archived at [19].

8 Competing Interests

We have no competing interests.

9 Author's Contributions

HE designed and ran the simulations and drafted the manuscript. SN and YH assisted in drafting the manuscript All authors contributed to the nature

and order of the experiments.

10 Funding

This study was partially funded by the University of Reading faculty funding for PhD studentship.

11 Research Ethics

We were not required to complete an ethical assessment prior to this study.

12 Animal Ethics

We were not required to complete an ethical assessment prior to this study.

13 Permission to carry out fieldwork

No fieldwork was performed for this study.

14 Acknowledgements

References

[1] Stepp N, Turvey MT. On strong anticipation. Cognitive Systems Research. 2010;11(2):148–164.

[2] Stepp N. Anticipation in feedback-delayed manual tracking of a chaotic oscillator. Experimental brain research. 2009;198(4):521–525.

[3] Foulkes AJM, Miall RC. Adaptation to visual feedback delays in a human manual tracking task. Experimental Brain Research. 2000;131(1):101–110.

[4] Vercher JL, Gauthier G. Oculo-manual coordination control: ocular and manual tracking of visual targets with delayed visual feedback of the hand motion. Experimental Brain Research. 1992;90(3):599–609.

[5] Miall R, Weir D, Stein J. Visuomotor tracking with delayed visual feedback. Neuroscience. 1985;16(3):511–520.

[6] Voss HU. Anticipating chaotic synchronization. Physical review E. 2000;61(5):5115.

[7] Voss HU, Stepp N. A negative group delay model for feedback-delayed manual tracking performance. Journal of computational neuroscience. 2016;41(3):295–304.

[8] Wolpert DM, Miall RC, Kawato M. Internal models in the cerebellum. Trends in cognitive sciences. 1998;2(9):338–347.

[9] Blakemore SJ, Frith CD, Wolpert DM. The cerebellum is involved in predicting the sensory consequences of action. Neuroreport. 2001;12(9):1879–1884.

[10] Miall RC, Wolpert DM. Forward models for physiological motor control. Neural networks. 1996;9(8):1265–1279.

[11] Oguchi T, Nijmeijer H. Control of nonlinear systems with time-delay using state predictor based on synchronization. Proc of ENOC 2005. 2005;p. 1150–1156.

[12] Smith AC, Hashtrudi-Zaad K. Smith predictor type control architectures for time delayed teleoperation. The International Journal of Robotics Research. 2006;25(8):797–818.

[13] Arcara P, Melchiorri C. Control schemes for teleoperation with time delay: A comparative study. Robotics and Autonomous systems. 2002;38(1):49–64.

[14] Alvarez-Aguirre A, van de Wouw N, Oguchi T, Nijmeijer H. Predictor-based remote tracking control of a mobile robot. IEEE Transactions on Control Systems Technology. 2014;22(6):2087–2102.

[15] Spong MW, Hutchinson S, Vidyasagar M. Robot modeling and control. vol. 3. Wiley New York; 2006.

[16] Ciszak M, Calvo O, Masoller C, Mirasso CR, Toral R. Anticipating the response of excitable systems driven by random forcing. Physical review letters. 2003;90(20):204102.

[17] Hayashi Y, Spencer MC, Nasuto SJ. A study of anticipatory non-autonomous systems. In: Awareness Science and Technology and Ubi-Media Computing (iCAST-UMEDIA), 2013 International Joint Conference on. IEEE; 2013. p. 316–318.

[18] Paul C. Morphological computation: A basis for the analysis of morphology and control requirements. Robotics and Autonomous Systems. 2006;54(8):619–630.

[19] Eberle H. hefebe/AS-Parallel-Serial: First release; 2017. Available from: `https://doi.org/10.5281/zenodo.888966`.

Synchronisation-Based Control for a Collaborative Robot

Abstract

Collaboration with another person requires a certain ability to anticipate their movements and respond proactively, a capability that most humans take for granted, but which robots do not yet possess. Modeling a human's intentional motor activity would be excessively complex, but Anticipation Synchronisation (AS) is a surprisingly versatile dynamical phenomenon that suggests that such a model is not needed. AS allows a dynamical 'slave' system to anticipate a similar 'master' through the use of delayed self-feedback, however the internal dynamics of a robot manipulator are very different from those of a human arm, so the coupling is prone to instability. Therefore, this manuscript defines a control system based around an internal feedback loop that enforces idealised 'slave' dynamics upon the robot such that it can anticipate the Cartesian trajectory of a target with substantially different internal dynamics. This is tested using a Baxter collaborative robot, which is designed to safely interact with humans at the cost of velocity limitations.

1 Introduction

To create a true collaborative robot, one which can physically cooperate with a human partner, the robot must be able to anticipate its user's behaviour. This is clearly understandable from human-to-human collaborative movements such as manipulating a large object, or even dancing; any delay in reacting to the partner may cause a breakdown in the collaborative movement and a failure of the shared task. It is particularly important that a

robot provides a seamless cooperative experience, because it cannot communicate with its human partner in order to improve its performance or defuse their frustration. Thus, conventional (that is to say, essentially reactive) closed-loop control is not the ideal paradigm for controlling a collaborative robot. The obvious alternative is to use one of the many predictive control frameworks that have been devised to control systems that incorporate delay, but this implies a need to comprehensively model the motor behaviour of the human partner. While many stereotypical human movements are well characterised (such as simple reaching motions, by the minimum-jerk model [1]), there is no complete model to predict what a human user is 'about to do'.

Instead of trying to build this model of the human, we can turn to another solution: strong anticipation. This relates to the idea that organisms like human beings anticipate events by continuously coupling their own (cognitive or somatic) processes to the dynamics of the environment, contrasting with methods that need to construct a model of the predicted system ('weak' anticipation). The most plausible implementation of this principle is anticipating synchronisation (AS), where a 'slave' dynamical system synchronises with the future of a 'master', rather than its instantaneous state [2]. This is not a violation of causality, but relies on the fact that a deterministic dynamical system's current state is strongly determined by its past. The difference between the state of the master and the delayed state of the slave constitutes a coupling term ($K[x(t) - y(t-\tau)]$) that will drive the slave towards the future of the master:

$$\dot{x}(t) = f(x(t)) \tag{1}$$

$$\dot{y}(t) = g(y(t)) + K[x(t) - y(t-\tau)] \tag{2}$$

if the vector spaces of the master (x) and slave (y) are similar, and the delay term (τ) is not too large, the synchronisation manifold will reach a stable state where $y(t) = x(t+\tau)$ and the coupling reduces to 0. Because on short timescales many dynamical systems exhibit similar behaviour, there is no need for f to equal g, and the slave can be governed by significantly simpler dynamics than the master. There is thus no need to model the complex cognitive processes of the human user, so long as a slave system can be designed that can aticipate the short-term dynamics of their motor behaviour. It has been suggested by Ishida and Sawada [3] that a control strategy with this characteristic is advantageous in minimising transient errors caused by

an unpredictably moving target, and may be how human beings cope in a constantly-changing environment.

The dissipative coupling term resembles proportional-derivative control, but differs in an essential way. While AS deals with the relationship between similar dynamical systems, a robot is expected to execute movements that may run counter to its autonomous dynamics. The crucial difference then is in the nature of the slave or plant. In order to connect the two the robot's behaviour must be altered such that it behaves as a slave with similar dynamics to the target, rather than as a merely kinematic object.

AS has typically been applied to isolated pairs or chains of autonomous systems since its discovery, but there have been studies that attempt to combine it with feedback control. An AS based predictor was used by Oguchi and Nijmeijer to replace a standard predictive model in a system that would otherwise be too nonlinear for most predictive control methods [4]. More recently, a similar method was used to enable the control of mobile robots via long-distance telecommunication [5].

AS allows a new relationship with delay: if the slave's self-feedback becomes delayed, it will actually respond by anticipating the master. If we substitute 'slave' for 'plant' we can see why this would be significant - while classical control becomes unstable and fails if the feedback from the plant is delayed, a system based on synchronisation would be expected to begin anticipating the user (the master) instead. This aligns strongly with the principles of proactive control [3]. Although leading the target in phase would seem equally as problematic as lagging it, it in fact allows the minimisation of transient errors when the target moves abruptly, at the cost of lesser accuracy during steady motion. Given the apparent unpredictability of a human user, this is a highly desirable property for a collaborative robot to have.

The nature of the plant's dynamics must be considered more carefully than when designing a classical control law. If the natural timescale of the plant is similar to that of the desired task, stable synchronisation can be achieved with a weak coupling term. If the timescale is significantly different, a larger coupling term will be needed, implying a greater energy expenditure and reducing the systems robustness to delay.

Due to these considerations, and the time and resources involved in producing a custom robotic platform, we will be tailoring the task to the capabilities of the existing Baxter compliant robot. This has two useful properties for how purposes: Baxter's compliant joints introduce dynamics that are more complex than those of a fully rigid robot arm, allowing synchronisation with a wider range of movements, and a fully-featured simulation of the robot already exists, which can be used to implement a master system.

2 Methods

2.1 Robotic Platform

The Baxter robot consists of two 7 degree of freedom arms mounted on either side of a central column capped with an articulated screen 'head', constituting a humanoid 'torso'. This is attached to a 91cm pedestal, giving the robot a total height of 185cm. The arm joints are referenced with alphanumeric labels from S_1 at the base to W_1 at the wrist, as seen in Fig. 1.

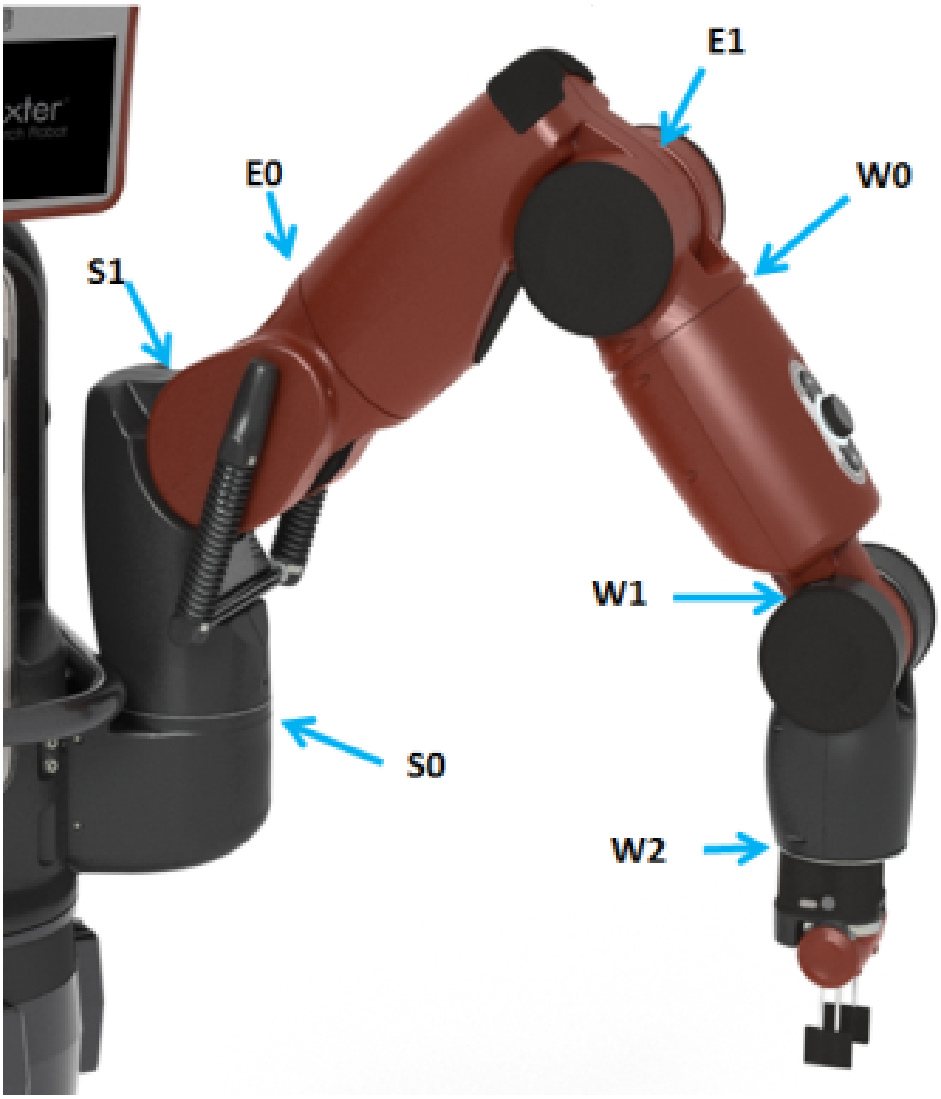

Figure 1: Joint positions on Baxter's left arm. All right arm joints are identical to those on the left, except that S_0, E_0, W_0 and W_2 are mirrored. Image from Rethink Robotics SDK wiki [6].

As a collaborative robot, Baxter is primarily designed for safety when interacting with humans, which is achieved through a combination of specialised hardware and software. Each arm joint contains a series elastic actuator [7] that allows control of joint stiffness and direct measurement of joint torque. Combined with a real-time onboard controller this allows the

robot to maintain arm velocities and forces that do not risk serious harm to the humans around it. A secondary effect of these safety constraints is that Baxter will not accept commands that cause self-collision (as defined by any element of its kinematic model intersecting any other).

In designing the task used to test our new control scheme, a conscious effort was made remain within some of these constraints by utilising Baxter's velocity control facility. This allows direct control of the velocities at each joint, but prevents them exceeding a maximum value of 2 rad/sec (or 4 rad/sec for the three terminal wrist joints) and automatically halts the robot in the event of a collision or a sustained 'crush' against an external object. The ability to control the robot's velocity is crucial to implementing AS, depending as it does on the time evolution of the slave, so this was considered the best compromise between safety and the requirements of the study.

2.2 Collaborative Task

The aim of this study is to demonstrate proactive cooperation with a partner, and we have chosen to concentrate on a task where the robot aims to maintain a constant displacement between its end effector and the user's hand. Many forms of bimanual manipulation involve this form of action, such as moving a piece of furniture, or operating one half of a saw, for example. The robot is considered to be the follower (or slave, for our purposes) in all these actions, in line with expected use cases for a collaborative robot.

We define an ersatz 'sawing' cooperative task where the robot must simulate holding one end of an object that must be moved back and forth with a partner by maintaining a constant displacement from the user's hand (in practice a tracking task). An unpredictable human partner is represented by a periodic oscillator with pseudorandom variation in its amplitude. This is not intended to be a faithful reproduction of a true human movement, but to model the unpredictable variations that proactive control is intended to address.

2.3 Parallel AS Controller

Anticipation requires a degree of autonomous behaviour that is sufficiently similar to the master, and preliminary results suggested that despite its in-

built elasticity, Baxter's unmodified dynamics did not meet this requirement. Therefore it was necessary to define a control input that would force Baxter to exhibit the required autonomous dynamics. This was achieved by creating a simulated control loop where a 'robot' with identical kinematics to Baxter, but modified joint dynamics, tracks the target without feedback delays. Provided the new joint dynamics are chosen correctly, this model produces a control signal that enforces the same behaviour in the real robot's joints, allowing it to act as an effective slave. Two distinct forms of joint dynamics are used in this way, chosen because of their proven individual success at anticipating smooth continuous master signals; leaky integrators (relaxation dynamics) as in Eq.3 and harmonic oscillators (Eq.4).

$$\dot{\boldsymbol{u}}(t) = -\boldsymbol{A}\boldsymbol{u}(\boldsymbol{t}) + G\boldsymbol{M}[\boldsymbol{x_T}(t) - f(\boldsymbol{u}(t))] \tag{3}$$

$$\begin{aligned} \dot{\boldsymbol{u}}(t) &= -\boldsymbol{A}\boldsymbol{n}(t) + G\boldsymbol{M}[\boldsymbol{x_T}(t) - f(\boldsymbol{u}(t))] \\ \dot{\boldsymbol{n}}(t) &= \boldsymbol{A}\boldsymbol{u}(t) - G\boldsymbol{M}[\boldsymbol{x_T}(t) - f(\boldsymbol{u}(t))] \end{aligned} \tag{4}$$

In both cases $\boldsymbol{u}$ is a vector corresponding to the three arm joints under active control, while in Eq.4 $\boldsymbol{n}$ is a harmonic feedback term. Both slave systems are subject to a self-feedback term, $G\boldsymbol{M}[\boldsymbol{x_T} - \boldsymbol{x_e}]$, where G is a gain constant, $\boldsymbol{x_T}$ is the spherical coordinate vector of the target and $\boldsymbol{x_e}$ is the spherical coordinates of the slave's 'end effector', derived using the robot's forward kinematics (adapted from [8]) and the spherical transformation (Eq.5). This feedback term causes the slave to track the course of the target as if it shares the robot's kinematics.

$\boldsymbol{M}$ is a static linear transformation matrix, based on the Joint Relationship Matrix from [9], adapted to a three-dimensional spherical workspace and a robot with three active joints. The use of spherical coordinates allowed a direct relationship between the joints S0, S1 and E1 and the azimuth, delta and radius coordinates of the end effector, ensuring convergence over the entire reachable workspace.

$$\begin{aligned} r &= \sqrt{x_1^2 + x_2^2 + x_3^2} \\ \theta &= \arccos \frac{x_3}{r} \\ \phi &= \arctan \frac{x_2}{x_1} \end{aligned} \tag{5}$$

In our sensory coupling the human partner (or synthetic surrogate) is considered the 'master' system and the output of the robot's encoders represents a measurement of the slave's state. However, the differences between the modelled dynamics and those of the robot mean it is more stable to couple the robot to the output of the model, treating it as an approximation of the target's state. In order to construct the AS coupling, the difference between the spherical position vectors of the 'end effector' within the model ($\boldsymbol{x_e}$) and Baxter's end effector ($\boldsymbol{x_R}$) with feedback delay τ is calculated and multiplied by a constant, K, and transformation matrix, $\boldsymbol{M}$. This is added to the output of the internal feedback loop ($\dot{\boldsymbol{u}}$), multiplied by a scaling constant B, creating the velocity command vector for the robot.

$$\boldsymbol{v}(t) = B\boldsymbol{u}(t) + K\boldsymbol{M}[\boldsymbol{x_e}(t) - \boldsymbol{x_R}(t-\tau)] \tag{6}$$

The final result is a variation on the 'parallel system' from [10] where stable anticipation arises from the interaction between a model of a conventional PD control loop and an AS coupling term. In that case, the internal feedback loop identically reproduced the dynamics of the robot, but the interaction between Baxter's compliant joints and safety firmware makes its dynamics very difficult to accurately simulate, motivating the use of a simpler model. The block diagram of this system is shown in Fig.2.

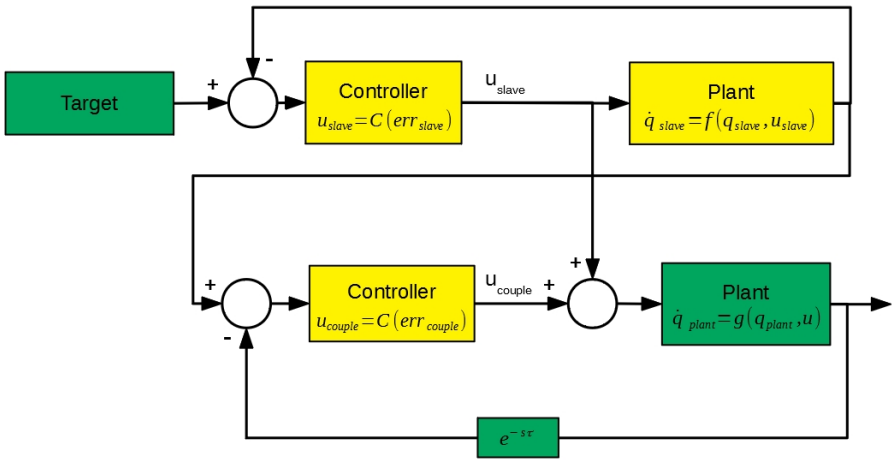

Figure 2: Block diagram of the proposed control scheme, where the plant (Baxter) anticipates a target with unknown dynamics through the combination of a primary control signal u_{slave} produced by an internal control loop with specific 'ideal' dynamics and a second 'coupling' control signal u_{couple} based on delayed feedback from the robot itself. Green blocks represent intrinsic elements of the underlying system, while yellow blocks have been added to enable anticipation. The internal control loop imposes a specific dynamical behaviour on the plant which is suitable to act as an AS slave that can anticipate the target's movements. Thus, the addition of the coupling term causes the robot to lead the target, if the feedback delay (τ) is large enough.

Position control is based around the transformation $\boldsymbol{M}$ which maps the individual spherical coordinates on to the s_0, s_1 and e_1, with all other joints fixed via an independent high-gain control loop. The coordinates θ and ϕ are controlled by joints s_0 and s_1, respectively, while the radial coordinate can be controlled by using joint e_1 to extend the arm, increasing r. Because s_1 also effects the radial coordinate, M is not a true coordinate transformation, however since the joints are effectively coupled through the forward kinematics, e_1 can continuously compensate for s_1's effects on r. This limits the arm to variations on a single pose, allowing the static linear transformation to

ensure convergence on the target. This is preferable to using inverse kinematics because, in particular, the use of a Jacobian-based methods becomes difficult when the instantaneous pose of the robot is not available, as in the scenario we present here.

Finally, the feedback delay term is implemented as last-in-first-out buffer that holds the holds the endpoint coordinate vectors received from Baxter's internal forward kinematics solver and holds them for a specified period.

3 Testing

In order to test this control method a faithful simulation of the Baxter robot attempts to follow a 'partner' that oscillates along the X-axis with a constant frequency of 0.5Hz, but pseudo-random amplitude (generated by applying a moving average filter to the output of NumPy's random() function). Both candidate slave systems are presented with a low ($\tau = 0.01s$) and high ($\tau = 0.2s$) feedback delay condition and this is compared against the performance of a basic PD controller that uses the same transformation matrix (Eq.7).

$$v(t) = K\boldsymbol{M}[\boldsymbol{x_T}(t) - \boldsymbol{x_R}(t - \tau)] \tag{7}$$

The degree of anticipation (or lag) is measured by taking the X-axis motion of the target and the robot end effector over 10 minutes, removing the DC offset from both and cross-correlating them, extracting the lag with the highest correlation coefficient down to a resolution of 0.01s. All analysis is performed using Cartesian coordinates, as this is the format in which Baxter natively publishes its position data.

4 Results

4.1 Leaky Integrator Slave

At 0.01s feedback delay, the lag is 0.01s, as displayed in Fig.3a, and in the cross correlation peak. This is considerably lower than that achieved by the PD controller in the same low-delay condition (0.46s, as seen in Fig.4), despite optimal gain. Once τ is raised to 0.2s, the robot begins leading the

target by 0.09s, albeit with reduced fidelity to the original waveform (Fig.3b). The difference in lead time can be observed in the cross correlation function between target and robot depicted in Fig.5, where the peak for the 0.2s condition clearly indicates negative lag.

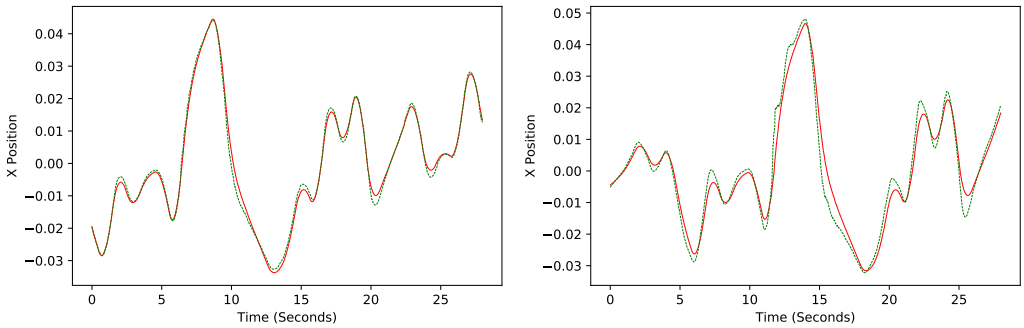

(a) 0.01s feedback delay (b) 0.2s feedback delay

Figure 3: An example of the parallel controller with leaky integrator slave dynamics tracking a pseudo-random oscillating target along the X-axis, with 0.01s (a) and 0.2s (b) feedback delay. The target is represented by a solid line, while the robot's end effector is shown as a dashed line. An increase in feedback delay causes the robot to lead the target on average, at the cost of reduced accuracy.

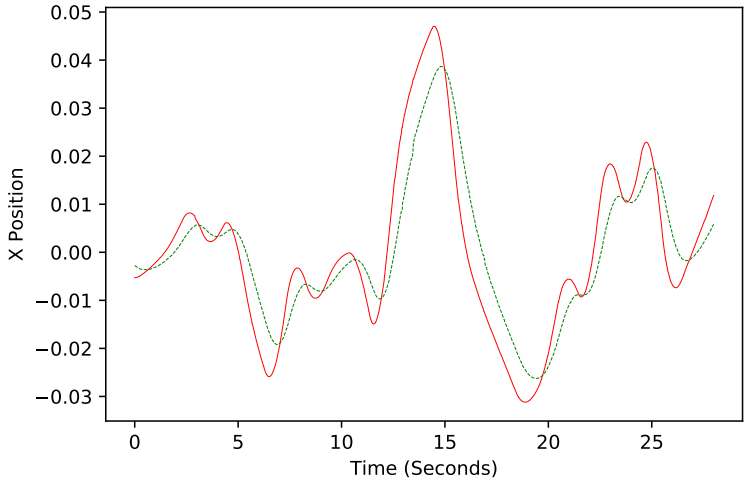

Figure 4: PD controller tracking a pseudo-random oscillating target along the X-axis, with 0.01s feedback delay. The target is represented by a solid line, while the robot's end effector is shown as a dashed line.

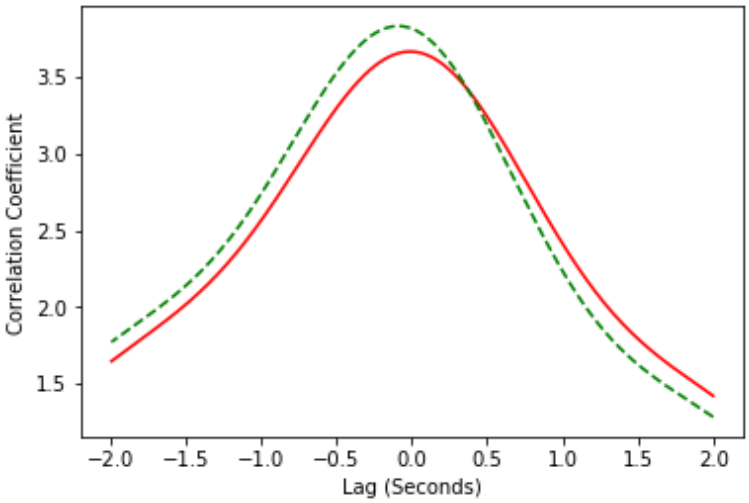

Figure 5: Cross-correlation between the target and robot end effector X-axis trajectories for the parallel controller with leaky integrator slave dynamics at 0.01s feedback delay (solid line) and 0.2s feedback delay (dashed line). The peak correlation coefficient for the 0.2s feedback delay condition is located at 0.09s, indicating that the robot is leading the target..

4.2 Harmonic Oscillator Slave

The harmonic oscillator-driven slave actually slightly leads the target by 0.03s at 0.01s feedback delay (Fig. 6a), but exhibits the same time response as the leaky integrator at τ=0.2s, with a lead of 0.09s (Fig. 7). However, the harmonic oscillator produces fewer erroneous oscillations when anticipating certain features of the target motion (compare the 5-10s period in Figs.3b and 6b).

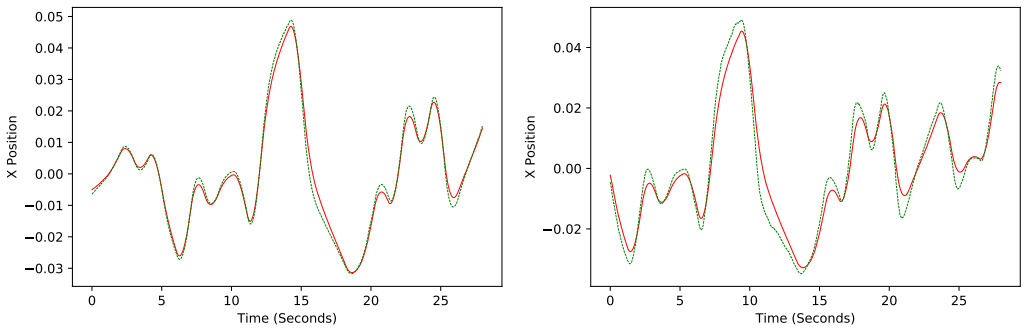

(a) 0.01s feedback delay

(b) 0.2s feedback delay

Figure 6: An example of the parallel controller with harmonic oscillator slave dynamics tracking a pseudo-random oscillating target along the X-axis, with 0.01s (a) and 0.2s (b) feedback delay. The target is represented by a solid line, while the robot's end effector is shown as a dashed line. Where feedback is delayed by 0.2 seconds the robot noticeably leads the target

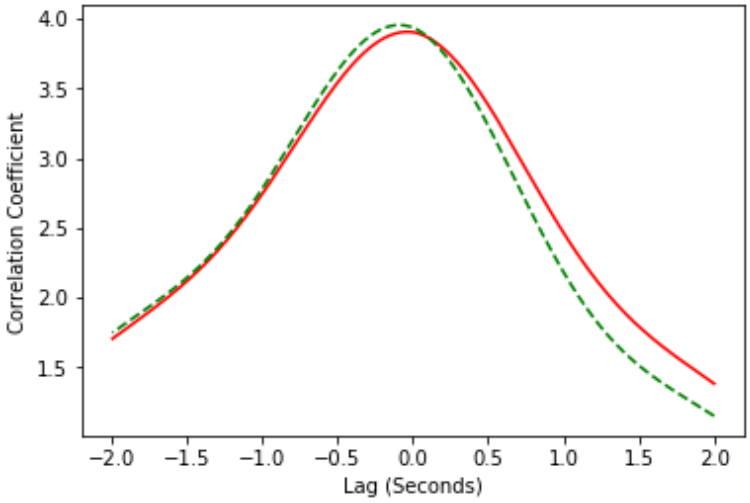

Figure 7: Cross-correlation between the target and robot end effector X-axis trajectories for the parallel controller with harmonic oscillator slave dynamics at 0.01s feedback delay (solid line) and 0.2s feedback delay (dashed line). Both peaks are located at a negative lag, indicating the robot is anticipating the target, but the anticipation time is greater in the 0.2s feedback delay condition (at 0.09s) than in the 0.01s condition (0.03s).

5 Discussion

In both the oscillator and relaxation cases there was a clear correspondence between feedback delay and anticipation, consistent with Stepp's observations in [11], but in neither case did the robot's lead time approach the full value of the feedback delay. This is expected, as neither of the slave dynamics used fully matches those of the target, reducing the maximum possible anticipation. Nonetheless, this result is consistent with Stepp's human studies, where the delayed cursor actually perceived by the subjects never overtook the target - the robot is only 'aware' of the delayed feedback, and it is this delayed version of the end effector that converges on the target. This is qualitatively different from the behaviour of systems where a forward model is placed in serial with the target and the plant such as Oguchi and Nijmeijer's [4]. In such systems the prediction horizon is fixed, and any additional delay will 'subtract' from the prediction time.

Of the two slaves the harmonic oscillator-based slave exhibited a greater tendency to anticipate, unambiguously leading the target even in the lowest delay condition. This is in one way unsurprising, because the master signal resembles an oscillation at the same natural frequency as the slave, with only the amplitude pseudo-randomised. In another respect this is curious, because the target motion is generated by low-pass filtered noise - i.e. a leaky integrator. Since the master is driven by a pseudo-random process, neither slave can be considered a perfect match, but it is clear that the oscillators' local behaviour (sinusoid-like peaks) is sufficiently similar to the master to produce a prediction comparable to that of the leaky integrators'. Additionally the slave is not one, but three systems connected through nonlinear kinematics. The fact that they can cooperate to anticipate a single target signal is a very novel result.

Finally, although adding feedback delay to the system validated its ability to predict a target, the system's behaviour when the delay is minimal is also worth examining. Both the oscillator and relaxation dynamics successfully eliminated the lag displayed by the PD controller under the same conditions. This strongly indicates that anticipation is occurring in response to the delay already present in the robot control loop, increasing the overall responsiveness of the system.

6 Conclusions

Although AS has properties that could be usefully applied to collaborative control, where predicting a human partner's movements is crucial, it relies on a similarity in dynamics between robot (slave) and partner (master) that simply may not exist. This chapter has resolved this issue by expanding upon the parallel system developed in Chapter 4. What would ordinarily be a single control loop is split into two: the first a forward model responsible for setting the robot's behaviour as a dynamical 'slave', and the second acting like an AS coupling term, driving the thus-modified robot to anticipate the target. The resulting controller can counteract any feedback delay the system experiences with a proportional degree of anticipation, without requiring exact knowledge of the delay value. Our use of both leaky integrators, and harmonic oscillators as the basis for the forward model to predict a pseudo-random oscillation firmly establishes that this parallel structure relaxes any

requirement that the model should exactly match the robot's dynamics. In its stead is the principle that the model should represent the dynamics the robot would need to anticipate the target - a much easier condition to meet.

The results in this chapter demonstrate that an existing collaborative robot can display the same adaptive anticipation capability observed in human delayed-feedback tracking experiments, which is an optimal behaviour for reducing lag and transient error. Outside of manipulators, a similar control system would be useful in an assistive exoskeleton, which while not commonly described as a collaborative robot, is judged by the same metrics of continuous, safe physical interaction with a human partner. Describing such a system is beyond the scope of this study, but a form of the parallel controller could theoretically be used to force a rigid exoskeleton to behave more like the user's own musculoskeletal system, allowing safe anticipation of their movements in the absence of more suitable biomimetic materials.

References

[1] Reza Shadmehr. *The computational neurobiology of reaching and pointing: a foundation for motor learning*. MIT press, 2005.

[2] Henning U Voss. Anticipating chaotic synchronization. *Physical review E*, 61(5):5115, 2000.

[3] Fumihiko Ishida and Yasuji E Sawada. Human hand moves proactively to the external stimulus: an evolutional strategy for minimizing transient error. *Physical review letters*, 93(16):168105, 2004.

[4] Toshiki Oguchi and Henk Nijmeijer. Control of nonlinear systems with time-delay using state predictor based on synchronization. *Proc. of ENOC 2005*, pages 1150–1156, 2005.

[5] Alejandro Alvarez-Aguirre, Nathan van de Wouw, Toshiki Oguchi, and Henk Nijmeijer. Predictor-based remote tracking control of a mobile robot. *IEEE Transactions on Control Systems Technology*, 22(6):2087–2102, 2014.

[6] Rethink Robotics. Baxter arm, 2014. [Online; accessed July 29 2018].

[7] Gill A Pratt and Matthew M Williamson. Series elastic actuators. In *Intelligent Robots and Systems 95.'Human Robot Interaction and Cooperative Robots', Proceedings. 1995 IEEE/RSJ International Conference on*, volume 1, pages 399–406. IEEE, 1995.

[8] Robert L Williams II. Baxter humanoid robot kinematics© 2017 dr. bob productions robert l. williams ii, ph. d., williar4@ ohio. edu mechanical engineering, ohio university, april 2017. 2017.

[9] Henry Eberle, Slawomir J Nasuto, and Yoshikatsu Hayashi. Integration of visual and joint information to enable linear reaching motions. *Scientific reports*, 7, 2017.

[10] Henry Eberle, Slawomir J Nasuto, and Yoshikatsu Hayashi. Anticipation from sensation: using anticipating synchronization to stabilize a system with inherent sensory delay. *Royal Society open science*, 5(3):171314, 2018.

[11] Nigel Stepp. Anticipation in feedback-delayed manual tracking of a chaotic oscillator. *Experimental brain research*, 198(4):521–525, 2009.

General Discussion

1 General Discussion

This thesis has charted the development of a robotic control scheme with a novel 'parallel' design that combines direct feedback control with the simultaneous usage of a dynamical forward model. This allows the robot to anticipate its target's motion in proportion to the feedback delay it experiences, mimicking the phenomenon of anticipating synchronisation (AS) first described by Voss in 2000 [1] and drastically reducing the delay's effects.

Existing predictive controllers ranging from the MOSAIC framework [2] to even the AS-based controller developed by Oguchi and Nijmeijer [3] are organised serially in an intuitive 'sense-calculate-act' loop: the state of the system is sensed, the correct movement command is calculated with the aid of a model, and this command is executed by the robot. In these cases, it is important that the model match the robot's desired behaviour near-exactly, because errors can only be corrected post-hoc by altering the model parameters. The parallel controller differs significantly, because the robot is governed by two parallel, simultaneous feedback loops, one simulated and one 'real', with neither fully describing the desired system behaviour. In fact, the only 'prediction' in this scheme is that observed in the robot's movement, which consistently leads the target - a reflection of the AS relationship in which a 'slave' system anticipates a 'master'.

The first step towards the goal of a controller with these properties was described in Chapter 2: "Integration of Visual and Joint Information to Enable Linear Reaching Motions". In this chapter I explored how a simple linear transformation matrix could be used instead of inverse kinematics to produce a specific path (a straight line) with a robot arm's end effector,

building on work by Nishida et. al [4] that established the conditions for such a matrix to ensure convergence on a target. Such an effect can only be achieved by ensuring that the elements of the arm, the joints, 'cooperate' so that when one moves in a way that draws the end effector off the desired path the others react and compensate. If the reaction is slow or delayed the resulting trajectory will be 'bumpy' and inefficient so, in other words, the joints must behave as if they are synchronised. Anticipation is simply an extension of synchronisation, as established by Voss [1], and can be produced by introducing delayed self-feedback to the driven system, but the relationship between a robot and its target is not the same as the robot's joints with each other. Therefore, success in this study did not necessarily imply that the robot as a whole could predict a target as I desired. In fact, attempts to treat the target and the robot as the master and slave in an AS manifold by simply adding feedback delay inevitably led to the system becoming unstable.

The reasons for this were made clear in Chapter 3: "Renormalized time scale for anticipating and lagging synchronization ". For this manuscript I performed the numerical simulations necessary to validate the hypothesis that AS could be well-approximated by its second-order Taylor expansion - equivalent to renormalising the time constant of the slave. This describes the majority of stable AS behaviour well because where the master and slave are similar and the delay is sufficiently small the anticipation manifold $[master(t) - slave(t - \tau)]$ is approximately linear, regardless of the nonlinearity of the systems themselves. From this it was clear that standard robotic feedback control cannot lead to successful anticipation because the relationship between the robot and its target remains inherently nonlinear, due to the large differences in their dynamics.

In Chapter 4 "Anticipation from Sensation: Using Anticipating Synchronisation to Stabilise a System with Inherent Sensory Delay" I explored two avenues for resolving this obstacle and creating a stable anticipation manifold between target and robot. The 'serial' controller simulates a nested feedback loop in which a copy of the target is tracked by a copy of the robot, and treats this model as the AS slave system. So long as slaves's dynamics are correct, it's output can be used to drive the robot's motion and the error term between the target and the robot's end effector drives the slave's anticipation. This enables the robot to lead the target by an impressive period, and the system can cope with large changes in feedback delay, but any dis-

turbance will break the correspondence between the model and the robot and cause immediate instability. Overcoming this flaw required stepping outside of the traditional serial structure seen in so many predictive control laws and combining the output of the model with direct feedback. This led to the first iteration of the parallel controller, which retained the ability to adapt to changing delay while being much more resilient to disturbance and no longer requiring a copy of the target dynamics.

This version of the parallel controller used a full copy of the robot's dynamics to construct its forward model, simulating a version of the robot that tracks the target without delay. When there is no feedback delay or disturbance, the system's behaviour is identical to a basic PD control law, but when delay increases the two feedback loops diverge in function. The forward model imposes a stable dynamical behaviour on the robot that allows it to behave similarly to an AS slave system, while the 'real' control loop acts like the AS coupling term, driving the robot to anticipate and lead the target. The model is effective not because it uses a copy of the robot's dynamics, but because the feedback loop has leaky integrator-like properties, which as shown by Voss and Stepp [5] allow a system to exhibit a phenomenon similar to anticipation. This was validated in Chapter 5: "Synchronisation-Based Control for a Collaborative Robot" in which I implemented a modified version of the parallel controller where the robot's dynamics were replaced by a group of leaky integrators representing its joints, without disrupting its ability to anticipate. With the link between the model and the robot broken, it was possible to design a model based on the known behaviour of the target instead, with the potential for a higher quality of anticipation. In the case of an oscillatory pseudorandom target, a group of harmonic oscillators was also an appropriate choice, given that the target exhibits sinusoidal peaks.

The success using harmonic oscillators as the model component of the parallel controller merits further discussion, as the smooth, oscillatory movements it was able to anticipate are common in many applications. The oscillatory behaviour that was imposed on the robot in Chapter 5, and which allowed it to anticipate, could in fact already exist in a robot with sufficiently elastic elements. In that case the forward model would become obsolete: simple under-actuated feedback control would allow such a robot to anticipate the target without any further computation. For this reason I believe that the control methods developed in this thesis are very relevant to the emerg-

ing field of soft robotics, where the robot's kinematics and dynamics are often too computationally intensive to use or simply not available. Inverse kinematics-free control and consideration of how the robot's autonomous dynamics compare with those of its desired behaviour could resolve many of these issues now faced by researchers.

For example, coordination-based control as demonstrated in chapter 2 does not require the links or other elements of the robot to maintain a constant length or shape so long as their effect on each others' motion is consistent. This condition requires an additional rotational transformation when using Cartesian coordinates, but a more bio-inspired coordinate system based on, for example, arm extension/retraction and orientation could subsume this problem. Since this form of control requires a responsive feedback loop it could be problematic for robots based around elastic or pneumatic actuators - which is where the parallel controller's use becomes apparent. Turning the robot itself into an anticipator can compensate for actuator lag even if it may vary in ways that are difficult to model (such as external forces, and the effects of the soft robot's own deformation).

References

[1] Henning U Voss. Anticipating chaotic synchronization. *Physical review E*, 61(5):5115, 2000.

[2] Masahiko Haruno, Daniel M Wolpert, and Mitsuo Kawato. Mosaic model for sensorimotor learning and control. *Neural computation*, 13(10):2201–2220, 2001.

[3] Toshiki Oguchi and Henk Nijmeijer. Control of nonlinear systems with time-delay using state predictor based on synchronization. *Proc. of ENOC 2005*, pages 1150–1156, 2005.

[4] Ryosuke Nishida and Sadao Kawamura. A new feedback robot control method based on position/image sensor integration. In *Intelligent Robots and Systems (IROS), 2012 IEEE/RSJ International Conference on*, pages 5012–5017. IEEE, 2012.

[5] Henning U Voss and Nigel Stepp. A negative group delay model for feedback-delayed manual tracking performance. *Journal of computational neuroscience*, 41(3):295–304, 2016.

Conclusions

1 Conclusions

The field of robotics is crowded with predictive control systems, both theoretical and realised, so it is necessary to be clear on what is unique about strong anticipation through anticipating synchronisation. Strong anticipation has been primarily investigated in terms of how it can explain the behaviour of organisms, so not all of its properties are relevant to robotics. This thesis has focused on two that are: the ability to anticipate nonlinear systems, and non-parametric adaptation to changing or unknown feedback delay. The value of the first is relatively obvious; nearly every conventional robotic manipulator has highly nonlinear kinematics and dynamics, and advances in soft and compliant indicate that this trend will only accelerate. The second holds the promise of a robot that will execute with minimal lag even if the feedback delay affecting the robot cannot be modeled. Together these properties would enable predictive control that is both simple and robust.

Despite the usefulness of AS in predicting nonlinear systems being previously recognised, the specific case of robotic manipulators which has the master (target) and slave (robot) defined in different coordinate systems (Cartesian and joint rotation, respectively) is under-investigated. This is only natural given that AS research has concentrated on highly similar master/slave pairs, but has left few indications on how to bridge the gap between AS and existing robotic control methods. Defining a control law based on a static linear transformation in chapter 1 acted as a first step here, making it simpler to formulate the task of reaching towards a target as a dynamical process that could be synchronised or synchronised with. In addition to being surprisingly effective as an implicit path-planning method, using this method to track a moving target with feedback delay revealed that a robot driven by

PD control can show some of the properties of anticipating synchronisation. The reason this has not been considered an important result in the past is twofold: firstly it occurs in the absence of explicit path planning, which is an unusual condition, and secondly the effect is only visible in the small range of feedback delay within which the control remains stable. Turning this observation into the basis of a practical anticipatory system thus required a significant change in the role of the controller.

The serial system presented in chapter 4 resolves this problem by treating the whole of the feedback loop containing target, controller and robot as the basic unit of the AS slave. A copy of these combined dynamics is placed between the real target and robot, and the control signal generated within this model control loop is used to drive the latter. The difference term between the real target and robot becomes the AS dissipative coupling term. As a result the slave model (and as a result, the robot itself) anticipates the target in proportion to the feedback delay, even if the length of the delay changes during the course of the movement. However the serial system could not tolerate any disturbance which caused the motion of the robot to diverge too much from that of the target, and this lack of robustness makes it unsuitable for the unstructured environments in which changing delays are most likely to occur.

Much more promising is the parallel system where there is no attempt to model the target dynamics, and an internal feedback loop is used to alter the behaviour of the robot so that it can be used as the anticipating slave. In this way the dynamical 'model' is actually acting as a controller that constrains the robot's dynamics in order to preserve stability. In chapter 3, this desired behaviour was identical to the robot tracking the target without delay, so the robot's 'body' dynamics were reproduced in full, but this is not the only viable form of slave. Chapter 4 applies the parallel system to Baxter, a humanoid robot with inbuilt compliance designed for safe human-robot collaboration. Baxter's compliant joints and safety-preserving firmware mean that its dynamics are very complex in practice, and a full dynamical model would not have been a feasible solution. Instead, two types of simple dynamics known to be able to anticipate a wide range of continuous dynamical systems were used - harmonic oscillators and relaxation dynamics/leaky integrators. Imposing these dynamics onto the joints of the robot's arm allowed it to act as a predictor for a smooth, pseudorandom oscillation as predicted by Stepp and Voss. The explicit anticipation in this case is the result of an

imposed feedback delay, and under 'normal' circumstances a system based on this principle will merely seem to have minimal lag, as the anticipation period will be in proportion to (but not exceeding) the delays naturally present in the system. This is in line with Stepp's original findings, which showed a gradual transition from lag to anticipation, and subjective human experience, which is reactive.

This use of highly simplified dynamics runs directly counter to the standard practice in control engineering that a model must be as close to reality as possible. However this convention is borne out of the needs of feedforward control, where even small parameter errors can cause the system to diverge from its desired behaviour over time. A controller built around negative feedback has no such limitation, as it can continually correct errors as they occur. When dealing with significantly delayed systems this would be considered a moot point - it is impossible to react to information one has not yet received, and closed-loop controller are notorious for losing stability when subject to feedback delay. However, it has been shown here that a system based on AS can take delayed feedback and respond proactively to its target, despite not possessing anything even approaching an accurate model.

In fact, an exact model of the plant may be counterproductive - the central conceit of the parallel system is that the robot being controlled does not have suitable autonomous dynamics to anticipate the external master, but while this is certainly true of Baxter and most other robotic manipulators, it does not have to be. To take the example of the 'sawing' task in chapter 5, a robot with natural elasticity that predisposes it to oscillate passively would almost certainly be able to synchronise with the partner as an ordinary AS slave, without additional control inputs. Thus, the natural extension of this research is to examine soft robotic systems as platforms for AS-based control. The design of many soft robots is already task-specific, but in the future it may be advantageous to examine how their dynamics relate to their desired behaviour (the master) in addition to the more common question of how their many degrees of freedom affect their kinematics.

What this thesis cannot do is shed any light on how (or whether) the human body and brain exhibit strong anticipation. The human body has much more complex autonomous dynamics than any of the robots examined here (or any robot yet designed), and it is plausible that this means its dynamics do not

need to be altered in order for it act as an anticipating slave. On the other hand, and in contrast to other animals, humans execute a huge variety of motor tasks, well beyond the scope of those for which it could be considered an 'optimal' slave. The differences between bouncing a ball and driving a car, for example, are such that it is hard to conceive of a single control rule that would encompass them both. The parallel system, in a modular form, might represent a way in which the body's dynamics could be modulated so that it adopts the 'correct' dynamics to anticipate the dynamics of the environment. The author does not not foresee a means to separate this form of AS from any other using purely behavioural data. However, if the body is acting as the slave, then one would expect that the signals from the brain to the muscles do not relate to the anticipated future position of the body, as the AS coupling is based on current state of the master and the past of the slave. It may be possible to construct a suitable causality measure between a target a subject is manually tracking with feedback delay and their EMG, but this is beyond the scope of this thesis.

In terms of immediate applications of this work, chapter 4 presents a complete framework for how a robot with known dynamics can continue to operate normally in the presence of sensory and/or feedback delay that cannot be accurately modeled. This could easily occur if the sensor system is connected via an unreliable network or if the robot itself exhibits lag time before executing instructions. Neither of these scenarios correspond to an optimised classical robotic system, but as such the parallel controller could be a means of extracting improved performance from inferior, damaged or aged components. This method could also be used to increase the responsiveness of robots with compliant elements, from robots with series elastic actuators (such as Baxter in chapter 5) to genuinely soft robots. Such machines can only become more common as more and more roles that require human contact (carer, nurse, assistant) are desired to be filled by robots.